AD-A202 921

NAVAL OCEAN SYSTEMS CENTER, SAN DIEGO, CA
LOW-COST POINTING-AND-TRACKING SYSTEM FOR OPTICAL COMMUNICATIONS (PATSOC) BY: KH JOYCE

1 OF 1
NOSC TD 1287
UNCLASSIFIED
JUN 1988

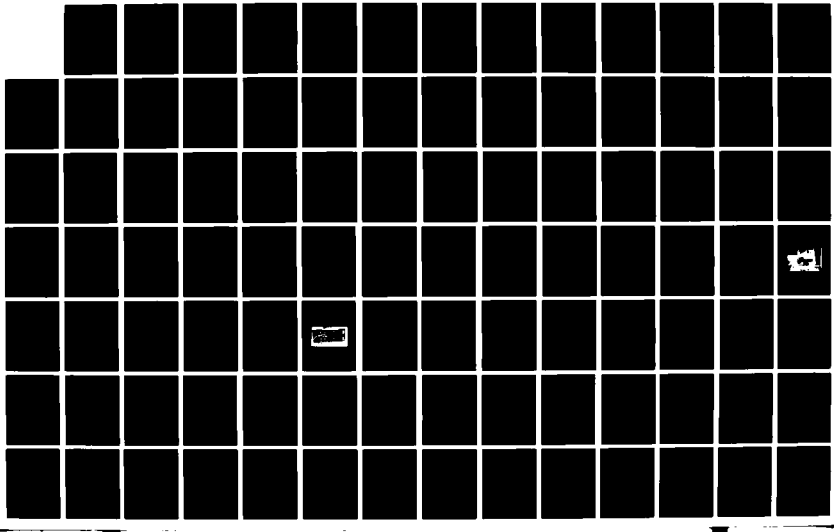

Technical Document 1287
June 1988

Low-Cost Pointing-and-Tracking System for Optical Communications (PATSOC)

K. H. Joyce

Applied Technology Associates, Inc.

NAVAL OCEAN SYSTEMS CENTER

San Diego, California 92152-5000

E. G. SCHWEIZER, CAPT. USN
Commander

R. M. HILLYER
Technical Director

ADMINISTRATIVE INFORMATION

This report was prepared by Applied Technology Associates, Inc., under contract N66001-88-C-0004 for the Naval Ocean Systems Center.

Released by
R. November, Head
Industry R&D Programs
Office

Under authority of
J. Silva, Head
Program Director for
Technology

JJ

REPORT DOCUMENTATION PAGE

1a REPORT SECURITY CLASSIFICATION UNCLASSIFIED	1b RESTRICTIVE MARKINGS
2a SECURITY CLASSIFICATION AUTHORITY	3 DISTRIBUTION/AVAILABILITY OF REPORT Approved for public release; distribution is unlimited
2b DECLASSIFICATION/DOWNGRADING SCHEDULE	
4 PERFORMING ORGANIZATION REPORT NUMBER(S) ATA Memo SBIR-025	5 MONITORING ORGANIZATION REPORT NUMBER(S) NOSC TD 1287
6a NAME OF PERFORMING ORGANIZATION Applied Technologies Associates, Inc.	6b OFFICE SYMBOL (If applicable)
7a NAME OF MONITORING ORGANIZATION Naval Ocean Systems Center
6c ADDRESS (City, State, and ZIP Code) 1900 Randolph Road, SE P.O. Box 4154 Albuquerque, NM 87196	7b ADDRESS (City, State, and ZIP Code) San Diego, CA 92152-5000
8a NAME OF FUNDING/SPONSORING ORGANIZATION Space and Naval Warfare Systems Command	8b OFFICE SYMBOL (If applicable)
9 PROCUREMENT INSTRUMENT IDENTIFICATION NUMBER N66001-88-C-0004
8c ADDRESS (City, State, and ZIP Code) Washington, DC 20363	10 SOURCE OF FUNDING NUMBERS PROGRAM ELEMENT NO: 0502N; PROJECT NO: XD36; TASK NO: XD15; AGENCY ACCESSION NO: DN307 551
11 TITLE (Include Security Classification) LOW-COST POINTING-AND-TRACKING SYSTEM FOR OPTICAL COMMUNICATIONS (PATSOC)	
12 PERSONAL AUTHOR(S) K.H. Joyce	
13a TYPE OF REPORT Final	13b TIME COVERED FROM Oct 1987 TO May 1988
14 DATE OF REPORT (Year, Month, Day) June 1988	15 PAGE COUNT 129
16 SUPPLEMENTARY NOTATION	
17 COSATI CODES FIELD / GROUP / SUB-GROUP	18 SUBJECT TERMS (Continue on reverse if necessary and identify by block number) optical communications pointing tracking

19 ABSTRACT (Continue on reverse if necessary and identify by block number)

This report describes the development of a low-cost, ship-to-ship optical communications system (OCS) under a six month Phase I Small Business Innovative Research (SBIR) contract.

Laser communication systems have been developed for use at fixed ground stations, aircraft, and satellites. However, they have not been successfully used in ship-to-ship applications. The difficulty is that ships have large, random linear and angular motion which interferes with holding a narrow-beam laser on an optical receiver. This study prepared a conceptual design of a relatively short range, low-power ship-to-ship system that would operate under severe sea conditions. The emphasis of the study was on the design of a low-cost gimbal set and its associated tracking system.

20 DISTRIBUTION/AVAILABILITY OF ABSTRACT ☐ UNCLASSIFIED/UNLIMITED ☒ SAME AS RPT ☐ DTIC USERS	21 ABSTRACT SECURITY CLASSIFICATION UNCLASSIFIED
22a NAME OF RESPONSIBLE INDIVIDUAL R. November, CODE [illegible]	22b TELEPHONE (Include Area Code) [illegible]

DD FORM 1473, 84 JAN

83 APR EDITION MAY BE USED UNTIL EXHAUSTED
ALL OTHER EDITIONS ARE OBSOLETE

UNCLASSIFIED
SECURITY CLASSIFICATION OF THIS PAGE

TABLE OF CONTENTS

FIGURES

TABLES

FINAL REPORT FOR LOW-COST POINTING AND TRACKING SYSTEM FOR OPTICAL COMMUNICATION

1. EXECUTIVE SUMMARY AND CONCLUSIONS

This final report describes the development of a low-cost ship-to-ship optical communications system (OCS) under a six-month Phase I Small Business Innovative Research (SBIR) contract.

Laser communication systems have been developed for use at fixed ground stations, on aircraft, and on satellites. However, they have not been successfully utilized in ship-to-ship applications. The difficulty is that ships have large, random linear and angular motion, which interferes with holding a narrow-beam laser on an optical receiver. This study prepared a conceptual design of a relatively short range, low-power ship-to-ship system that would operate under severe sea conditions. The emphasis of the study was on the design of a low-cost gimbal set and its associated tracking system.

1.1 Goals

The requirements for a ship-to-ship OCS are not well-defined and the requirements selected as part of this study are viewed as goals. The three goals that influenced the design significantly are:

1) To communicate over a distance of 15km under favorable atmospheric conditions, i.e., transmission greater than 30%.

2) To transmit 5×10^7 bits per second with an error rate less than 10^{-6}; this will handle two real-time video signals.

3) To communicate continuously under a condition of severe ship motion, i.e., that correspond to sea state 8.

There are many other characteristics of an OCS having to do with operation and maintenance that make an OCS a desirable addition to an overall naval communication system. The general characteristics are described in this summary. Subsequent sections contain more details.

1.2 Design

The design was considered in terms of three subsystems: 1) gimbals, beam pointing, and controls, 2) optics, laser, and detector, and 3) data transmission systems. A relatively detailed design was developed for the gimbals, beam pointing, and associated controls. The optics and data subsystems were considered in sufficient detail to estimate the size and mass of the components that the control system must drive and to estimate the beam pointing errors.

A schematic of an OCS in which the laser transmitter, the tracker, and the data receiver share the same optical path is shown in Figure 1-1. A system with separate transmitting and receiving options on the same coarse gimbal was considered but is not illustrated. Figure 1-2 gives another view of the shared aperture design.

The mechanical configuration of the emerging design consists of a coarse azimuth gimbal which drives a sealed cylindrical unit which contains all of the optics and the coarse elevation drive. A separate computer not shown in the figures handles the signal processing, control algorithms, and interfaces with the other ship's communication functions.

Commercial, preloaded ball bearings are used for both gimbals. The coarse gimbals are driven by electric motors through a unique but inexpensive capstan and cable system. The fine pointing of the laser beam is accomplished by fast steering mirrors. The illustration shows separate azimuth and elevation fast-steering mirrors; however, a single 2-axis mirror is available. A single system can provide complete 360° communication; however, obstructions on most ships will dictate the need for two systems.

The unique feature of the design is the use of nested control loops which receive azimuth and elevation error signals from a quad cell. These control loops reject both the large-amplitude, low-frequency angular motion of the ships due to sea state and the high-frequency, small-amplitude vibrations induced by the ship upon which the system is mounted.

The laser, which is a small, inexpensive 40 mW GaAlAs diode laser, serves the dual function of acquisition and data transmission. The beam will be defocused to speed up the search and target acquisition process.

Other features of the system include a retro-reflector inside the exit window augmented by reflector tape on the outer surface to establish contact between pairs of systems. Other components not shown in the illustration are the position encoders on the coarse gimbals, a horizon sensor, or a gyro. The latter sensors are needed to provide an inertially stable search pattern. A summary of the important characteristics of the conceptual design are:

Field-of-regard azimuth	360°
Field-of-regard elevation	±45°
Coarse gimbal bandwidth	15 Hz
Coarse gimbal rejection at 1 Hz	50 dB
Fast steering mirror bandwidth	350 Hz
Fast steering mirror rejection at 100 Hz	40 dB
Input LOS jitter, rms	50 μr
Residual beam jitter, rms	1[illegible] μr
Focused beam width for communication	3[illegible] μr
Defocused beam width for acquisition	1 mr
Aperture (primary mirror)	15 cm dia.
Detector	Si Avalanche photo diode quad cell
Laser	40 mW GaAlAs diode
Laser wavelength	82[illegible] nm

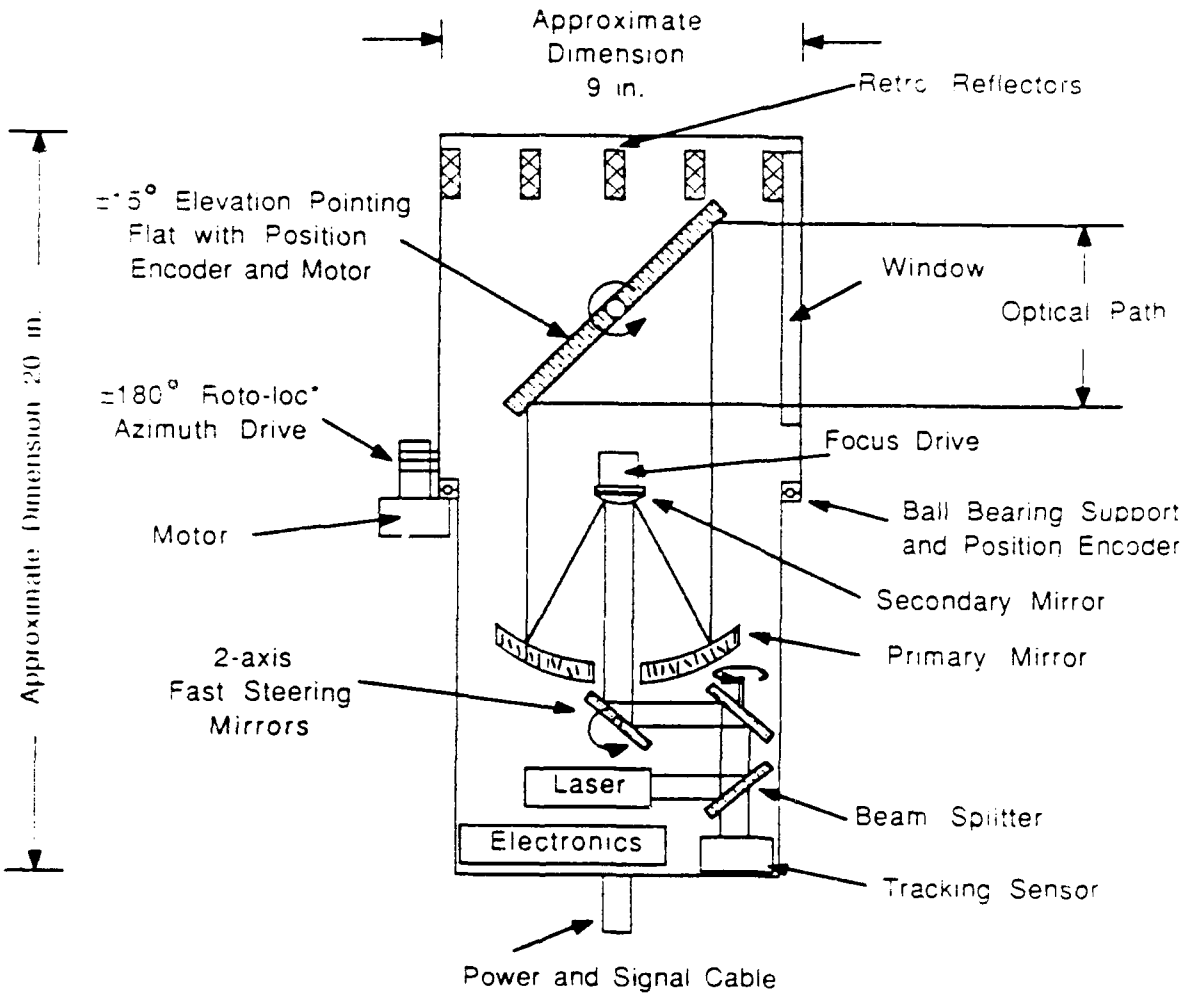

Figure 1-1. Schematic of an Optical Communication System

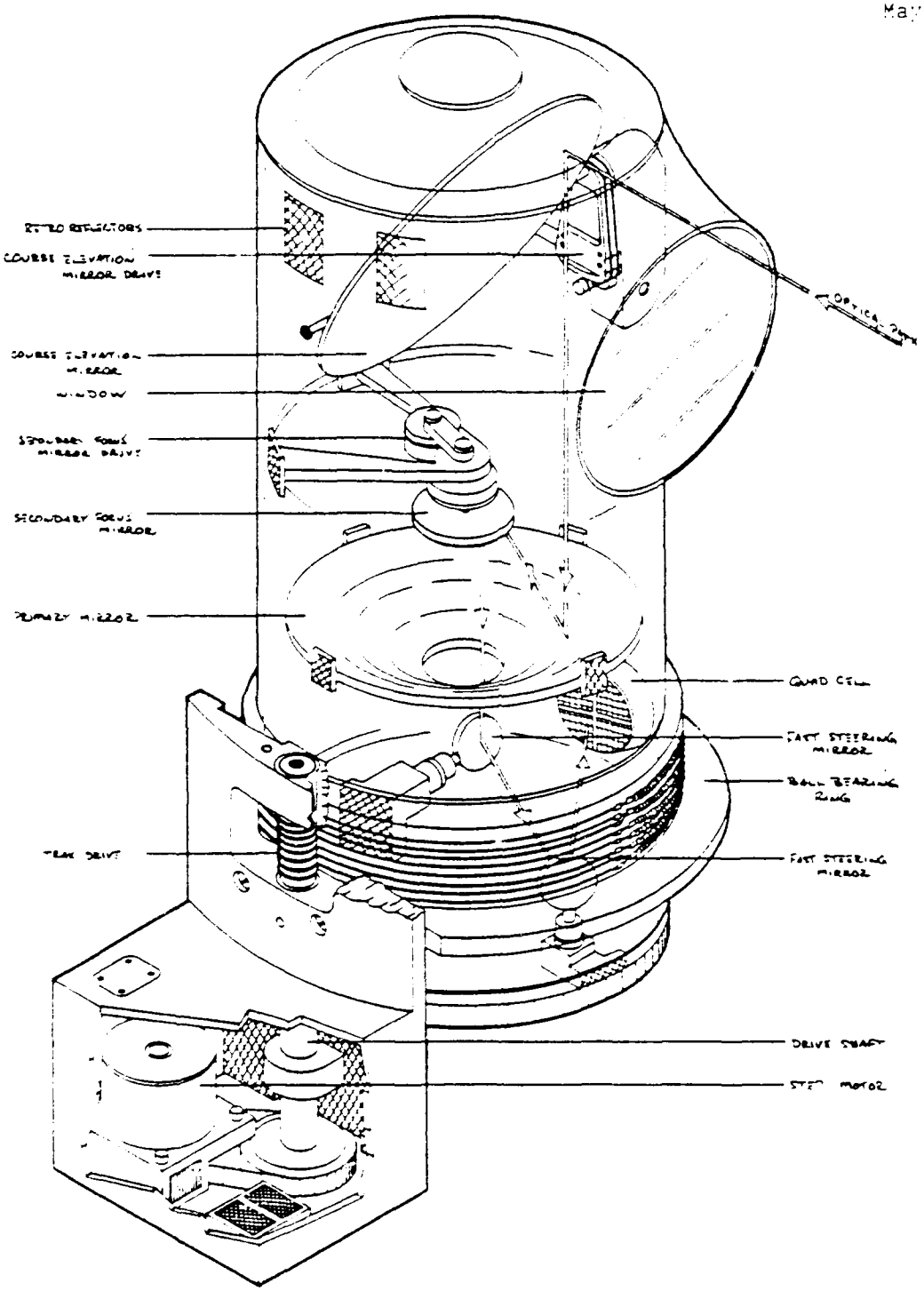

Figure 1-2. Schematic of an Optical Communication System

1.3 System Operation

The first step in initiating communication is the receipt of a command by the OCS computer to contact another specific OCS. An approximate direction to the specified OCS will shorten the acquisition time. If the uncertainty in the direction is greater than 1 degree, the transmitted beam will be defocused to 1 mr and a search will be started near the approximate direction to the other OCS. The search with the defocused beam will scan the horizon at 1 radian per second. An internal vertical direction sensor will determine the direction to the horizon. When a return above a preset threshold is received, it is assumed to be from the retro-reflector on the other OCS.

The beam will rescan the direction of the return. If it is a persistent return, the beam will be refocused to 30 µr and a 300 Hz spiral scan will be used to acquire the target. The target will then be maintained in track using error signals produced by the quad cell.

The second OCS will identify itself by either modulating the retro signal or by propagating its own beam to the first system. At this point two-way communication is established and the systems are ready to transmit data.

Under poor-seeing conditions laser backscatter or scattered sunlight from the atmosphere may inhibit acquisition of the retro-reflector at long ranges. In this case a pulse mode can be used to gate out scatter energy from the beam path. This mode requires an approximate knowledge of the range to the target. A second poor-seeing mode uses a search beam modulated at 1 MHz. In this case the target return is also modulated at the same frequencies; whereas atmospheric backscatter is relatively constant. The scan rate for these poor-seeing modes must be reduced; therefore, a 360° search will take longer than the 6 seconds required by a normal search.

1.4 Benefits

The system will allow more effective command-and-control of defense and attack operations and will provide low-cost ship-to-ship optical communication.

The system could also be adapted to any application involving optical communication over a short range between moving vehicles. Commercial applications would include airport and harbor operations, remote site TV broadcasting, and command-and-control for medical, police, and fire emergency teams. Table 1-1 shows the advantages of an optical communication system for ship-to-ship use.

Table 1-1. Advantages of an Optical Communication System for Ship-to-ship Use

- High Data Rate
- Small Transmitter and Receiver
- Secure Communications

  Low Transmitter Power
- Rapidly Developing Laser Technology
- Similarity to Ship-to-Air and Ship-to-Satellite Communication

1.5 Conclusions

ATA's conclusions can be summarized follows:

1) Nested control loops will lead to an inexpensive optical system for ship-to-ship communication.

2) The concept can be demonstrated in the laboratory using mostly off-the-shelf components.

3) The concept is low-risk and based on current technology.

4) A phased program will demonstrate the tracking, acquisition, and communication functions.

2. INTRODUCTION

2.1 Advantages

Optical communication links have several advantages for ship-to-ship applications over current operational systems at radio frequencies. Key features that make a laser-based, optical communication attractive include:

1) High data bandwidth;
2) Potentially small transmitter and receiver hardware;
3) Ease of protection from interception;
4) Low transmitter power requirements;
5) Promising technology advances to implement optical signal generation, multiplexing, detection, and demultiplexing;
6) Potential similarity with surface-to-satellite and surface-to-aircraft communication systems.

The advantages of optical communication, however, are linked explicitly to reliable, maintenance-free, low-cost pointing and tracking systems to link the transmitter and receiver in the presence of large amplitude ship motion. These systems are required so that a small optical beam from the transmitter can be placed onto the receiver and held there to facilitate low-error data transfer over the beam. A low-cost ship-to-ship optical communication system would provide a very attractive short range alternative to radio and microwave systems.

2.2 Technology Review

Design, fabrication, assembly, alignment, and performance verification of the optical and mechanical subsystems historically have been responsible for significant fractions of the budgets of experimental projects involving precision laser pointing-and-tracking. In the late 1960's and early 1970's the Air Force, the Navy, and the Army each began R&D programs to exploit high-energy lasers in weapons applications. The pointing-and-tracking requirements of these programs are similar in technical difficulty to the pointing and tracking problem of ship-to-ship optical communication. Both situations involve gimballed telescopes carried on a host vehicle which is undergoing intentional trajectory changes and unintentional vibrations. The propagation path through which the optical communication (laser) beam must traverse is affected by atmospheric phenomena (natural, meterological, and man-made) and by boundary layers surrounding the host vehicles.

The lessons learned from previous programs confirm the need for cost improvements in technology for precision pointing and tracking systems. (Reference 1: L. Sher, Editor, "Lessons Learned from the Airborne Laser Laboratory," AFWL-TR-83-5, June 1983. (Confidential).) While disturbances, size and other requirements may differ between weapons and communications systems, many of the technical challenges in areas of cost and performance are similar and have been recognized as significant research needs. Currently, significant amounts of research resources are being expended in the areas of sensors, optics, and associated structural systems for

acquisition, tracking, and pointing. (Reference 2: Mikatymon, "Laser Satellite Communications.) However, the emphasis is on very large space-based and ground-based systems suitable for strategic defense roles. Optical communication involving intersatellite laser links is also receiving a great deal of attention. (Reference 3: R.D. Nelson, T.E. Ebben, R.G. Marshale k, "Experimental Verification of the Pointing Error Distribution of an Optical Intersatellite Link," SPIE Proceedings, 1987). Unfortunately, little emphasis and few research resources are currently being devoted to identification of low cost pointing-and-tracking technology that will be applicable for optical communication applications involving short ranges, high vibration, and moving host vehicles such as ship-to-ship communication links.

The performance requirements for pointing-and-tracking systems for optical communication links are demanding when either the transmitter or receiver is on a moving vehicle. Consequently, such systems have in the past been costly to design and manufacture. This research program seeks cost-effective technology and conceptual designs for the pointing-and-tracking system. Phase I provides a design of a low-cost pointing-and-tracking system which is free of undesired complications and cost impacts on the overall communication system.

Table 2-1. Previous Work in Optical Pointing and Tracking

Name Manufacturer	Application	Range (km)	λ (μm)	Beam Width (μr)	Data Rate (Mb/s)
APT Hughes	Weapon	5	10.6	10	CW
AFTS/McDD	Air-ground	100	0.53	100	1 Gb/s
ISL/Ball	Satellite	42,000	0.8	10	360 Mb/s
Comm. System/ Optronics	Ground	0.6	0.8	800	70 Mb/s

3.1 DESIGN APPROACH

The design of a ship-to-ship optical communication system involves many scientific and engineering disciplines. It requires a knowledge of many aspects of the ship/sea environment and the design must consider the needs and operational constraints on naval ships. The optimum design, where cost is a major concern, requires a large number of trade-offs, many of which are beyond the scope of this paper. The empnasis in this paper is on the design of the gimbal control system. This section presents the approach, the requirements and some alternate conceptual designs. Subsequent sections will present detailed analyses of the control, the optical, and the data subsystems.

3.1 Study Emphasis

Previous R&D efforts have demonstrated the ability to perform accurate pointing and tracking in benign environments such as ground based or aircraft-based systems. The pointing jitter measured during these demonstrations has been in the tens of microradians range which is adequate for optical communication. There has been no demonstration of this accuracy in the shipboard, high-amplitude vibration environment. The same R&D efforts have demonstrated high transfer rates over laser links at ranges of hundreds of kilometers. The data rates and ranges have been adequate for the ship-to-ship system. With the exception of short-range, ground-based laser communication systems, the cost of these previous R&D efforts has been in the tens to hundreds of millions of dollars. What has not been demonstrated is the technology to transmit in the high linear and angular vibration environment of an ocean-going ship. Therefore, the emphasis in this study is to develop, in a preliminary design sense, the gimbals, controls, and stabilization systems needed for a low-cost pointing and tracking system.

A conceptual design of the entire optical communication system including the laser and the data transmission subsystem will be developed because the size and weight of these subsystems impact the control subsystem.

For example, the current technology of small, light-weight, easily modulated diode lasers can be used to reduce the weight on gimbals without the complex beam transfer optics for an off-gimbal laser; however, it places certain constraints on the beam width and the allowable jitter resulting from the tracking system.

3.2 Operational Scenarios

Many of the requirements and constraints placed on an optical ship-to-ship system become evident by following the steps that must be performed to establish communication. In the following scenario the ship initiating communication is referred to as the transmitting ship or system. The ship being contacted contains the target which is the aperature of the receiving

system. Once two-way communication is established, both systems will transmit and receive.

3.2.1 Target Acquisition

Before tracking of the receiving system and two-way communication with it can be established, several steps must be executed which are defined here as target acquisition. These steps are:

1) The person or computer responsible for initiating communication will identify the ship to be addressed and its approximate direction;
2) The communication system will perform a search for the target;
3) Detect the target;
4) Establish closed loop tracking of the target; and
5) Receive an answer back from the target system to confirm two-way communication.

The last step is not required in cases where the receiver has no transmitter or does not care to go on the air. Both systems in the communicating pair are identical and each must perform target acquisition. The time required to complete acquisition is an important parameter and will depend upon what is known about the target location. Possible situations are:

1) Approximate location of the receiving ship is known through visual or radar sightings;

2) Several ships need to be contacted and their locations are unknown; however, the order in which they are contacted is not important;

3) One ship of several in the area is to be contacted and its location is unknown.

The communication system processor will have several acquisition algorithms to choose from, based on the input information accompanying the request to initiate a communication link and on the motion of the transmitting ship. The following paragraphs describe the steps listed above.

3.2.2 Initial Inputs to Transmitting System

The identification code of the ship to be addressed is a required input. A desired input is the direction to the ship. This information will reduce the search time. Without initial pointing data, the search may take times on the order of 10 seconds which is acceptable in most situations. An issue is how initial pointing information might be obtained, in what coordinates would it be measured, and how would it be provided to the optical communication system.

Two angular coordinate systems can be used: 1) azimuth and elevation relative to the ship and 2) an inertial system. The relative azimuth and

elevation of the target will change rapidly during maneuvers or rough weather; therefore, if ship-based coordinates are used, the information must be transferred very rapidly. An approximate ship-based azimuth and the fact that the target will be near the horizon can be used to reduce the search time.

The OCS will incorporate an inertial angle system. This is required: (1) to maintain a systematic search pattern while the ship is rolling, (2) to know where the horizon is, and perhaps (3) to provide inputs to the tracking loops if excessive beam jitter is encountered. The types of sensors which were considered were gyros, magnetic compass, artificial horizons or, turn and bank indicators of the type used in light aircraft, and an inexpensive angular rate sensor developed by ATA. Incorporating some combination of sensors of this type in the OCS will permit the system to slew to a given azimuth and elevation measured in an inertial coordinate system.

The OCS should be designed to accept an initial pointing direction in either ship or inertial coordinates and, depending on the accuracy of the information, begin a limited search or go directly to closed loop tracking.

The OCS may be slaved to a remote manual acquisition device through azimuth and elevational position sensors. The manual acquisition device may be binoculars, a telescope, or a simple gun sight. When the operator has the target centered in the optical system, a button is pressed transferring control to the OCS. If the OCS is located within easy reach of the operator, a telescope mounted on top of the case, joy stick control on the gimbals, and a button to turn control over to the tracking system provide a convenient acquisition means under good viewing conditions.

3.2.3 Target Search

The system computer will contain one or more search patterns which will send the appropriate commands to the fast steering mirror and gimbals. The pattern could be a spiral which begins at the estimated target positions and moves outward. The maximum spiral frequency will be limited by the fast steering mirrors to approximately 300 Hz. The radial advance per cycle is approximately one beam width. The transmitter has a defocus capability; therefore, the radial advance could range from 30 ur using the narrowest beam to 1 mr, which has sufficient beam energy density that can detect the retro-reflector. A linear search along the horizon would reduce the acquisition time, under some circumstances. Figure 3-1 and figure 3-2 illustrate several search patterns.

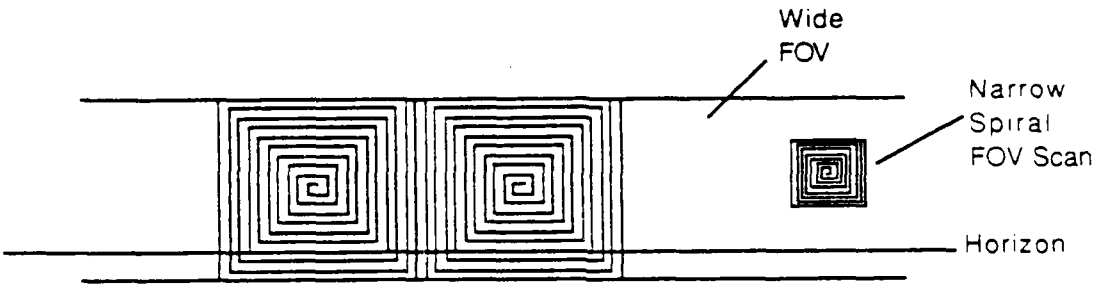

Figure 3-1 Spiral Scan

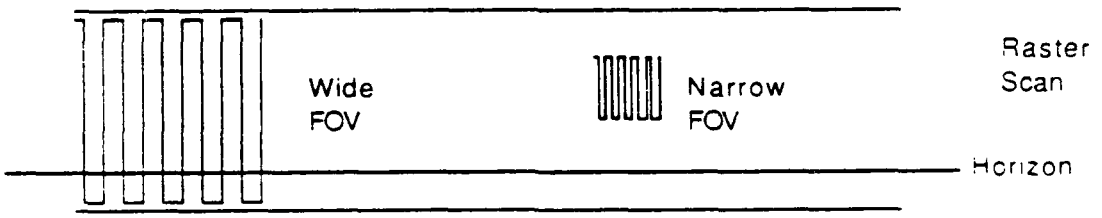

Figure 3-2 Raster Scan

3.2.2 Target Detection

A return above a given threshold will be interpreted by the system as the target. The target of interest is the retro-reflector on the receiving system. The system will occasionally receive false alarms from other parts of the receiving ship's structure and possibly from the sea surface. The ratio of the signal from the retro-reflector to the detector noise is high enough that the probability of false alarms resulting from detector noise is very small. The probability of false alarms from other sources will be investigated during Phase II. Because each return above a threshold will be considered automatically by the system for tracking, the number of false alarms must be kept very low so as not to overwhelm the system. This system, as do most detection systems, will have a threshold adjustment which can be changed by the operator.

3.2.3 Tracking

Each time a return is detected, the system will go into a tracking mode and analyze the position of that return and establish that it is a persistent return. The return from a retro-reflector could be modulated by the receiving ship to indicate its ID, thereby confirming acquisition of the desired receiver.

A search pattern for use when track is momentarily broken would be available: in this case, the system would immediately go to a spiral scan in which the beam is spiraled above the position of last contact with the receiving system. An alternative approach is that the receiving ship could come on the air and identify itself with its laser. Each system would have a repertoire of search patterns and the amount of beam defocus available to the operator. By experience, the operator would select the appropriate pattern for the situation at hand. The parameters the operator would use to select search patterns are: 1) the uncertainty of the position of the receiving system to be contacted; 2) the motion of the ships; 3) a threshold which would be set depending on the number of false returns expected.

The construction of the system could be a shared aperture system as described in the summary of a two-aperture system in which the transmitting aperture and receiving aperture are on the same gimbal but are separate.

Acquisition mode is completed when more than one return above threshold is received at a particular location or if the unique ID of the receiving system is detected. The system then transfers to the track mode. The method of closing the track loop depends on the type of system involved. Two choices are possible: 1) a singular frequency system in which both the two communicating systems are on the same wavelength: a protocol would be established to interweave the transmitting and receiving functions while maintaining track. 2) Using two frequencies, one for each communicating system, the systems could transmit simultaneously and use the incoming signal from the opposite system as the tracking signal.

Data Transfer

Once track is established, data transfer could begin immediately. The bit rate for data transfer would be in the 10-100 megahertz range. The tracking loop would be in the kilohertz range; therefore, the data bits superimposed on the signal would be invisible to the tracking circuitry.

3.3 Requirements

Requirements for the conceptual system designed in this paper reflect the goal of the program, which is that a low-cost system be developed which can track while subjected to the large amplitude motion of ships. The field-of-regard of the system will be 360° in azimuth and 45° in elevation. The laser must be an off-the-shelf, inexpensive device that will handle up to 100 megabits per second. The maximum range that can be expected of such a system is about 15 kilometers which is limited by the curvature of the earth. The system will be designed to communicate under atmospheric conditions up to 15 kilometers.

3.3.1 Identification of Lower Level Constraints

ATA derived the following list of lower-level subsystem requirements and constraints:

1) Pointer/tracker azimuth/elevation coverage;
2) Maximum gimbal slew rate;
3) Maximum search/acquisition time;
4) Minimum information capacity of the system;
5) Maximum error rate of the system;
6) Bandwidth of disturbance rejection loops;
7) Maximum aperture size;
8) Budgets for volumes, weights, power.

These lower-level subsystem requirements and constraints were essential ingredients in the process of selecting the evaluation criteria to identify the optimum overall communication system.

3.3.2 Pointer/Tracker Azimuth/Elevation Coverage

Based on calculations of maximum sea conditions, a gimbal coverage of 45 degrees should be sufficient.

The need to achieve maximum range, maximum protection from sea water, and 360° field-of-regard suggests an installation as high above the water line as possible. The desire for minimum linear and angular motion, requires an installation on a rigid structure. The desirability of short communication paths for high data rate signals suggests a location near the communication center. This latter location is probably a reasonable trade-off between the competing requirements. The need for 360° field-of-communication would tend to place the unit on top of the bridge, for example. Two systems may be required on a ship to give a full 360° field-of-view. The need to maintain the unit would also place it in a relatively accessible location. A size and weight that can be managed by a single person, and that would fit through a

nation are desirable. The electronic and optical components would be contained in an air-tight unit to prevent deterioration of the [illegible] equipment.

3.- Conceptual Design

The work described here did not attempt to design an optimum system in complete detail. A candidate design was established in sufficient detail that the control system and gimbals could be designed and their performance estimated. Alternative designs for various subsystems are suggested at several points. In order to illustrate that current technology does allow variations which might be needed to overcome certain difficulties. This section discusses the candidate design first, and then possible alternatives are suggested. The candidate design is a single shared-aperture system. The optical systems, the optical component and much of the electronics are contained in a single, air-tight, cylindrical structure. The only optical component exposed to the elements is the exit window. The pointing controls consist of a coarse azimuth drive that rotates the sealed unit and a coarse elevation mirror which is enclosed in the sealed unit. The fine tracking is accomplished by a two-axis mirror.

The major elements of the pointing and tracking subsystem for which components, materials, and technologies were identified are:

1) Gimbal sets, including actuators;
2) Fixed and steered optical elements;
3) Tracking electronics;
4) Digital control electronics;
5) A tracking illuminator or beacon (optional).

ATA has developed the following design as being the most practical for the low-cost ship-to-ship optical communication system (see Figure 3-3).

The top of the system rotates, while the bottom part is attached to the base with isolation built into it to prevent transmission of vibrations of low-frequency motion caused by the waves and ship. A 15-centimeter telescope is used. The shared aperture is also time shared. The whole azimuth housing turns and is driven by a motor. The bottom part is fixed and does not need to turn. This design also uses an optical window. It is possible to spoil the beam during acquisition and then to narrow it during tracking. The glass has a secondary glued to it.

ATA calculated the worst roll would be plus or minus 40 degrees, with a pitch of plus or minus 10 degrees. Therefore, we used plus or minus 45 degrees in this design.

ATA believes that the shared aperture system in this design, which eliminates the redundancies, volume, weight and power penalties of a separate aperture system, is another key element in achieving a cost effective ship-to-ship optical communication system. Even though additional optical complexity, such as beam splitters and optical filters, are some of the penalties associated with a shared aperture system, they are more than offset by the reduced inertia of the shared aperture system. Reduced inertia allows the shared aperture gimbal set to be fabricated with lighter materials and still have the

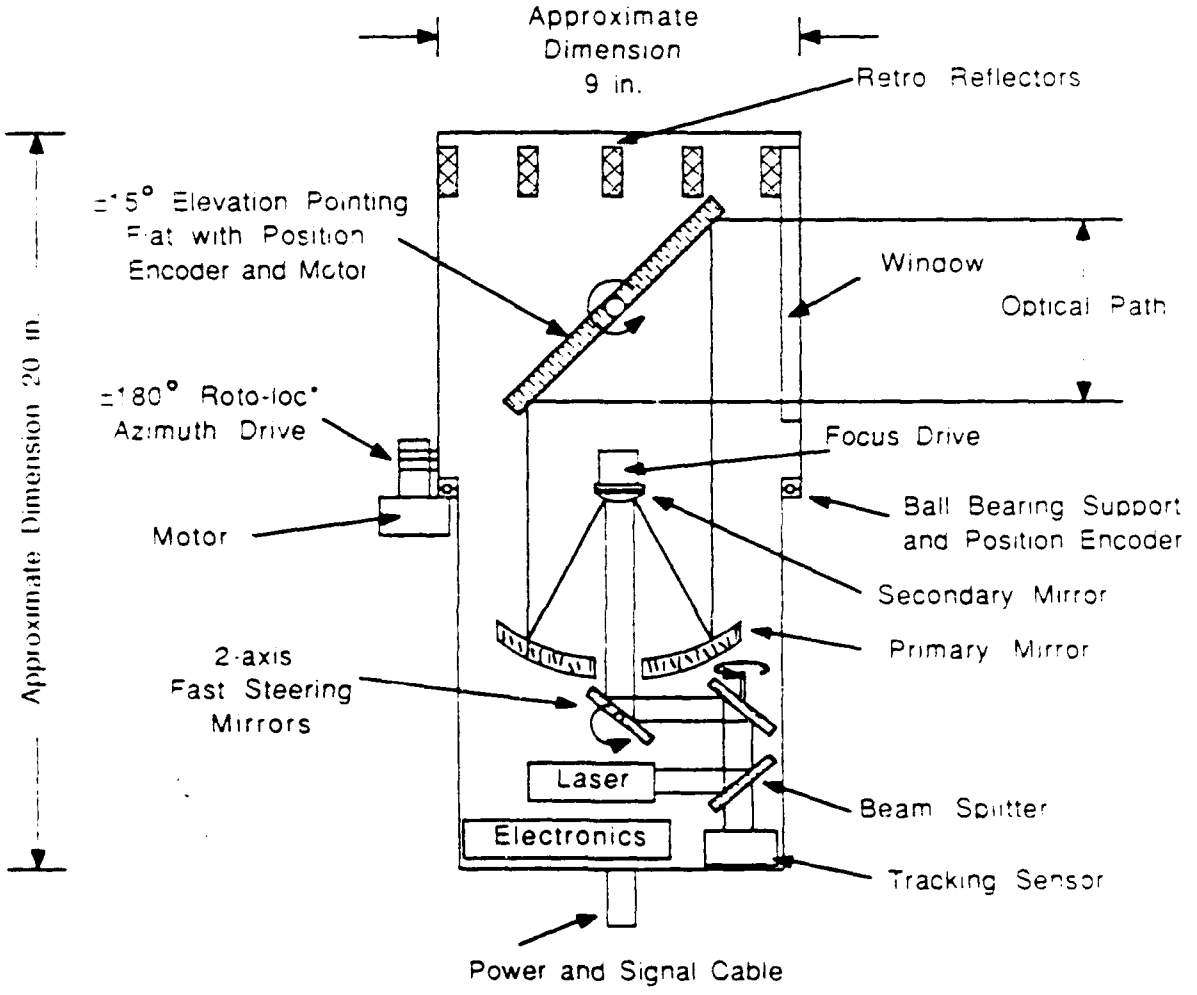

Figure 3-3 Schematic of an Optical Communication System

required structural stability under dynamic load. Use of lighter materials for the gimbals, such as composites and plastics, results in lower cost.

Figure 3-4 shows a schematic of a two-optical path system.

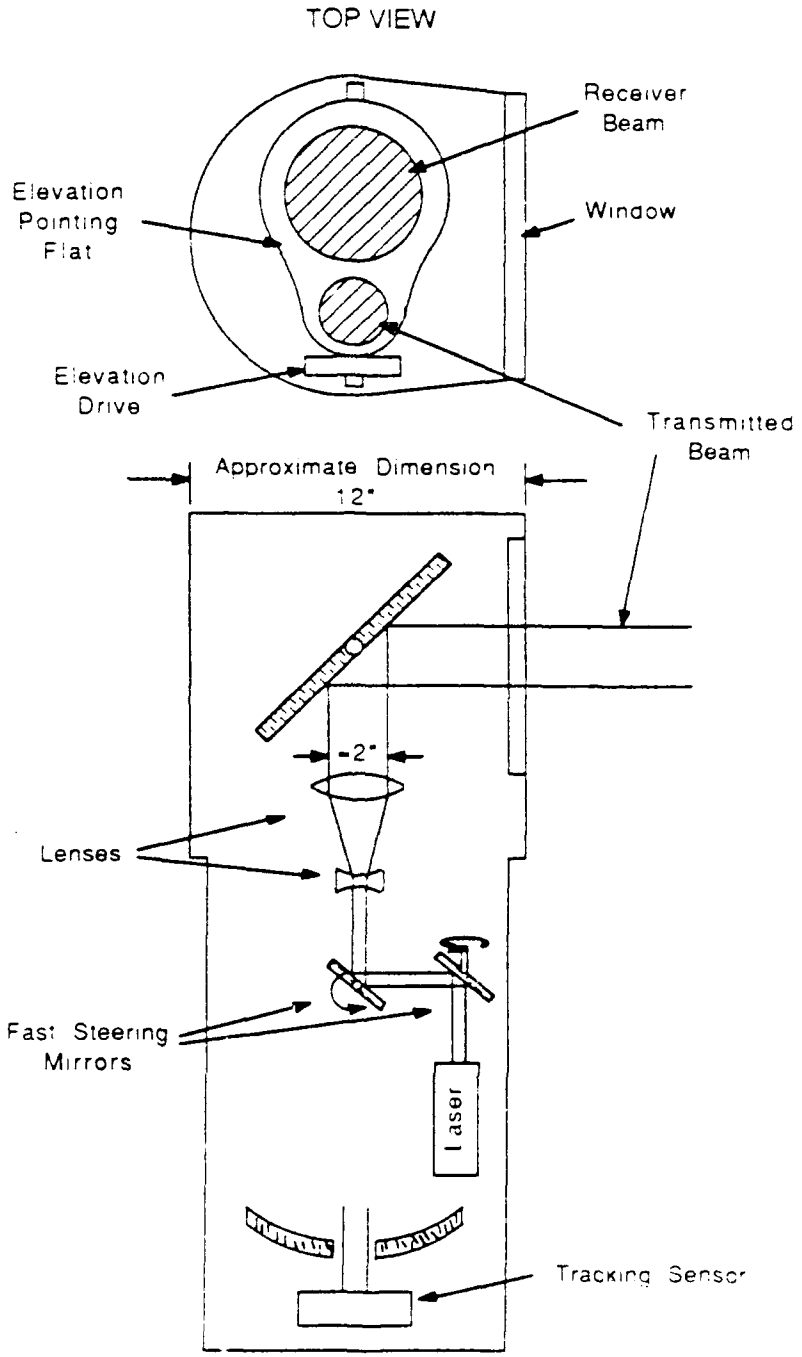

Figure 3-4 Schematic of a Two Optical Path and a shared aperture System (Showing Transmitted Beam Path).

4.0 CONTROL SYSTEMS

4.1 Definition of Requirements and Constraints

The definition of requirements and constraints is the most critical element in the identification of the optimum system for low-cost ship-to-ship optical communication. ATA has identified these constraints in a two-level process that starts with top-level requirements and then derives lower-level subsystem constraints.

4.1.1 Identification of Top-Level Requirements and Constraints

ATA started by identifying the following top-level requirements and constraints:

1) Maximum/minimum distance between ships;
2) Maximum relative motion between ships, worst-case sea state;
3) Worst-case pitch/roll;
4) Worst-case base disturbance spectra;
5) Worst-case propagation medium characteristics;
6) Type/quantity of information to be transferred;
7) Maximum transfer time;
8) Maximum volumes, weights, power.

The above constraints were then quantified with figures and ranges, and are described in the following subparagraphs.

4.1.1.1 Maximum/Minimum Distance Between Ships

ATA is designing its system for a maximum range of 15 kilometers and a minimum range of 0.3 kilometers. Major considerations include maintaining line-of-sight between the two ships while accounting for the earth's curvature and degraded optical path. Considerations at short range include adequate slew rate and gimbal angle coverage in worst case sea state.

4.1.1.2 Maximum Relative Motion Between Ships, Worst Case Sea State

One can place an upper bound on relative motion between ships by estimating each ship's maximum heave and pitch response to heavy seas. Dynamics of Marine Vehicles, by Rameswar Bhattacharyya presents the pertinent data as a function of sea state and Beaufort wind force. Table 4-1 presents typical values.

The ship's response to waves sets the low frequency inputs and bounds. To estimate the relative motion of ships in these seas, the ship's heave, pitch, and roll response to these amplitudes must also be known.

Table 4-1. Wave Characteristics

Sea State	Wind Force	Wind Velocity (kt)	Significant Wave Height (ft)	Average Period (sec)	Average Wavelength (ft)
1	2	5	0.5	1.3	6.7
1	3	8.5	1.3	2.3	20
2	3	10	1.8	2.7	27
2	4	13.5	3.3	3.6	52
3	4	16	4.7	4.3	71
4	5	19	6.6	5.1	99
5	5	20	7.3	5.4	111
5	6	24	10.5	6.4	160
6	6	26	12.3	7.0	188
6	7	28	14.3	7.5	212
7	7	32	18.6	8.6	285
7	8	36	23.6	9.6	363
7	3	40	29.1	10.7	444
8	9	44	35.2	11.8	534
8	10	50	45.5	13.4	700
8	10	54	52.1	14.5	810

"Ship Relative Motions and Related Phenomena" by M.F. Van Shijis presents results of experiments of the heave and pitch response of a ship and showed a strong dependency on Froude number ($F_n = V/\sqrt{gl}$) and the ratio of ship length to wavelength. The worst case response presented was at a Froude number of 0.5 and a ship length that was half the wavelength. As shown in Table 4-1, in high seas the wavelengths can be very long (400 to 800 feet). Some destroyers, frigates, and submarines are around 400 feet long, but would have to be making 30 knots to achieve this Froude number. Since this is unlikely in such high seas, a more realistic estimate would be that the relative ship heave would be equal to three-quarters of the wave height which corresponds to a Froude number of 0.3 and a length-to-wavelength ratio of 0.5.

Using this factor, the worst case pointing-and-tracking requirements occur when the ships are $\frac{2n+1}{2}$ waves apart. For most ships, n must be greater than one since ship separation will likely be at least two ship lengths, particularly in rough seas. Accordingly, for this calculation minimum separation of 1000 feet (0.300 km) is assumed required. Table 4-2 presents the elevation angle coverage for the two worse rough sea conditions.

Table 4-2. Relative Displacement Induced Angle

Significant Wave Height (ft)	Wavelength (ft)	Heave (ft)	Separation (ft)	Angle°
53.1	810	40	1215	1.9°
45.5	700	34	1050	1.9°
35.2	534	26	1335	1.1°
29.1	444	22	1110	1.1°
23.6	363	18	1270	0.8°
18.6	285	14	1000	0.8°

For an angular pointing system, the pitch and roll of the ships must also be considered since these can be significantly larger than the relative displacement. From the Van Shijis' book, we see a maximum pitch response of $\theta = 1.25(360)/\lambda$ at $L/\lambda = 0.65$ at a Froude number of 0.5. In Table 4-3, for the sea states previously analyzed, we find the following pitch response for a 400-foot ship at a Froude number of 0.3 (17 kt):

Table 4-3. Pitch Characteristics

Significant Wave Height (ft)	Wavelength (λ) (ft)	Pitch $\theta/K\xi a = 1$	Pitch (Degrees)
53.1	810	11.8	13.3
45.5	700	11.7	13.2
35.2	534	11.9	11.3
29.1	444	11.8	6.5
23.6	363	11.7	5.3
18.6	285	11.7	1.2

Since the maximum pitch would occur in a different part of the wave than maximum relative displacement, the two effects cannot be added. The maximum combined effect would be where one ship is pitched down and the other is at the top of a wave. This would occur when the ship was $\frac{4n+3}{4}$ wavelengths apart. The worst case for the 53-foot waves would result in a 14.4 degree look angle. To estimate roll motion a typical roll response to a wave was simulated (see Section 4.1.1.4) and the response to the 53-foot wave was calculated. This resulted in an estimated RMS roll motion of 8.7°. If we assume a Gaussian distribution, one can say that 90% of the time the roll would be less than $\pm 26°$ (3σ). If one wanted to include 99% of the occurrances, the limit would be $\pm 43°$. Based on these calculations, plus input from operational Navy personnel, the gimbal limits for the pointing system will be $\pm 45°$, driven primarily by roll.

4.1.1.3. Worst-Case Pitch/Roll, Worst-Case Sea State

ATA is using values which allow up to plus or minus 45 degrees of pitch and roll. Yaw motion is minimal and azimuth requirements drive the outer gimbal. Wave periods of up to 10-15 seconds are fairly typical.

4.1.1.4. Worst-Case Base Disturbance Spectra

Perhaps the most widely accepted spectra of wave motion is the Pierson-Moskowitz spectrum from D. Hoffman's paper "Analysis of Measured and Calculated Spectra", of the form:

$$S(w) = \frac{H_{1/3}^2}{4\pi} \left(\frac{2\pi}{T_2}\right)^4 \omega^{-5} \exp\left[-\frac{\left(\frac{2\pi}{T_2}\right)^4 \omega^{-4}}{\pi}\right]$$

where: $H_{1/3}$ is the significant wave height in feet

T_2 is the average apparent period in seconds

$S(\omega)$ is the wave energy spectrum in $ft^2/(rad/sec)$

ω is the frequency in radians/second.

The Hoffman paper compares this analytic form with many measured spectra and shows general agreement. Figure 4-1 shows this spectra, plotted logrithmically, using the same values of $H_{1/3}$ and T_2 as were used in the Hoffman paper. Figure 4-2 presents the wave spectra for the worst case wave we have previously considered with $H_{1/3}$ = 53.1 feet and T_2 = 14.5 seconds.

The Bhattacharvya book presents analytical methods for constructing the resulting pitch and roll motion from wave amplitude spectra. There are two effects: (1) the natural frequency response of the ship and (2) the exciting moment for the ship, which is a function of the ship design and the wavelength-to-ship length or wavelength-to-ship width ratio.

The angular frequency response of a ship to an applied moment is an underdamped second-order response. Table 4.9 in the Bhattacharvya book gives typical values of the pitching time constants. These range from 4.4 seconds for a 500-foot destroyer to 9.0 seconds for a 1,040 foot aircraft carrier. This would correspond to a natural pitching frequency of between 0.7 and 1.3 radians/second with the higher frequency corresponding to the smaller vessel. For roll, Bhattacharvya states that roll periods are typically twice as large as pitch and gives typical values ranging from 9 seconds for a destroyer to 17 seconds for a battleship. Furthermore, Bhattacharvya states that the roll damping coefficient is very small and "the magnification factor may reach a value between 5 and 10."

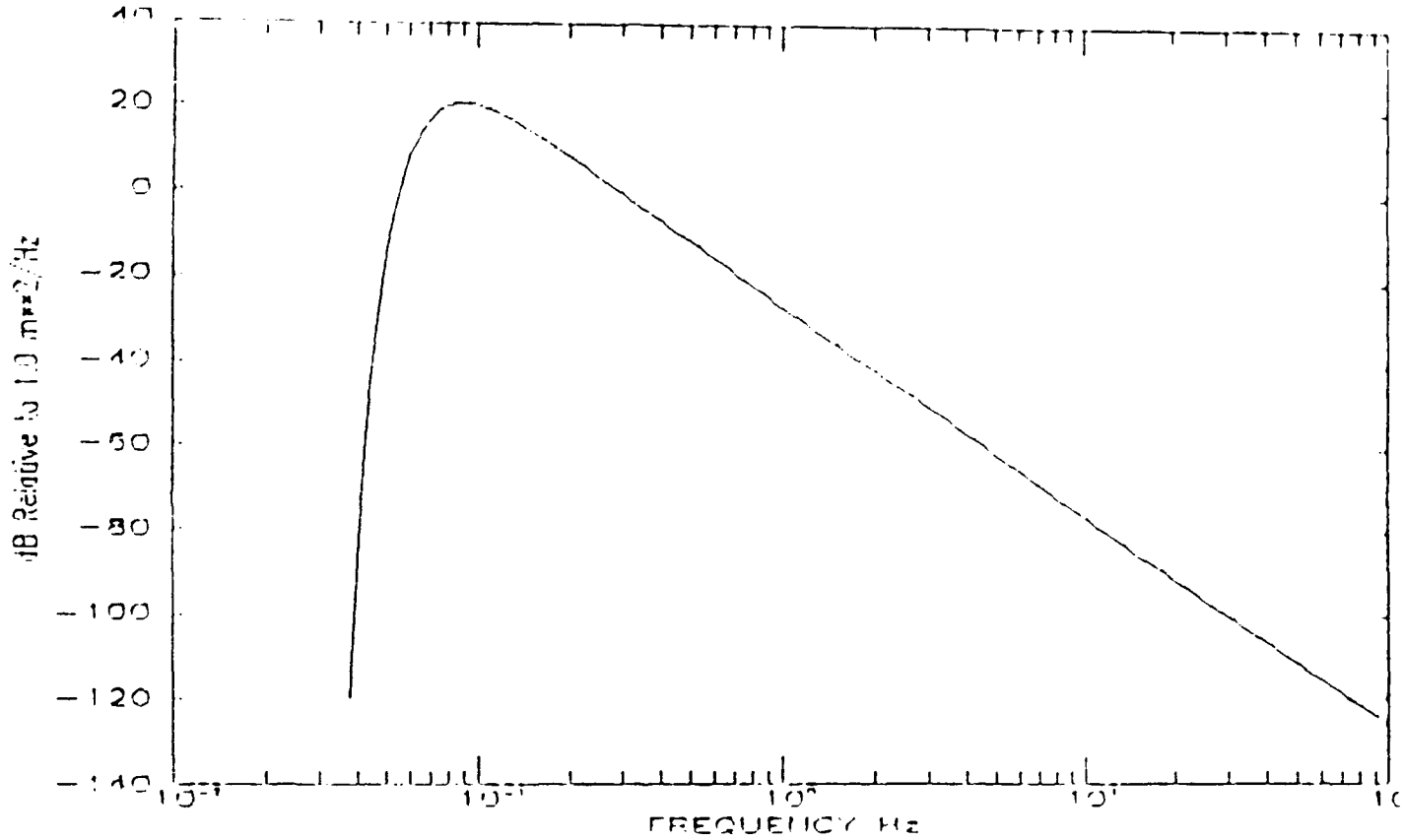

Figure 4-1. Wave Motion PSD [illegible]

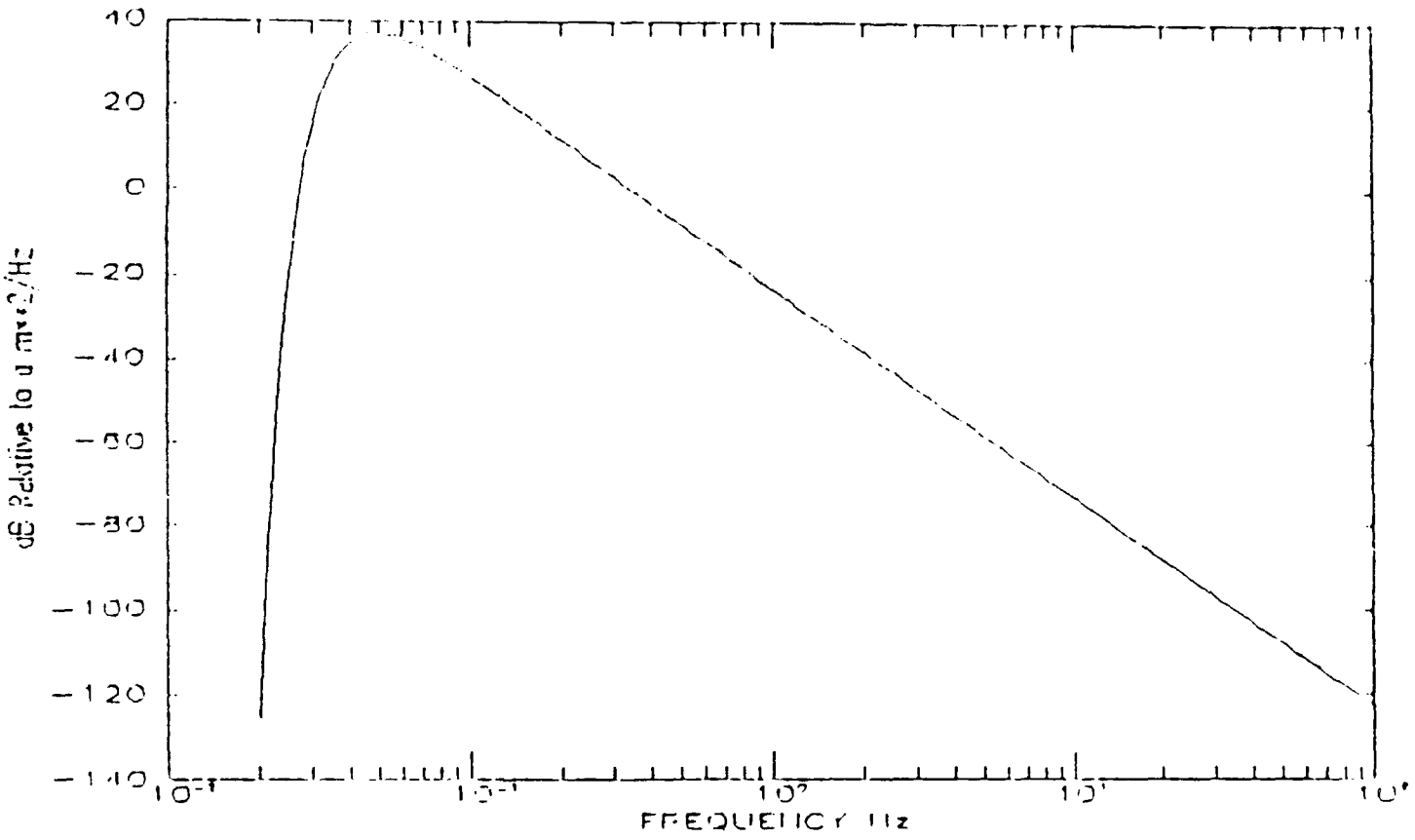

Figure 4-2. Wave Motion PSD T1(1.2)=53.1 T2=14.5
(Spectral Character of Extreme Case Wave Motion)

The other factor is how the pitching moment is related to the waves. The Bhattacharvya book shows that this pitching moment can be calculated by:

$$M_\theta = \rho g \int_{-L/2}^{L/2} 2y(x)\xi(x)dx$$

where: ρ = density of water
g = gravitational acceleration
$y(x)$ = location of the ship's hull in the vertical direction
$\xi(x)$ = wave amplitude as a function of horizontal ship station.

The Bhattacharvya book plots this as a function of the ratio of the wavelength to the length of the ship. As shown in this reference, this function falls off very rapidly where the wavelength is shorter than the ship's length. The Van Shijis' paper depicts the measured combined effects of both of these phenomenon for a scaled ship. This ship had a natural pitch period of 0.783 seconds which corresponds to a natural frequency of 8 rad/sec. However, the experiment was scaled so that this corresponded correctly to the dynamic response of a large vessel. Figure 4-3 shows the response of the vehicle in pitch versus the ratio of the ship length to the wavelength. Notice the sharp dropoff at $L/\lambda = 1.0$. By fitting a straight line to the data, this falloff goes like $(L/\lambda)^{-6}$. Since the circular frequency, ω, is related to the wavelength by $\omega = V/\lambda = \frac{2\pi}{T}$ where V is the velocity of the wave in the water, we can scale this by using the approximate wave velocity at a given sea condition. For the 53.1 foot wave condition, this velocity is approximately 350 feet/second. The ratio plotted in Figure 4-3 is $\theta a/k\xi a$. If we model the high frequency behavior of this ratio as a falling off by $(L/\lambda)^{-6}$, beginning at $(L/\lambda) = 1$, one can show that:

$$\frac{\theta a}{\xi a} = \frac{2\pi}{L^6}\lambda^5$$

By relating this to the circular frequency, ω, using the wave velocity relationship above, one finds that:

$$\frac{\theta a}{\xi a} = \frac{(2\pi V^5)}{L^6}\frac{1}{\omega^5}\ \frac{rad}{ft}$$

Using values from above, one has a high frequency behavior of:

$$\frac{\theta a}{\xi a} \simeq \frac{8}{\omega^7}\ \frac{mrad}{ft} \quad \text{in the region where} \quad L > \lambda.$$

Below that region $\frac{\theta a}{\xi a} = \frac{2\pi}{\lambda} = \frac{2\pi}{V}\omega = 18\omega\ \frac{mrad}{ft}$.

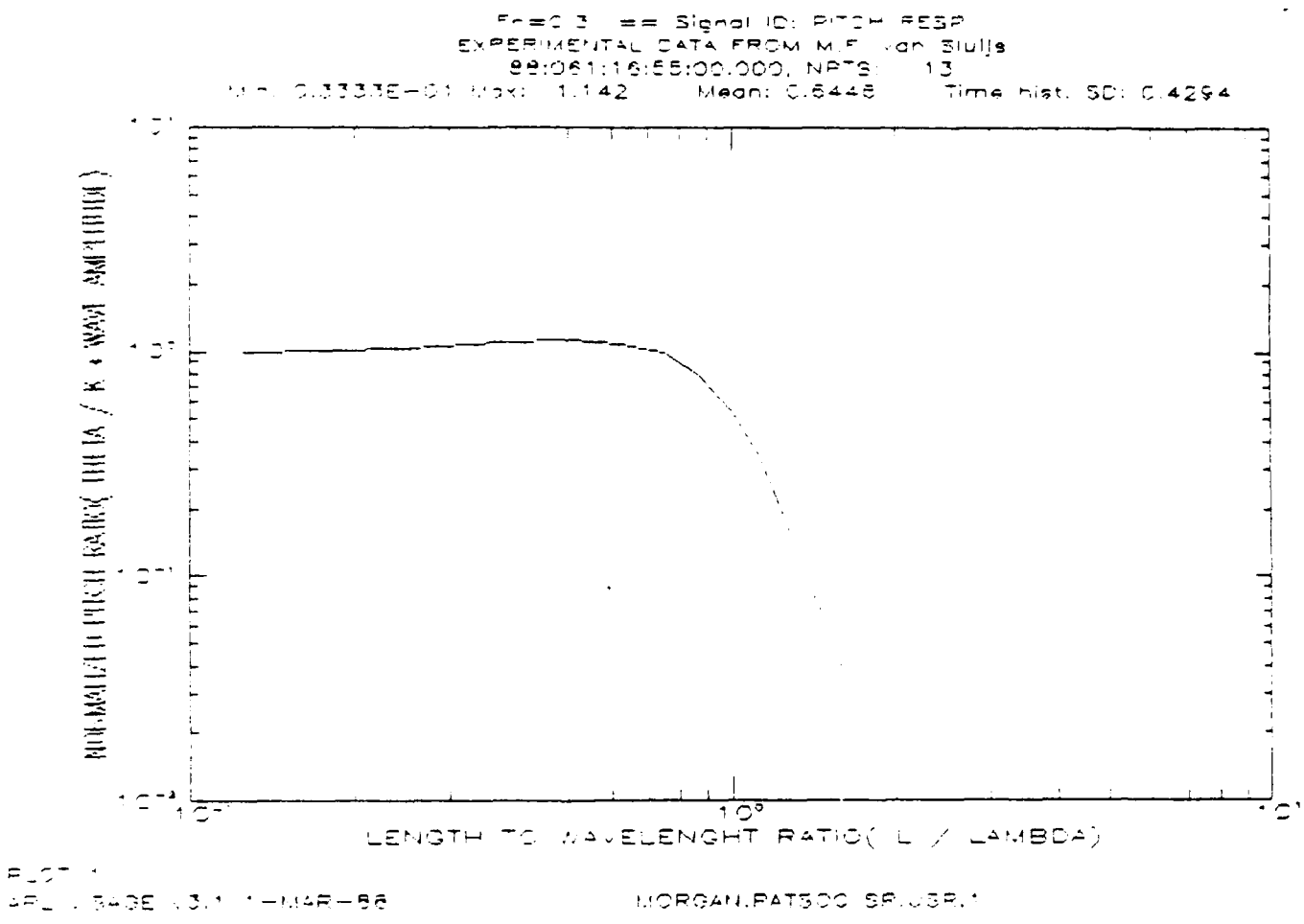

Figure 4-3. Response of the Vehicle in Pitch versus Ratio of Ship Length to Wave Length.

Using these two relationships, one can show that $L/\lambda = 1$ corresponds to $\omega = 0.90$ rad/sec for our 400-foot ship. To construct a frequency domain model of this response, it is assumed that the denominator can be approximated by three second-order systems with natural frequencies ω_1, ω_2, ω_3, and damping ratios ξ_1, ξ_2, and ξ_3. One of the natural frequencies, ω_1, will correspond to the natural pitching motion of a small ship, such as a destroyer. For this case $\omega_1 = 1.3$ rad/sec and we assume a damping ratio of $\xi_1 = 0.5$. For a Froude number of 0.3, there is a peak of about 14% at $L/\lambda = 0.5$. This would correspond to a damping ratio of $\xi_2 = 0.5$ and a natural frequency of $\omega_2 = 0.64$ rad/sec. The third natural frequency, ω_3, is set to that corresponding to $L/\lambda = 1$ which is $\omega_3 = 0.90$ rad/sec. The damping ratio was selected so that the normalized pitch response would have a unity gain at this frequency. This results in $\xi_3 = 0.60$. The resulting analytic frequency response is shown in Figure 4-4, which appears very similar to Figure 4-3. The analytic expression for this function is:

$$\frac{\theta}{K\xi a} = \frac{\omega_1^2\omega_2^2\omega_3^2}{(S^2+2\xi_1\omega_1 S+\omega_1^2)(S^2+2\xi_2\omega_2 S+\omega_2^2)(S^2+2\xi_3\omega_3 S+\omega_3^2)}$$

moving $K = 2\pi/\lambda = (\frac{2\pi}{V})\,\omega$ on the right side of the equation, one has:

$$\frac{\theta}{\xi a} = \frac{(0.018)(\omega_1^2\omega_2^2\omega_3^2)S}{(S^2+2\xi_1\omega_1 S+\omega_1^2)(S^2+2\xi_2\omega_2 S+\omega_2^2)(S^2+2\xi_3\omega_3 s+\omega_3^2)} \quad \frac{\text{rad}}{\text{ft}} .$$

This last response function is calculated and plotted in Figure 4-5. When this response is subjected to the wave spectra shown in Figure 4-2, the resulting base motion spectrum is as shown in Figure 4-6.

A similar process was followed to estimate the roll spectrum. In this case, the natural rolling motion of frequency was adjusted to be half that for pitch ($\omega_1 = 0.65$ rad/sec) and the damping ratio (ξ_1) was adjusted to be 0.05, which corresponds to an amplification factor of 10. The other two frequencies were adjusted for the difference between the rolling moment coefficient and the pitching moment coefficient. There was no data given in the Van Shijis' paper, therefore we assumed we could substitute the width of the ship (assumed to be 55 feet) for the previously assumed 400-foot length. This resulted in shifting ω_2 and ω_3 to 4.65 and 6.55 rad/sec respectively.

Figure 4-7 shows the roll response due to wave amplitude and Figure 4-8 depicts the resulting roll spectrum on the deck of a 55-foot wide ship.

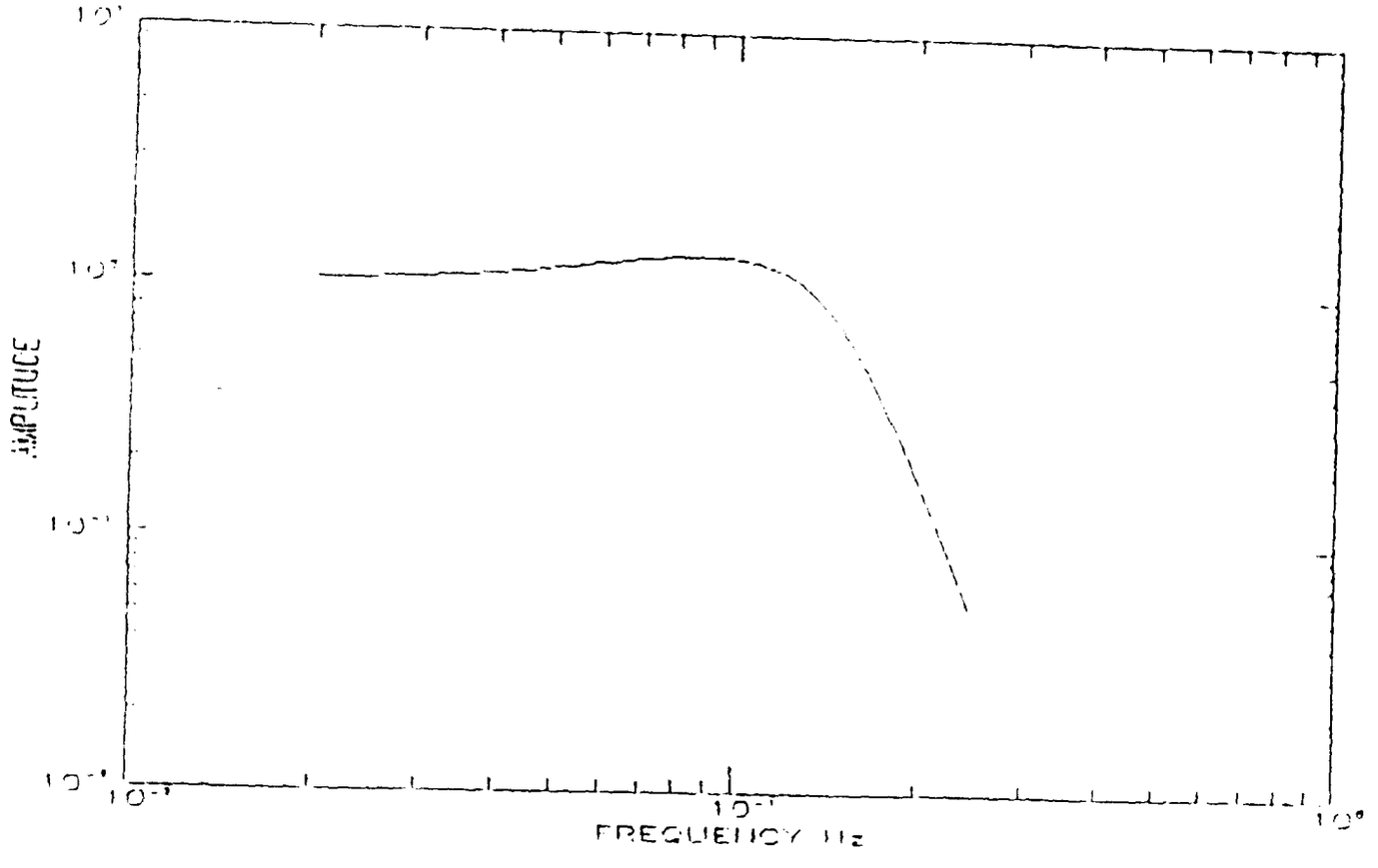

Figure 4-4. Amplitude Response Normalized Pitch.

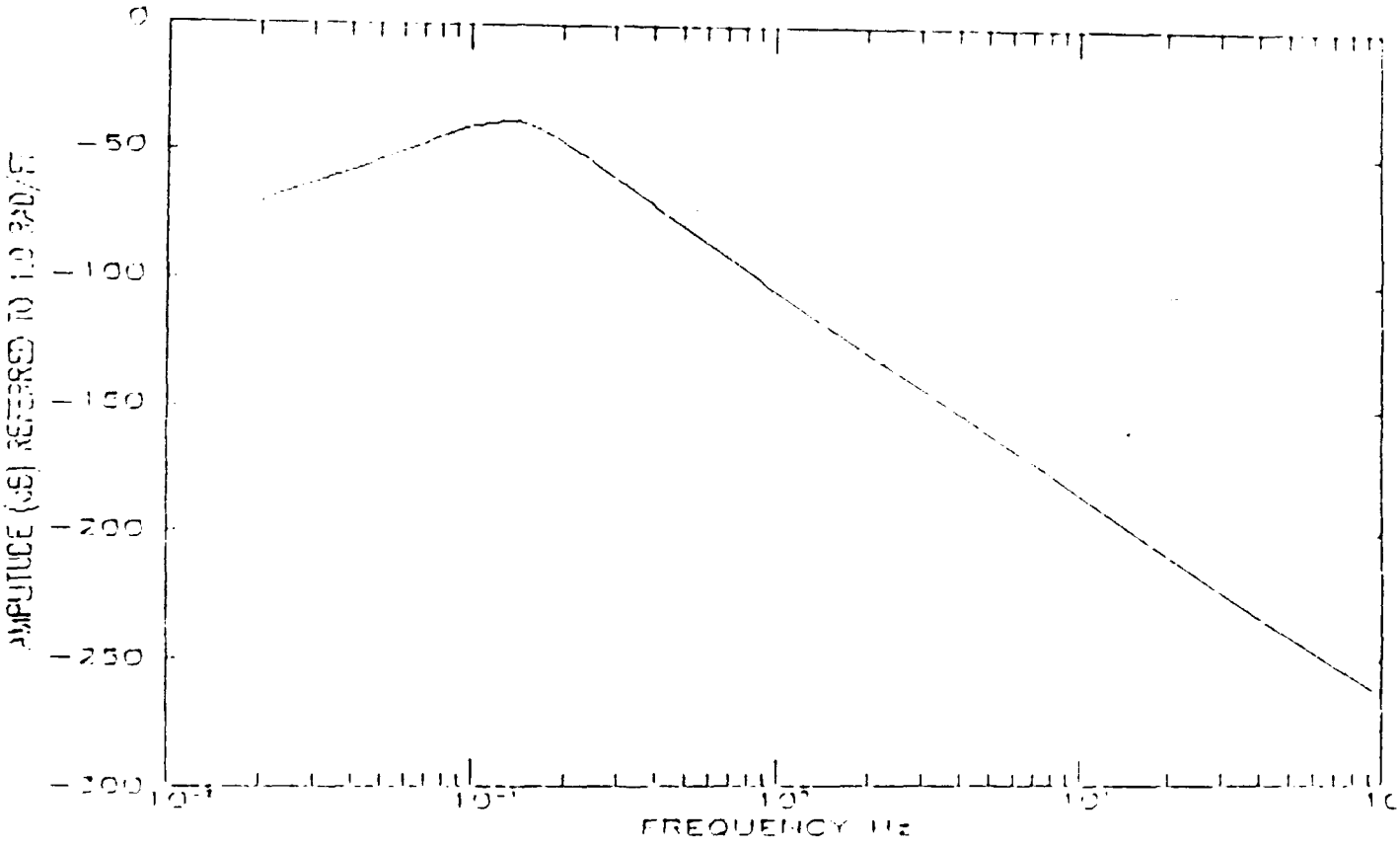

Figure 4-5. Pitch Response 400 ft. Ship, 51.1 ft. Waves.

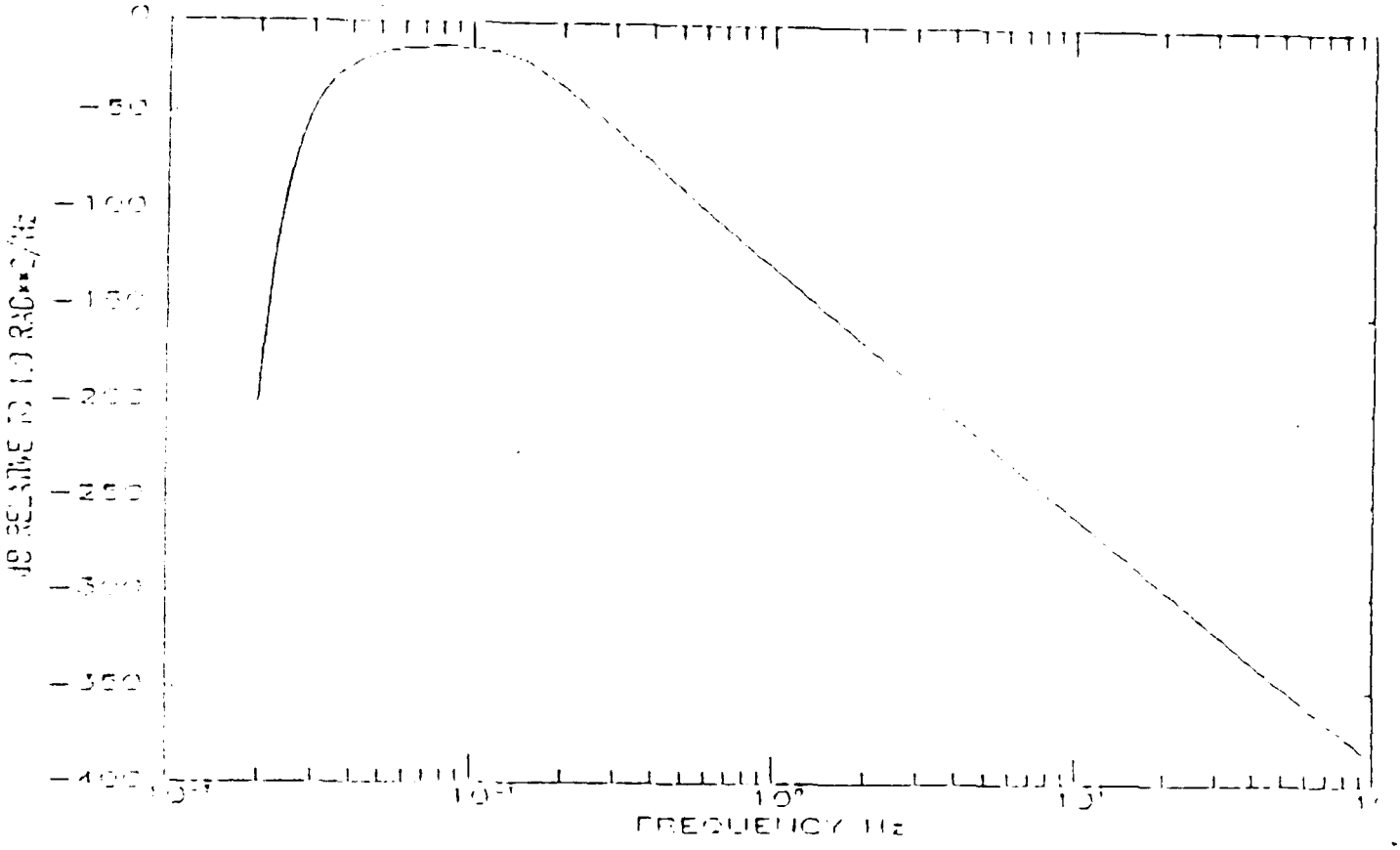

Figure 4-6. Pitch Disturbance Spectrum due to Wave Motion.

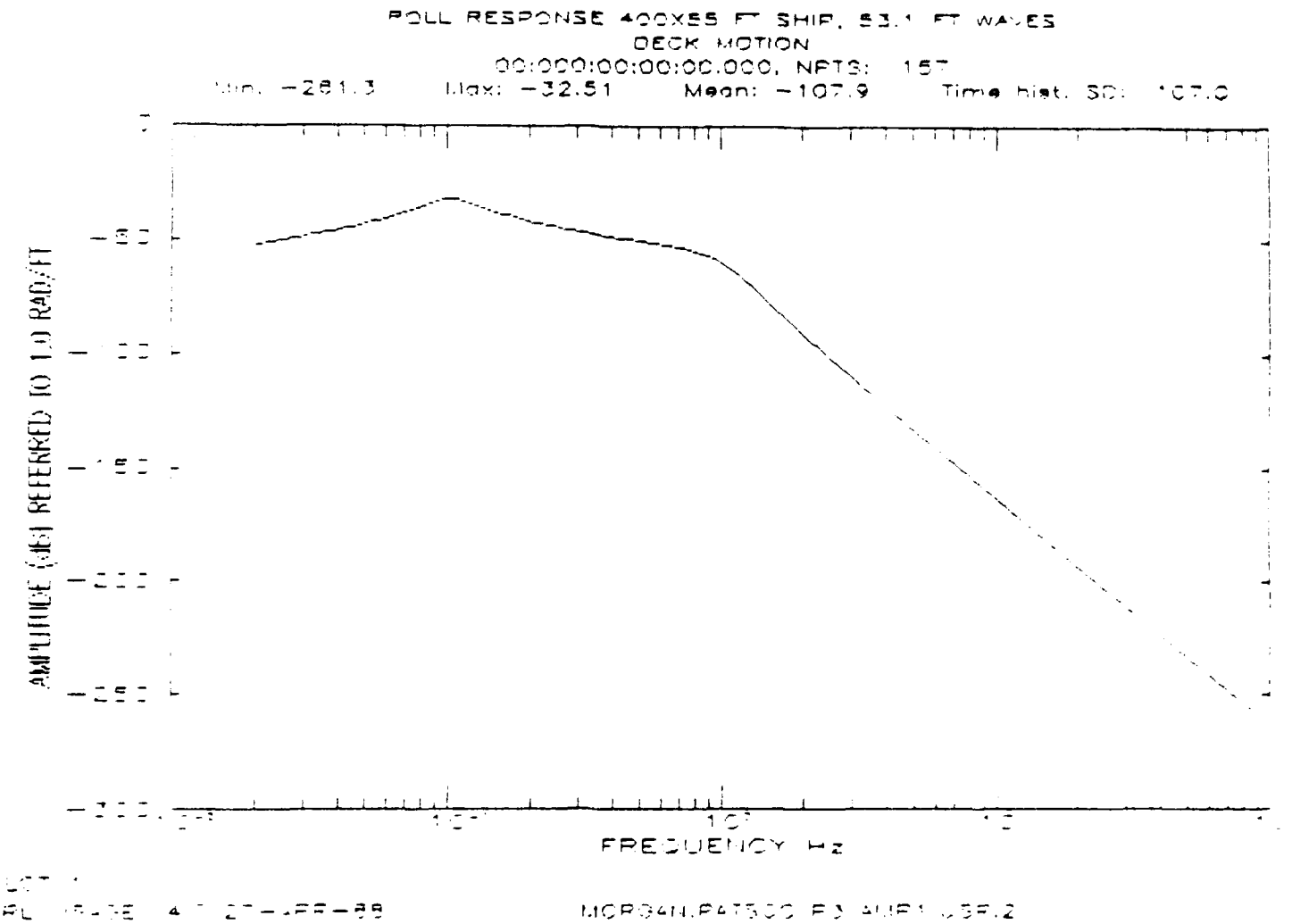

Figure 4-7. Roll Response 400 x 55 Ft. Ship, 53.1 Ft Waves

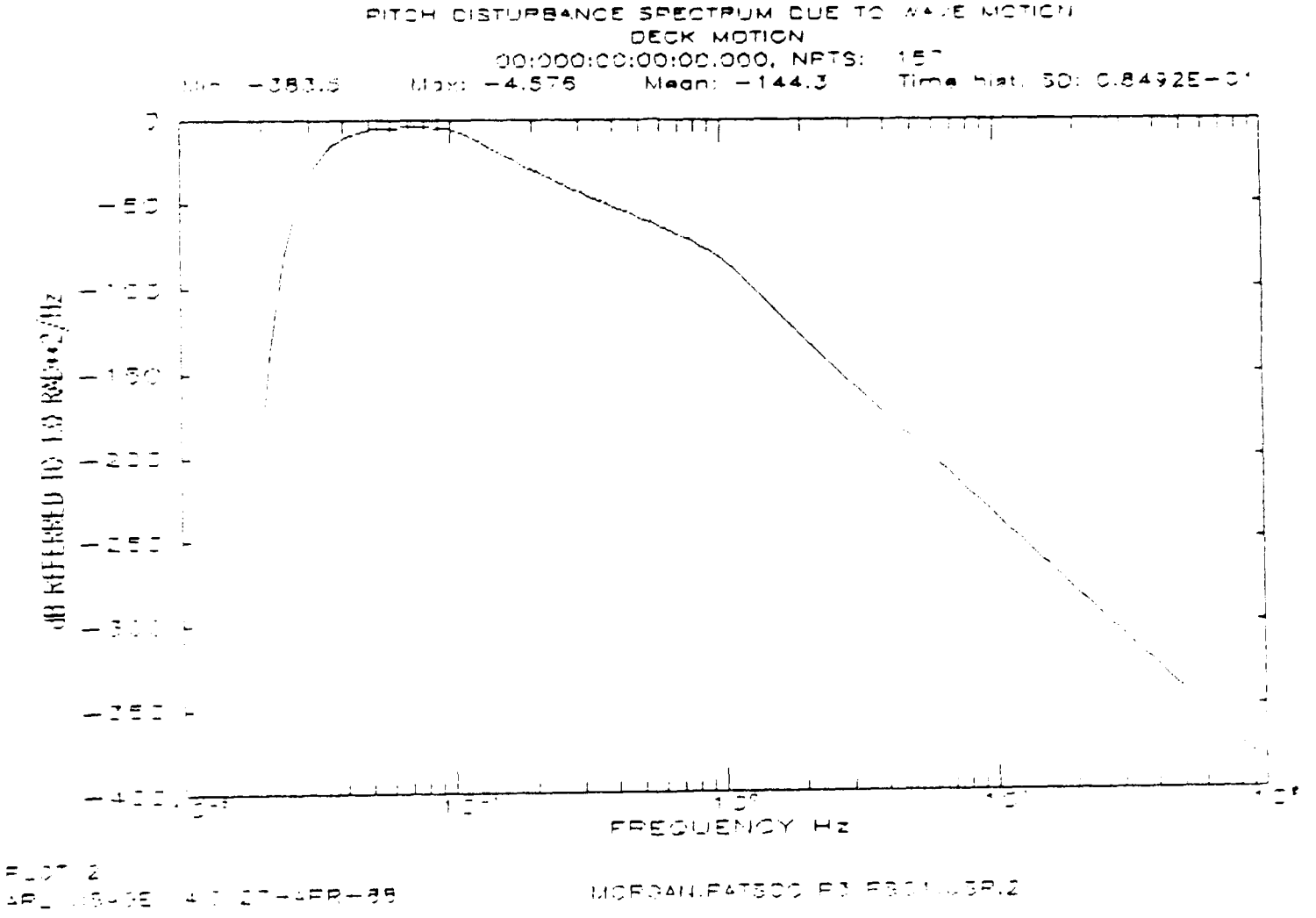

Figure 4-8. Roll Disturbance Spectrum due to Wave Motion

4.1.1.5 Calculation of LOS Disturbance

The system must also remove the relative motion of the two ships due to their individual heaving motions. The angle between the two can be calculated approximately as:

$$\theta_{LOS} = \frac{Z_2 - Z_1}{R}$$

where Z_2, Z_1, are the vertical displacements of two ships and R is the separation distance. If the motions were uncorrelated, one could calculate the PSD of the angular motion by adding the two displacement spectra and then dividing by R^2. However, in this case the motion is correlated at short distances, therefore we can bound the problem by calculating the angle spectrum as:

$$\Phi_{LOS}(\omega) = \frac{4\Phi_z(\omega)}{R^2} .$$

Again, we must compute the effective frequency response of the ship related to the circular frequency, ω. For a Froude number of 0.3, the normalized heave response is 0.7 at $L/\lambda = 1.0$. Accordingly, for the heave response, we will assign $\omega_1 = (0.75)(0.90)$ at 0.68 R/sec and $\xi_1 = 0.7$. We will maintain $\omega_3 = 1.3$ R/sec with $\xi_3 = 0.5$. To achieve a response of 0.57 at $\omega_2 = 0.90$, requires $\xi_2 = 0.5$. Therefore, the heave response has the following frequency responses:

$$\frac{Z}{\xi_a} = \frac{(\omega_1^2\omega_2^2\omega_3^2)}{(S^2+2\xi_1\omega_1 S+\omega_1^2)(S^2+2\xi_2\omega_2 S+\omega_2^2)(S^2+2\xi_3\omega_3 s+\omega_3^2)}$$

$\omega_1 = 0.68$ R/sec $\quad \xi_1 = 0.7$

$\omega_2 = 0.90 \quad \xi_2 = 0.5$

$\omega_3 = 1.3 \quad \xi_3 = 0.5$

Applying this transfer function to the wave spectrum shown in Figure 4-2 results in a ship displacement spectrum. Assuming a minimum separation of 1,000 feet, the resulting line-of-sight spectrum is shown in Figure 4-9. These spectra can now be used to design the pointing and tracking system.

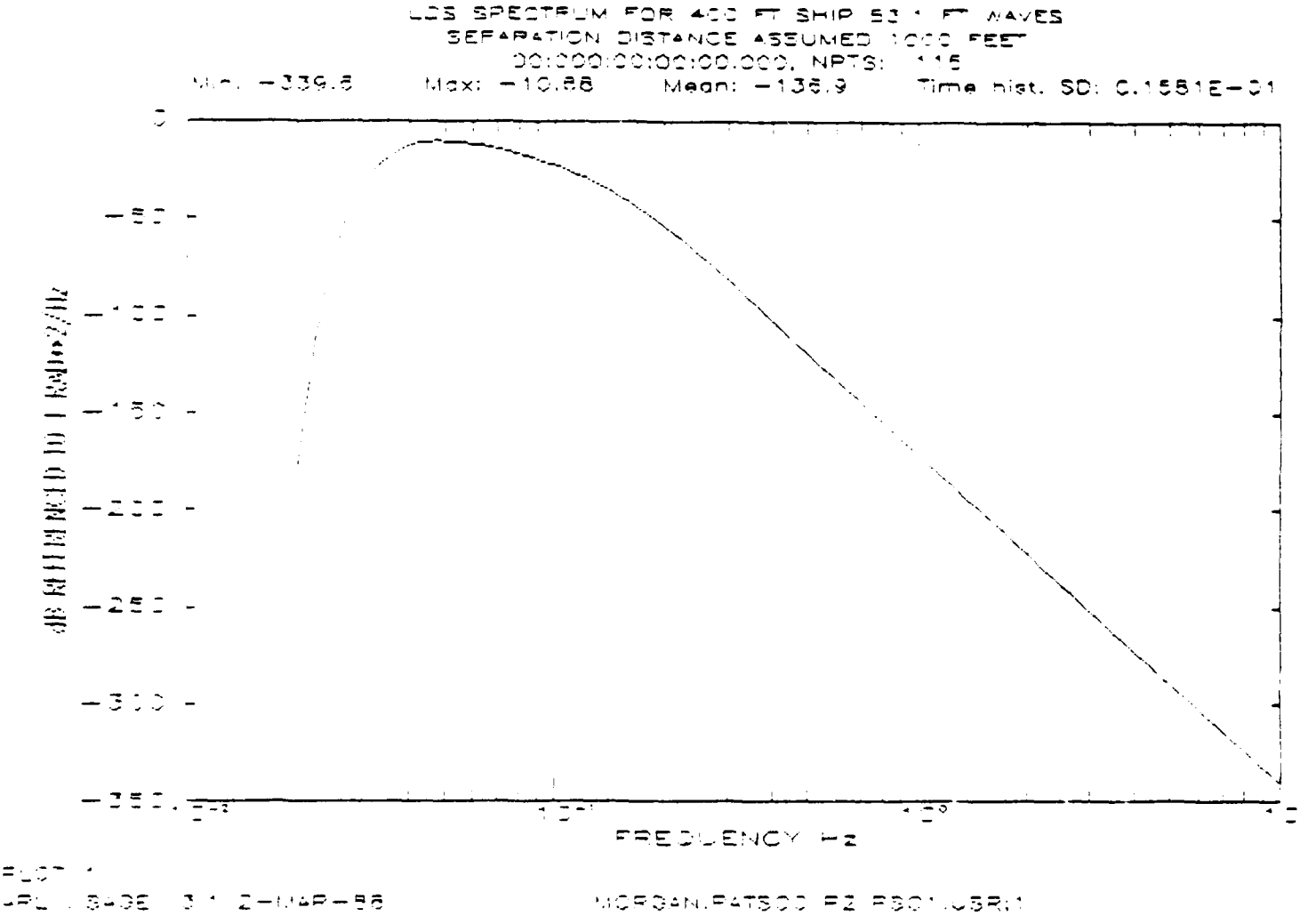

Figure 4.9. LOS Spectrum for 400 ft. Ship, 53.1 ft. Waves
(LOS Angular Spectrum Due to Relative Vertical Motion)

4.1.1.6 Worst-Case Propagation Medium Characteristics

When optical communications occurs over a direct line-of-sight path, as is the case here, the propagation analysis is concerned with radiant flux on a receiver aperture. Here we consider the losses due to the atmosphere. Atmospheric absorption/scattering at optical frequencies limits the separation between ships. This is due primarily to the high absorption and scattering coefficients of sea water. Beam clearance above the sea surface is of paramount importance for two major reasons: 1) in reducing the probability of waves breaking the line-of-sight and 2) in reducing the amount of sea mist and spray over the path to a minimum. Using simple geometry with two ships placed on the surface of the sea, we approximate the line-of-sight separation between the ships by

$$R = 2\sqrt{2\,(h_p - h_c)\,R_E}$$

where:

R_E = Radius of the earth ($= 6 \times 10^6$ m)

h_p = height above the sea level of the platform carrying the transmitter-receiver

h_c = height above the sea level of the line-of-sight, i.e., the line-of-sight clearance above sea level

R = line-of-sight range between the communicating ships (See Fig.10).

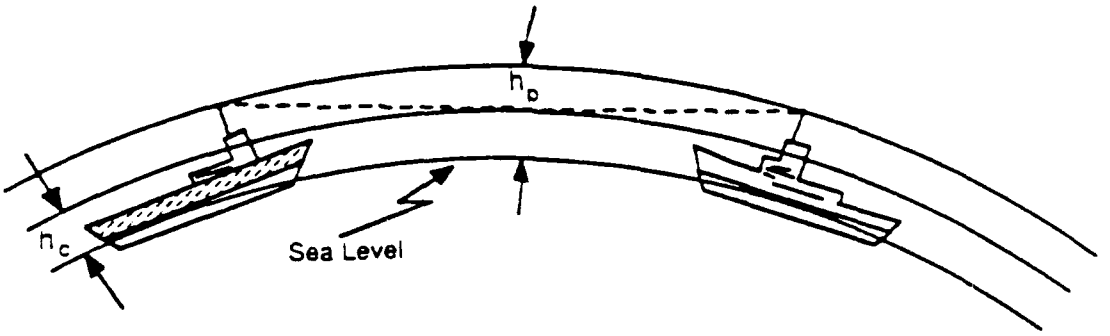

Figure 4-10. LOS Calculation

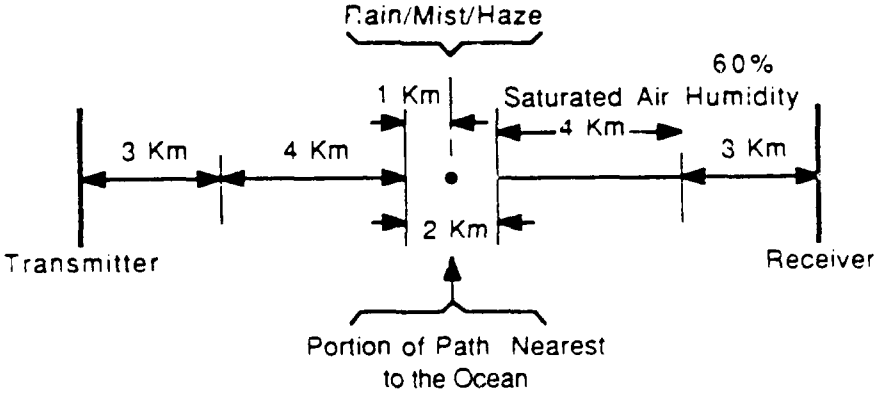

Figure 4-11. Atmospheric Conditions

For a clearance of 10 meters (h_c = 10) and package height of 15 meters (h_p = 15) the maximum ship separation is approximately 15.5 kilometers.

This derivation is shown below:

h_p = height of pole or mast carrying XTR/RCVR above sea level

h_c = beam clearance height above sea level

$\Delta = h_p - h_c$

R_E = Radius of earth $\approx 6 \times 10^6$m

$$\frac{R_E + h_p}{R_E + h_c} = \text{Sec}\theta = \frac{1}{\cos\theta} \simeq \frac{1}{1 - \frac{\theta^2}{2}} \simeq 1 + \frac{\theta^2}{2} =$$

$$\frac{(R_E + h_c) + \Delta}{(R_E + h_c)} = 1 + \frac{\Delta}{(R_E + h_c)} \text{ or } \theta^2 = \frac{2\Delta}{(R_E + h_c)}, \quad \theta = \frac{\sqrt{2\Delta}}{(R_E + h_c)}$$

(Range = R):

$$\frac{R}{2} = (R_E + h_c)\,\theta = \sqrt{2\Delta\,(R_E + h_c)} \simeq \sqrt{2(h_p - h_c)}\,R_E \simeq 2\sqrt{2\Delta R_E}$$

$R = 2\sqrt{2\Delta R_E}$ depends on Δ only (approximately) whereas h_p is determined by h_c.

Example: For h_p = 15m; h_c = 10m; Δ = 5m; $R = 2\sqrt{2x5x6}\ 10^3$m = 15.49 km.

4.1.1.7 Atmospheric Transmission Calculations

The path that the beam travels from one ship to the other passes closest to the water surface at the midpoint between ships, so let us break the path up into the following atmospheric conditions for calculation of one way transmittance for 15.49 km (approximately 16.0 km) range. See Figure 4-11.

First 3 km: 60% saturated air at 23°C
Next 4 km: saturated air at 23°C
Next 2 km: haze and mist
Next 4 km: saturated air at 23°C
Last 3 km: 60% saturated air at 23°C

The portion of the path nearest to the ocean surface (approximately 2 km) is modeled separately as a region of rain/mist/haze.

The path attenuation due to this atmospheric segment is calculated for several wavelengths as follows:

Γ (λ = 0.5μm) = 0.5
Γ (λ = 0.8μm) = 0.69
Γ (λ = 1.7μm) = 0.77

(Reference: Hudson's "Infrared System Engineering, Table 4-13; pg. 164).

An intermediate segment of 4 km is modeled as 100% saturated air and water vapor mixture. The outer segments are modeled as 60% saturated air and water vapor mixture. The amount of precipitable water in these segments

= 2 {4 x 20 + 3 x 12} = 232 mm of H_2O.

We will approximate it as 250 mm of H_2O.

Path attenuation at a given wavelength for this amount of precipitable water is obtained from standard references (Rand Report, pp. 898, July 1956).

Total one way transmittance for the assumed range model is

for λ = 0.5μm, Γ = 0.351125 x 0.5 = 0.1756
for λ = 0.8μm, Γ = 0.4618 x 0.69 = 0.3186
for λ = 1.7μm, Γ = 0.89 x 0.77 = 0.685

The table values for absorption and scattering vary with wavelength by orders of magnitude. A window for absorption and scattering resides in the range from a wavelength of 400 to 600 nanometers (nm). There are several choices of available lasers in this region. The EXIMER laser wavelength at 451 nanometers is an excellent choice but is expensive and bulky. The compact, inexpensive GaAs laser diodes present a poor choice with wavelengths from 750 nanometers to 880 nanometers. A good compromise, however, is the laser diode pumped doubled Nd:YAG laser. This gives a wavelength of 530 nanometers with good propagation characteristics through water saturated air and rain. This device is small and rugged, and with the pumping being performed with GaAs laser diodes, the lifetime is in the tens of thousands of hours.

For each of the beam pathway sections we use 500 nanometers, slightly lower than the 530 nanometers doubled Nd:YAG only because studies using a 500 nanometer wavelength are readily available in atmospheric tables. For the path sections, we find that the major contributor to losses is in scattering. We therefore ignore absorption losses and consider only scattering (reference Deirmendjian, 1964). For a rough order of magnitude of the transmission through the 16 km path, we have at 500 nm the sum of

precipitable H_2O = 250 mm with a transmittance of 0.3967 (Tables 4-3, 4-7 and Figure 4-3, Hudson). For the 2 km of haze we have a transmittance of about 0.5, the total transmittance is then:

$$T = (0.3967)\ (0.5) = 0.1983 \text{ (Table 4.13, Hudson)}$$

for the entire 16 km path which is very close to the T(λ=0.5μm) obtained from the Rand report above. For a more precise analysis of the propagation transmittance and boundry-layer effects the LOWTRAN simulation package can be run. For the next phase, an in-depth analysis will be run which should help narrow down the appropriate wavelength of operation.

Although we have presented only a rough order-of-magnitude analysis, we have found that we have atmospheric losses that are reasonable for incorporating into the design of the ship-to-ship line-of-sight link. The key point in this analysis is that an appropriate choice of the propagation wavelength can result in acceptable losses, that the doubled Nd:YAG or a GaAlAs laser diode may be a good choice.

Figure 4-12 shows atmospheric transmission results for mostly clear with light haze conditions.

The study also considered the condition of fog mixed with light rain and a snow storm. Both these conditions dramatically reduced transmission. The results obtained by ATA agree with the results obtained by A. Goroch, J. Davis, and G. Trusty in their article, "The Near-Ship and Ambient Marine Environment" in JDR (received Oct. 19, 1984).

In conclusion, ATA's study showed that the best available derived laser sources over all meteorological conditions were the GaAlAs and Nd:YAG which operate with approximate wavelengths of 0.80 μm and 0.53 μm, respectively.

For communication purposes, laser output must be modulated. The diode laser may be directly modulated by changing the input current. The Nd:YAG laser may be modulated via Q switching or cavity dumping.

4.1.1.8 Bandwidth of Disturbance Rejection Loops

Using the spectra presented in Figures 4-6, 4-8 and 4-9, one can determine the minimum error rejection bandwidth to achieve certain levels of residual beam jitter on target. To provide a quick analysis, we assumed a Type II Loop with 5, 7 and 10 Hz error rejection bandwidths. Table 4-4 below presents the residual jitter on the other receiver for this bandwidth.

- Naval Research Laboratory Conducted Study of Infrared Radiation Transmission over Chesapeake Bay under a Wide Range of Atmospheric and Meteorological Conditions

- Results of Study are:

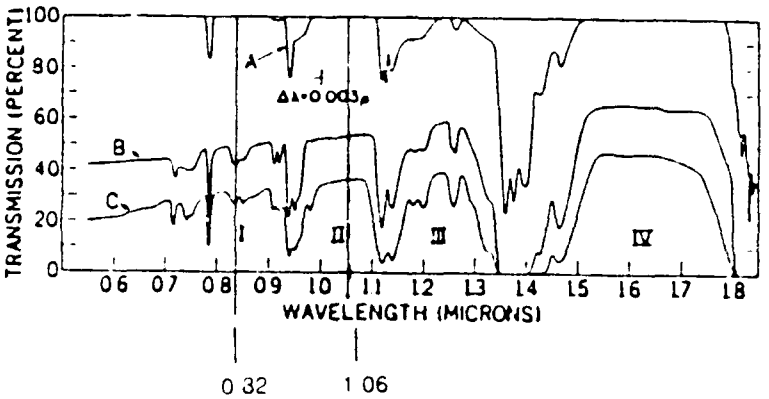

CURVE	PATH LENGTH	TIME	TEMP	R.H.	PRECIPITABLE WATER	VISUAL RANGE
A	1000'	3 PM	37°F	62%	11 MM	22 MI.
B	34 MI.	10 PM	34.5°F	47%	13.7 MM	16 MI.
C	101 MI.	12 AM	40.5°F	48%	52.0 MM	24 MI.

Taylor & Yates 1955-56

For Mostly Clear with Light Haze Conditions

Figure 4-12. Atmospheric Transmission

Table 4-4. Residual RMS Motion With Error Rejection Bandwidths

	RMS MOTION	ERROR REJECTION BANDWIDTH		
DISTURBANCE	NO CORRECTION	5 Hz	7 Hz	10 Hz
Roll Motion	151.2 Mrad	50.8μrad	25.4μrad	12.5μrad
Pitch Motion	59.4 Mrad	27.2μrad	13.9μrad	6.8μrad
LOS Motion	51.8 Mrad	9.2μrad	4.7μrad	2.2μrad

For a 1-meter beam at 15 km, a jitter less than 32 μrads would be sufficient. It is clear from Table 4-3 that the error rejection bandwidth needs to be between 5 - 10 Hz. For a 5 Hz loop, the roll motion is too severe while the LOS is adequately rejected. At a 10 Hz rejection bandwidth, even the worst case residual is adequate. The 10 Hz bandwidth is adequate for coarse gimbals. Actual loop implementations must be considered to pick the bandwidths more carefully. Also, when details of the noise introduced by the gimbal torquer and other high-frequency vibrations are considered, these bandwidths may need to be adjusted.

To make an attempt at doing this, a simulated spectrum was generated to add some high frequency vibration. These levels were chosen to provide, with a high-bandwidth loop, equal residual RMS noise in the high-frequency bands. Figure 4-13 gives a combined LOS angular spectrum low frequency plus this added high-frequency vibration.

4.1.1.9 Maximum Aperture Size

ATA plans a maximum aperture size of 25 centimeters.

4.2 Identification of Key System Elements

ATA identified the following components as being key to an optimal system:

1) Nested optical loops;
2) Digital controllers;
3) Gimbals.

The search for a ship-to-ship optical communication system that is optimal in cost and performance was therefore constrained to shared aperture systems employing digital controllers to position gimbals and steering elements in multiple, nested control loops. Such a configuration provides a system which is optimum in a global sense. These components are described in more detail in the following subparagraphs.

4.2.1 Nested optical loops

The use of nested optical loops is key to achieving a low-cost pointing-and-tracking system for the ship-to-ship communication. With nested loops, the

transmitting and receiving optics are implemented with multiple, controllable optical elements as opposed to a single large fixed optical mirror or telescope. Single loop systems usually have resulted in low bandwidth pointing-and-tracking subsystems because of the large inertias involved and finite actuator powers available. Further, they provide virtually no rejection of high-frequency base motions and disturbances which are inevitably coupled to the pointer/tracker line-of-sight to become optical communication beam jitter. This beam jitter becomes increasingly important as the size of the receiving aperture decreases in relation to the width of the optical beam as will be the case for a low-cost system.

With nested loops, the tracking error controls small, low-inertia, high-bandwidth steering elements, such as General Scanning Inc.'s Fast Steering Mirror (FSM) (shown in Figure 4-14). These steering elements can be controlled directly or indirectly, as described by Held and Barry of the Hughes Aircraft Company in "Precision Optical Pointing and Tracking from Spacecraft with Vibrational Noise", SPIE Vol. 616, pp. 160-166, Optical Technologies for Communication Satellite Applications, 1986. Such a mirror is currently being used in our conical scanning laboratory experiment.

When controlled indirectly, the steering elements follow a stabilized mass which is pointed along the desired LOS by the tracker. The steering elements follow the mass via high-bandwidth slave loops. In either case, the steering elements move the optical beam at high rates, decoupling it from the higher frequency base motions and disturbances.

The pointer/tracker gimbal set which houses these steering elements follows them or the stabilized mass to which the steering elements are aligned through low-bandwidth slave loops. The gimbals with their larger inertias only have to follow the faster beam-steering elements or stabilized mass with their smaller inertias in an average sense, just as single-loop low-bandwidth pointer/tracker systems follow their targets in an average sense. In either case, the gimbals move the optical beam at low rates, decoupling it from the lower-frequency base motions and disturbances without requiring precision pointing of the gimbals, as is the case in single-loop systems.

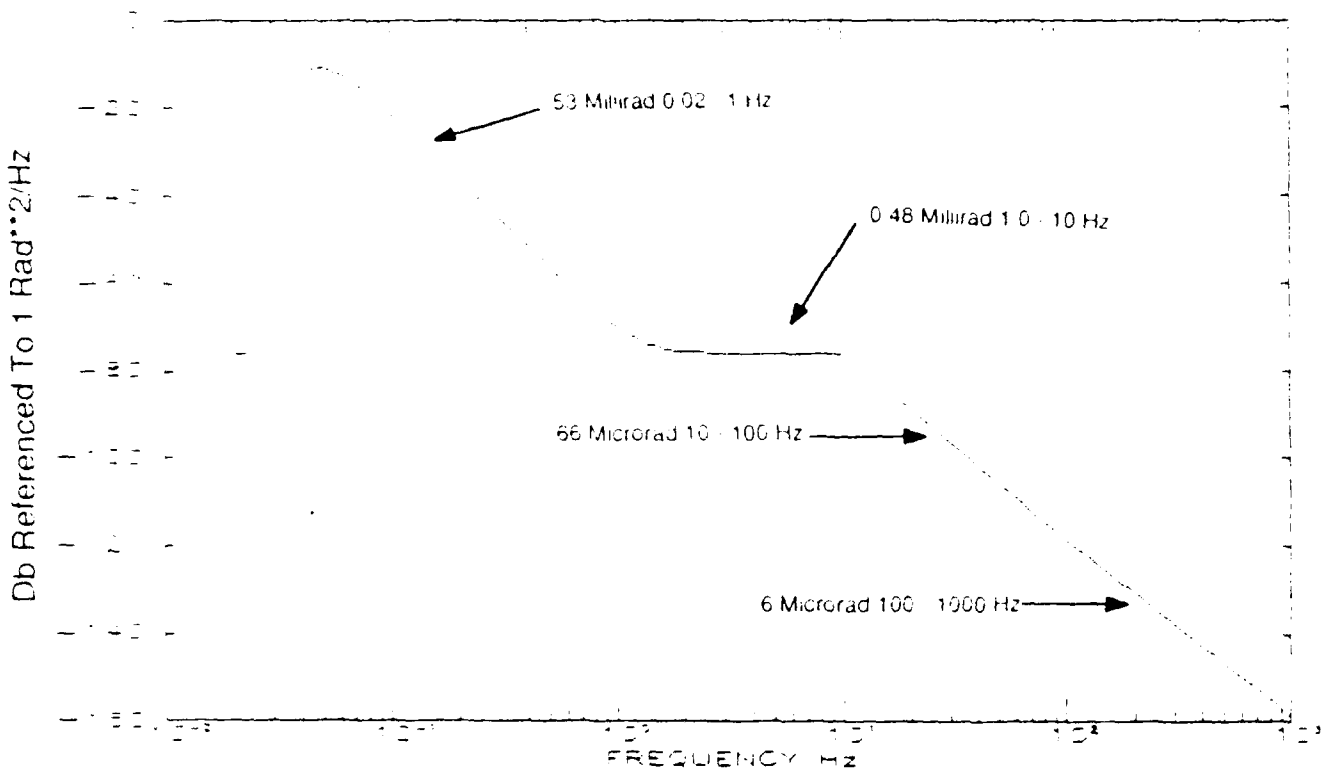

Figure 4-13. LOS Angular Spectrum Low Frequency Plus High Frequency Envelope.

Because the gimbals do not have to be pointed with great precision for the overall system to have high precision, they can be manufactured to considerably less rigid specifications than gimbals for single-loop systems. In effect, the requirements for precision have been distributed between gimbals and steering elements, thus relieving the gimbals of the burden for precision pointing. By so distributing the precision requirements, the gimbals can be manufactured very inexpensively, using lighter, less rigid materials such as composites or plastics. The small steering elements are themselves inexpensive and so the mechanical elements of the resulting nested control-loop system are considerably less expensive to manufacture than those for the single-loop system. Note that low-cost has not been achieved at the expense of performance; in fact, the performance of the nested multiple-loop system far exceeds that of the single-loop system, which further strengthens ATA's cost and performance rationale for using nested multiple-control loops.

4.2.2 Digital Controllers

ATA believes that digital controllers, as opposed to analog controllers, as a means to tie the multiple, nested control loops of the system together, represent another important area for cost reduction. Because of the rapid advances in semiconductor technology and manufacturing techniques, digital control hardware is both plentiful and inexpensive. Because this hardware is an off-the-shelf item, only the control laws and the software algorithms which implement the laws require development.

Intelligent decisions and algorithms can be implemented easily on digital computer control systems. Several models comprise a complete description of the digital controller of the tracker and communications system package. First, remote and local command of the package is simplified through an intelligent user interface such as a terminal connection and/or a status/command control panel. This facilitates quick communication link startup, acquisition of other ship commands, and communications system status. Aside from the intelligent front end, the digital controller must perform a systematic search or scan for a designated receiver. Conical, raster scanning, or other scanning techniques can be exercised by the controller. Large and narrow field-of-view (FOV) for coarse and fine tracking/scanning are decisions that the controller employs. To reacquire a lost or faint beacon, predictive algorithms can be used to minimize down and retransmission times. A low bandwidth controller for the pitch, yaw, and roll of the ship is inexpensive off-the-shelf hardware.

The digital controller for the high-frequency control will depend directly upon the base motion disturbance rejection necessary. Here, parallel processing can be incorporated if necessary.

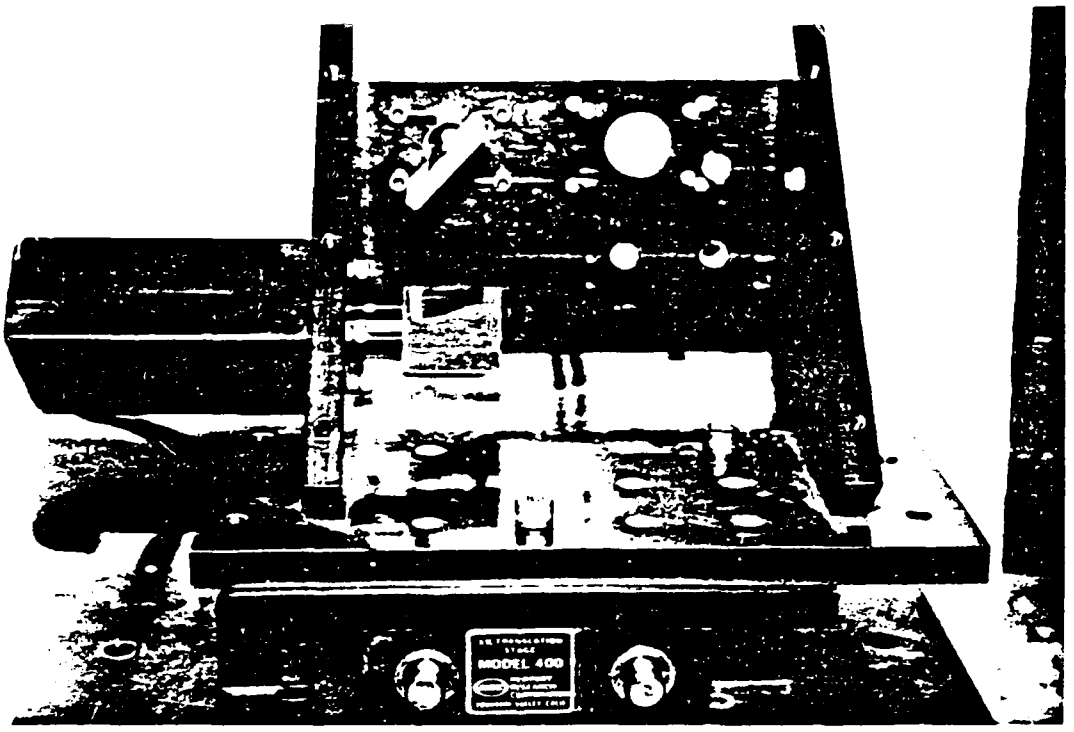

Figure 4-14. General Scanning, Inc., Fast Steering Mirror.

Digital signal processors are relatively new types of processors used for enhancing the computer and speeds often needed in signal processing applications. The DSPs are applicable in this control problem for the high frequency control loop. Here, in place of ganging multiple conventional type processor modules together to implement a parallel processing approach, one DSP coupled with one conventional processor may indeed provide the necessary computational requirements.

A digital controller can handle the scan-acquire-track logic and handoff operations. It can also be asked to control the low-frequency track loop and the high-frequency track loop, which is dependent upon base motion PSD. A $20,000-25,000 digital controller can handle a 1 KHz closed loop bandwidth. Figure 4-15 shows control modular flow. Figures 4-16 and 4-17 show two VME systems that ATA has under development, CONSCAN and SSP. Figure 4-18 shows a possible VME bus configuration for this project.

4.2.2.1 Digital Control Electronics

For the digital control electronics, MC68020-based boards, both with and without parallel processing capabilities were considered. However, due to the rapid involvement of digital semiconductor technology, a complete digital controller specification at this point may be rendered obsolete at the actual time of the prototype design effort. At this time, ATA has implemented a single degree-of-freedom ultra-precision controller using a VME computer architecture. This controller utilizes multiple CPU boards to perform parallel processing, and is currently being developed into a 6 degree-of-freedom controller.

A digital control system offers more flexible and adaptive means of controlling a gimballed type transmitter/receiver flat and associated components. The functional modules comprising the digital controller are:

1) Initialization;
2) NTDS Command front end;
3) Safety operation;
4) Cross-link receiver acquisition;
5) Receiver tracking;
6) Reacquisition;

Figure 4-19 is a photograph of a set of typical digital control electronics units.

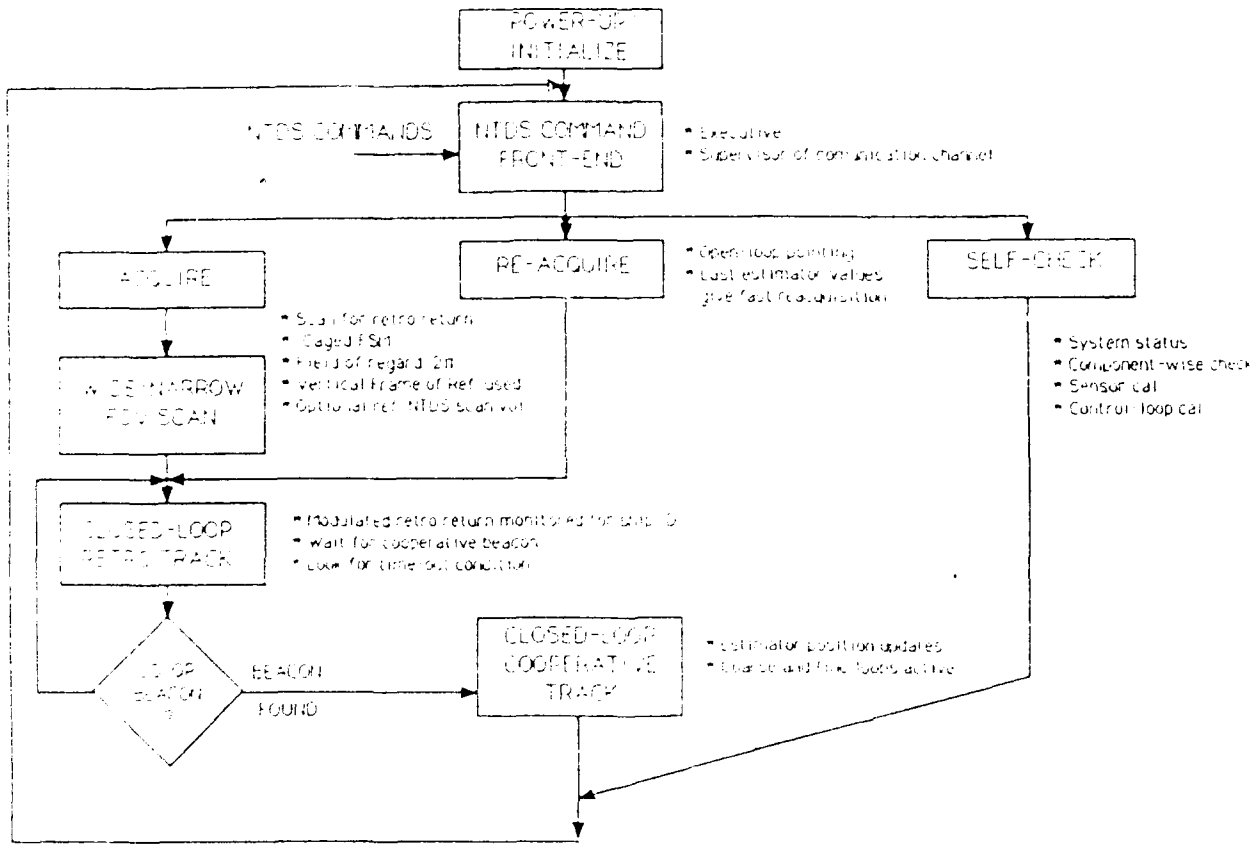

Figure 4.15. Control: Modular Flow

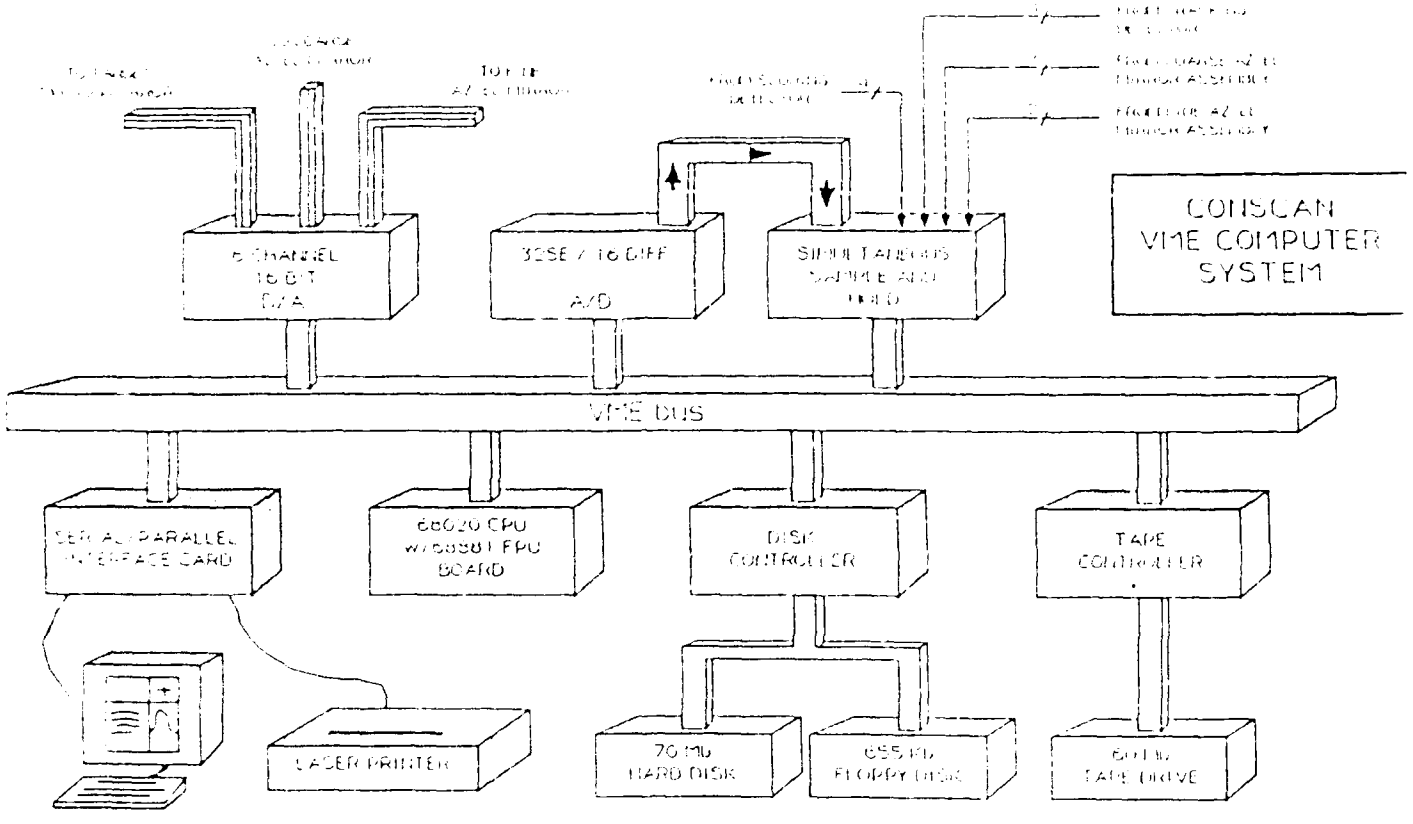

Figure 4-16. VME System Under Development: CONSCAN

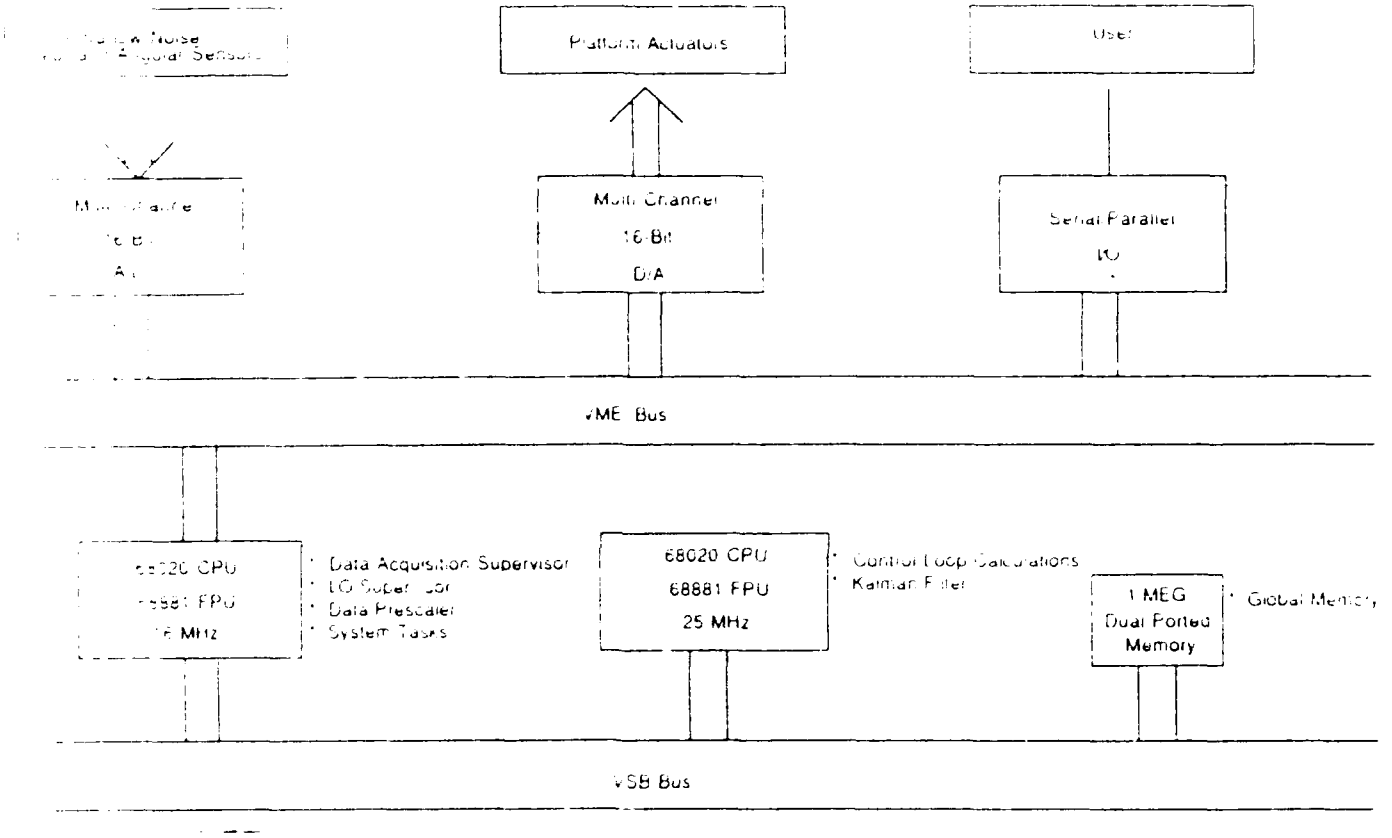

Figure 4-17. VME System Under Development: SSP

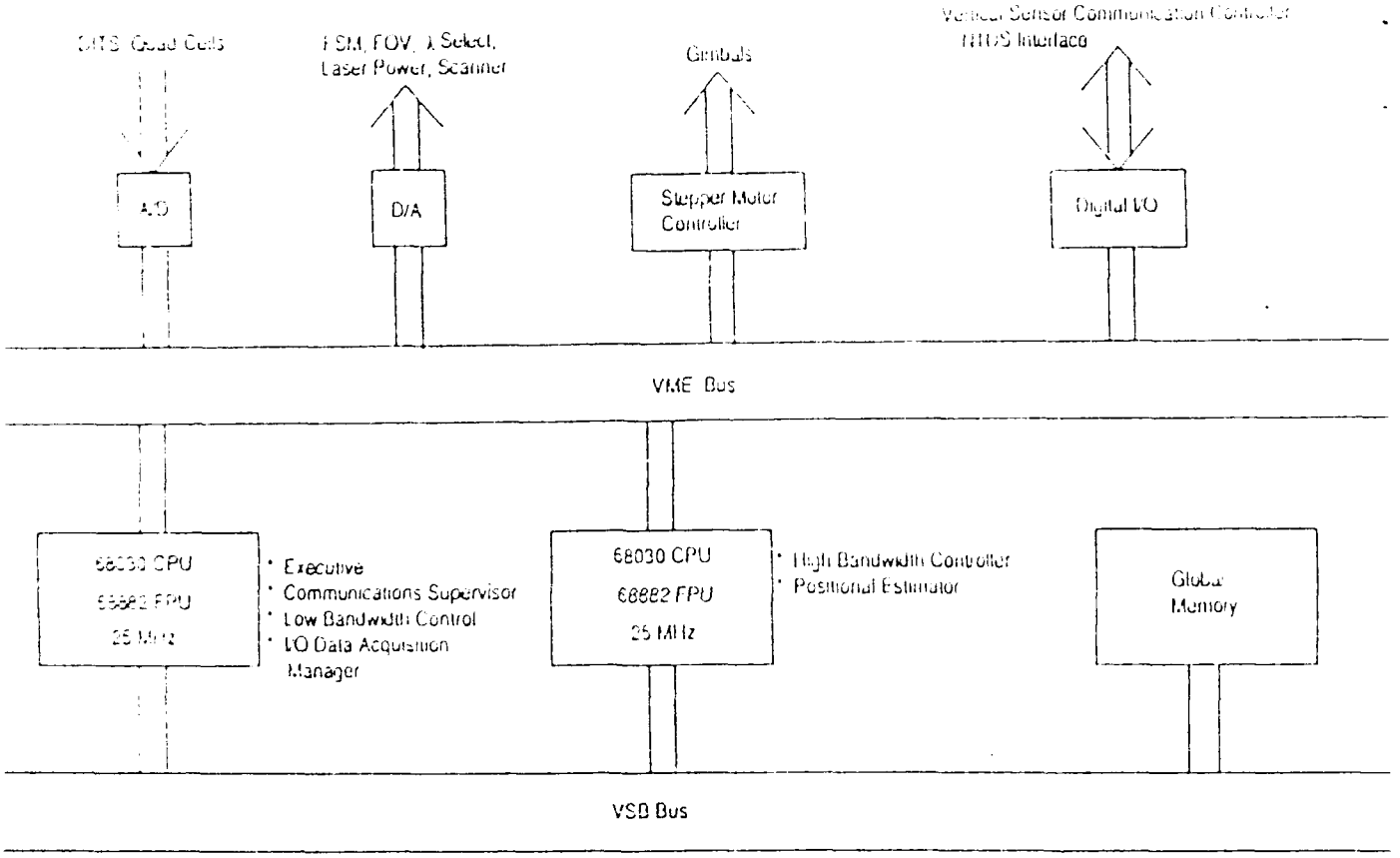

Figure 4-18. Possible Configuration

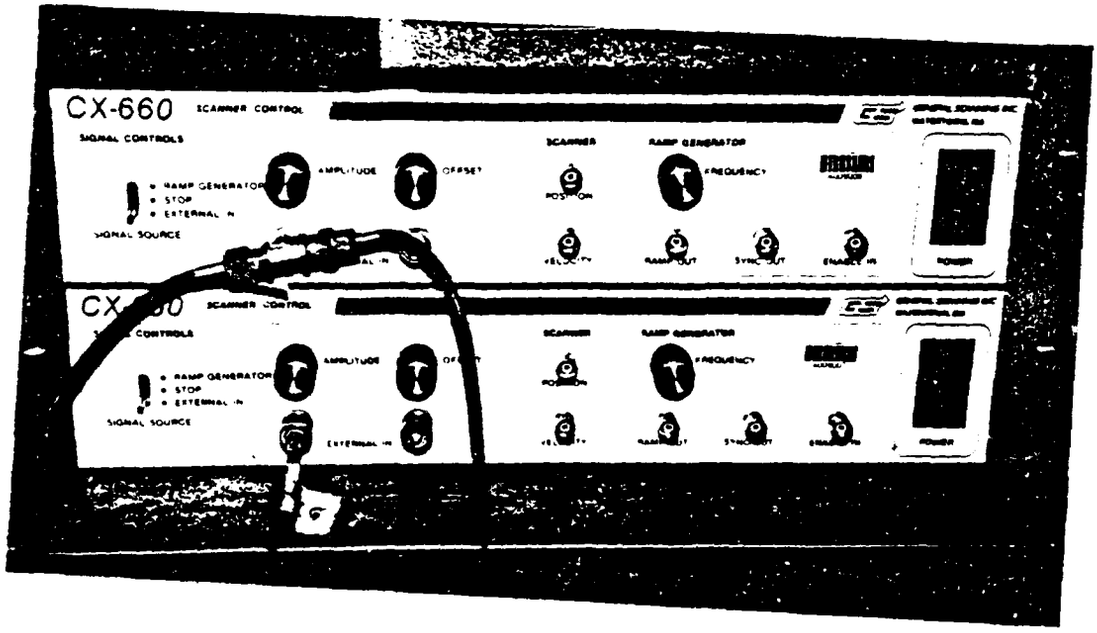

Figure 4-19. Digital Control Electronics

4.2.2.2. Initialization

In the initialization mode, the controller goes through a system status and health check and then identifies a vertical frame of reference via a one-axis vertical gyro, horizon sensor, or the Naval Tactical Data Systems (NTDS) computer. The system status and health check provide a self check to determine the working condition of the laser subsystem system, the communication subsystem, and the Fast Steering Mirror (FSM) and gimbal functionality. It then reports status to NTDS when queried. After assessing the functionality of the various subsystems, the vertical frame-of-reference sensor is monitored as the gimbals are commanded to a level position. The vertical frame-of-reference is needed to reduce the search volume in acquiring a receiver on a second ship as discussed earlier.

4.2.2.3 Naval Tactical Data System Command Front End

To facilitate operations training, all commands, status, and data are routed through a NTDS interface. The digital controller can therefore be treated as an intelligent peripheral or as a NTDS computer. Commands sent to the digital controller control which ship to scan and lock-on to, and control the dataflow to and from the communications subsystem.

4.2.2.4. Digital Tracking Controller

The nested digital control loops consist of one high-frequency loop closed around a low-frequency loop. The low-frequency loop controls the gimballed pointing flat and should maintain a pointing accuracy to within the field of view of the high-frequency beam steering mirror. In the process of locking-in on the target, the low-frequency control loop, using a wide field-of-view, tries to minimize the error on the quad-cell or avalanche photodiode array. Only one digital processor is needed to control the FOV and send error correction angles to the gimballed flat since this is a relatively slow control loop. Stepper motors can be used to achieve the desired accuracy and when the error angle is within the fast steering mirrors field-of-view, the second high-frequency loop kicks-in and tracks to the accuracy needed. Bandwidth requirements are still uncertain until actual platform measurements can be made. However, if bandwidth requirements are less than 1 kilohertz, a digital implementation is feasible with current off-the-shelf products. Here, if necessary, parallel processing may be needed to achieve the necessary calculations and control input/output signals. The parallel processing aspect is currently being implemented in a seismically stable platform controller at ATA (Figure 4-20).

4.2.2.5 Track Reacquisition

During the tracking control, the digital controller records the platform disturbances and trajectory of the target. This information is used to build an estimator of the target in the event of a lost track condition. This will allow the tracker to predict where the target will be in the next millisecond, second, or minute. This predictive controller is especially useful for high sea-state conditions when the receiver of one of the ships

is blocked by large waves. Here, fast reacquisition is realized and down time is minimized. The additional computation necessary to perform predictive tracking is of little consequence to the control bandwidth, since several processors may divide up the computation.

4.2.3 Gimbal

Structural grade plastics, composites, and traditional metals were considered for the gimbal structure. Geared and ungeared DC and AC motors were considered for gimbal actuation and unswitched and switched power amplifiers for the gimbal motors.

ATA determined that the gimbal sets supplied by TPAX would be the most appropriate. These gimbal sets utilize a unique Roto-Lok Rotary Drive that incorporates a patented friction-drive technology which smoothly couples a drive to a load using standard flexible cables in a figure-eight configuration. Multiple cables configured in this way increase torsional stiffness and improve smoothness through load sharing. The performance characteristics include:

1) No backlash;
2) Extreme stiffness;
3) Elimination of slippage;
4) Efficiencies of over 99%;
5) Environmental stability;
6) Reliability and long life.

Figure 4-21 shows the Roto-Lok Rotary Drive system; Figure 4-22 shows typical friction losses for different drive types; and Figure 4-23 shows backlash comparisons.

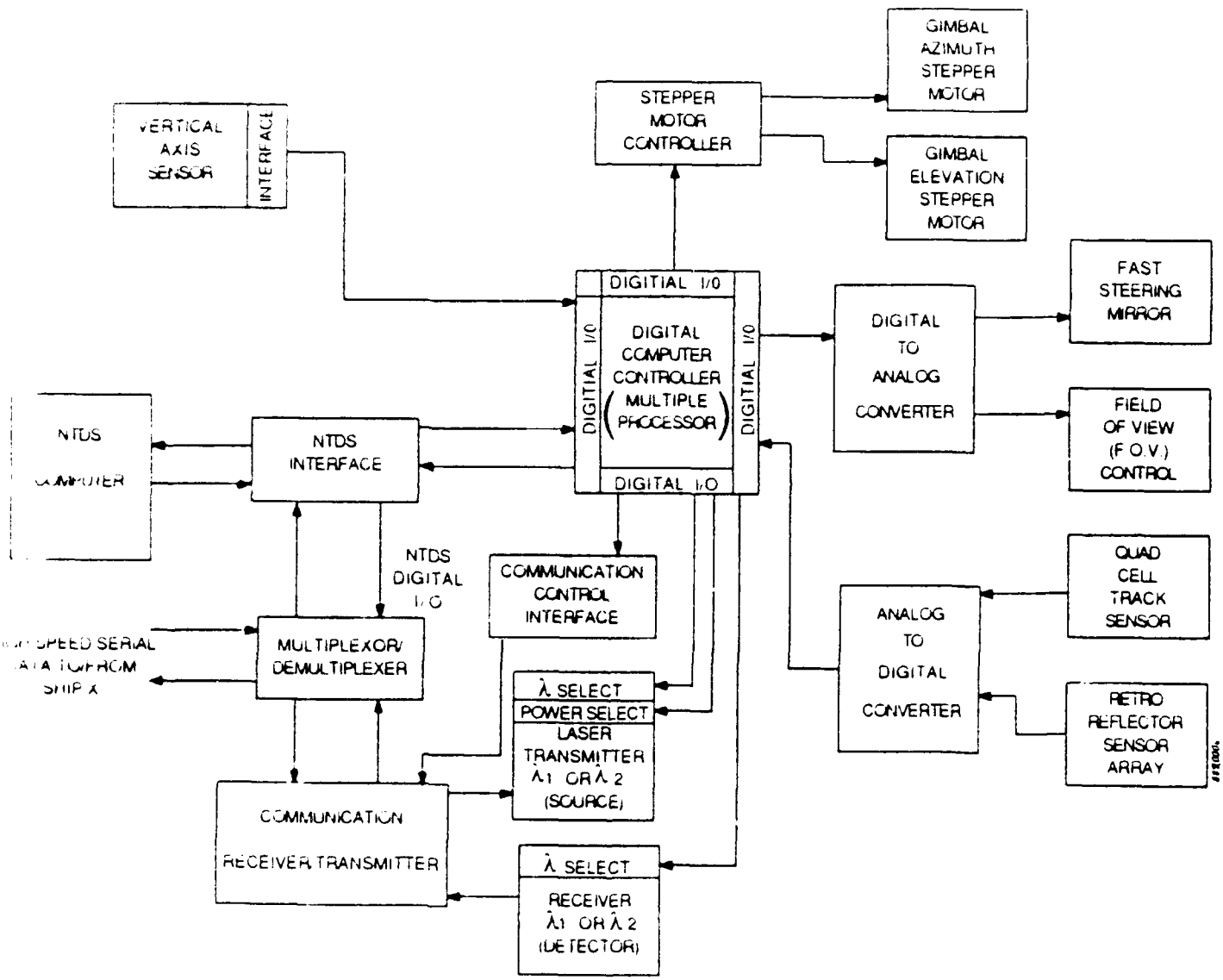

Figure 4-20. Digital Computer Controller

4.2.3.1 Maximum Gimbal Slew Rate

The largest angular excursions occur at the longest wave amplitudes due to their long wavelength and amplitude. However, due to the low frequency of these waves, the required line-of-sight rates are not maximum here. Again, the shorter the ship, the greater the bandwidth requirements. Based on our 400-foot ship, we calculate the maximum rate to be 7.3 degrees/second which occurs with a significant wave height of 29.1 feet. Therefore, an angular rate requirement of 7.5 degrees per second should be sufficient. ATA does not expect accelerations of more than 50 $\frac{\text{deg}}{\text{sec}^2}$ or = .87 $\frac{\text{radian}}{\text{sec}^2}$ on large gimbals, etc. We expect higher acceleration rates on smaller optics, i.e. 100 $\frac{\text{rads}}{\text{sec}^2}$.

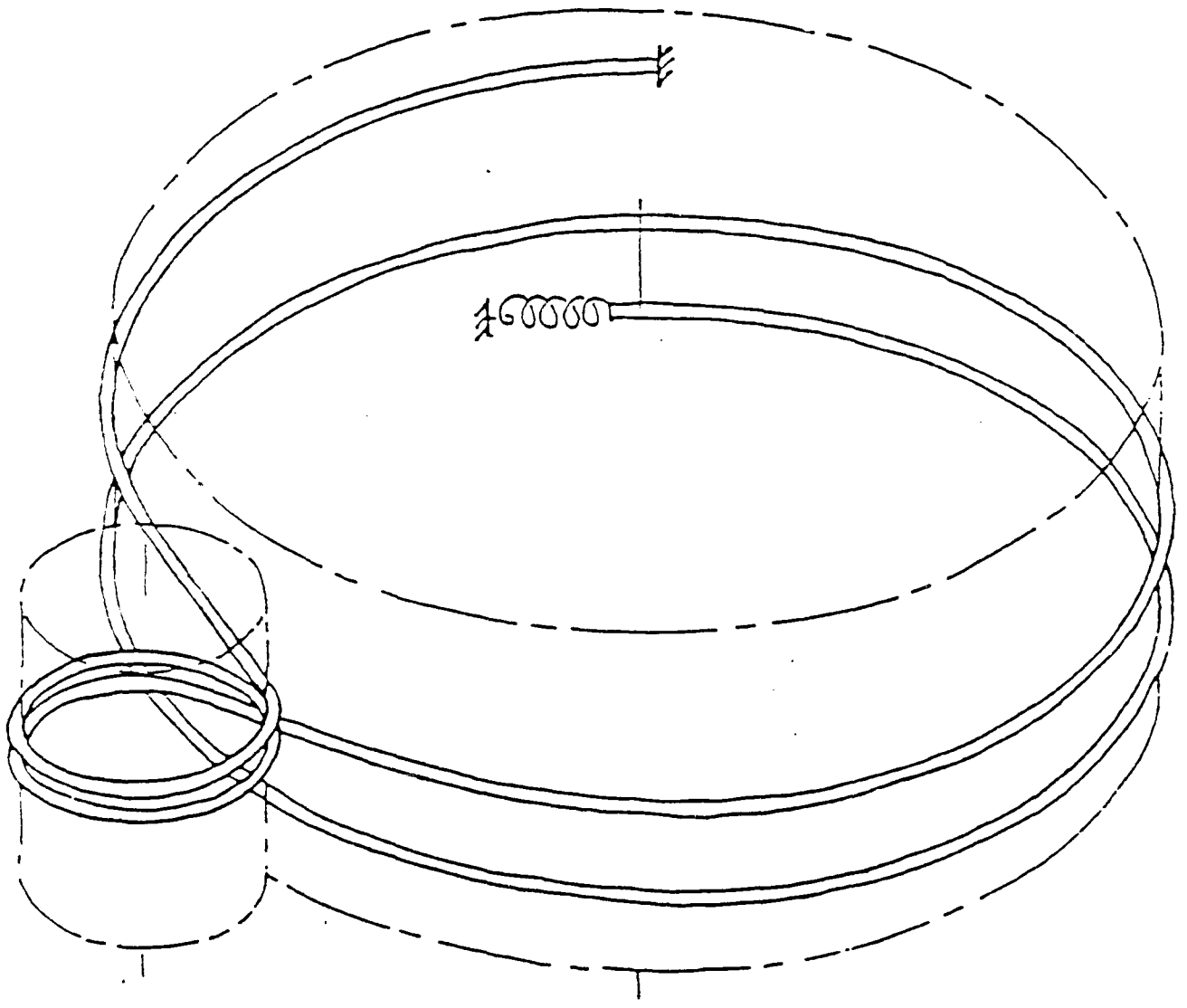

Figure 4-21. ROTO-LOK Rotary Drive Concept

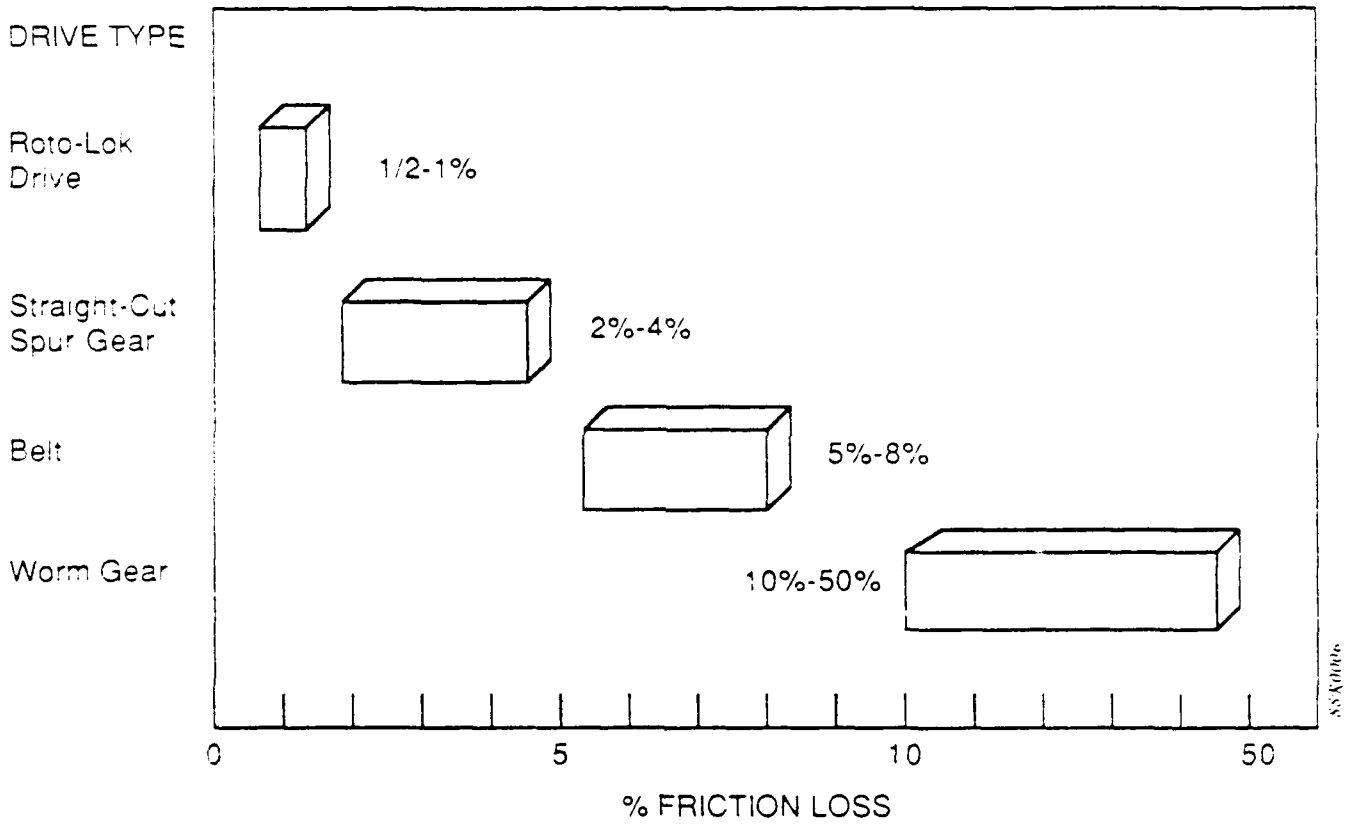

Figure 4-22. Drive Related Friction Losses less than 1%

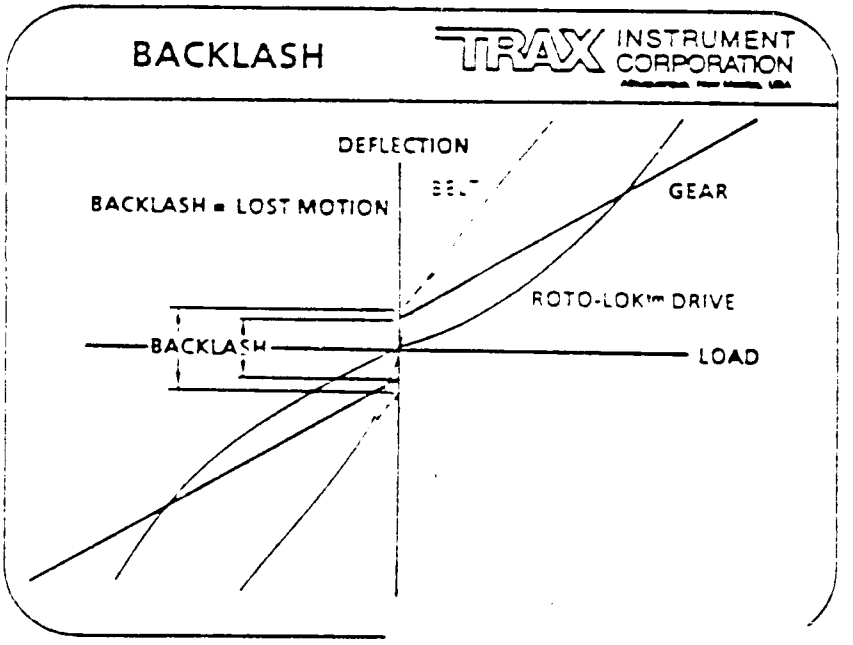

Figure 4-23. Blacklash Comparisons

4.3 Tracking

When a target is detected, the system will go immediately to tracking mode. This must be accomplished in less than a millisecond so that the ship's motion will not cause the target direction to change more than a beam width. The target will be maintained in track by rotating the beam about the target position.

Figure 4-24 shows a schematic of a demonstration tracker. Figure 4-25 gives the optical system schematic for a tracking demonstration, and Figure 4-26 gives the signal flow diagram for a tracking demonstration. Figure 4-27 shows a candidate configuration for ship-to-ship communication, and Figure 4-28 shows ship acquisition. Based on these configurations, the following calculations predict the tracker performance.

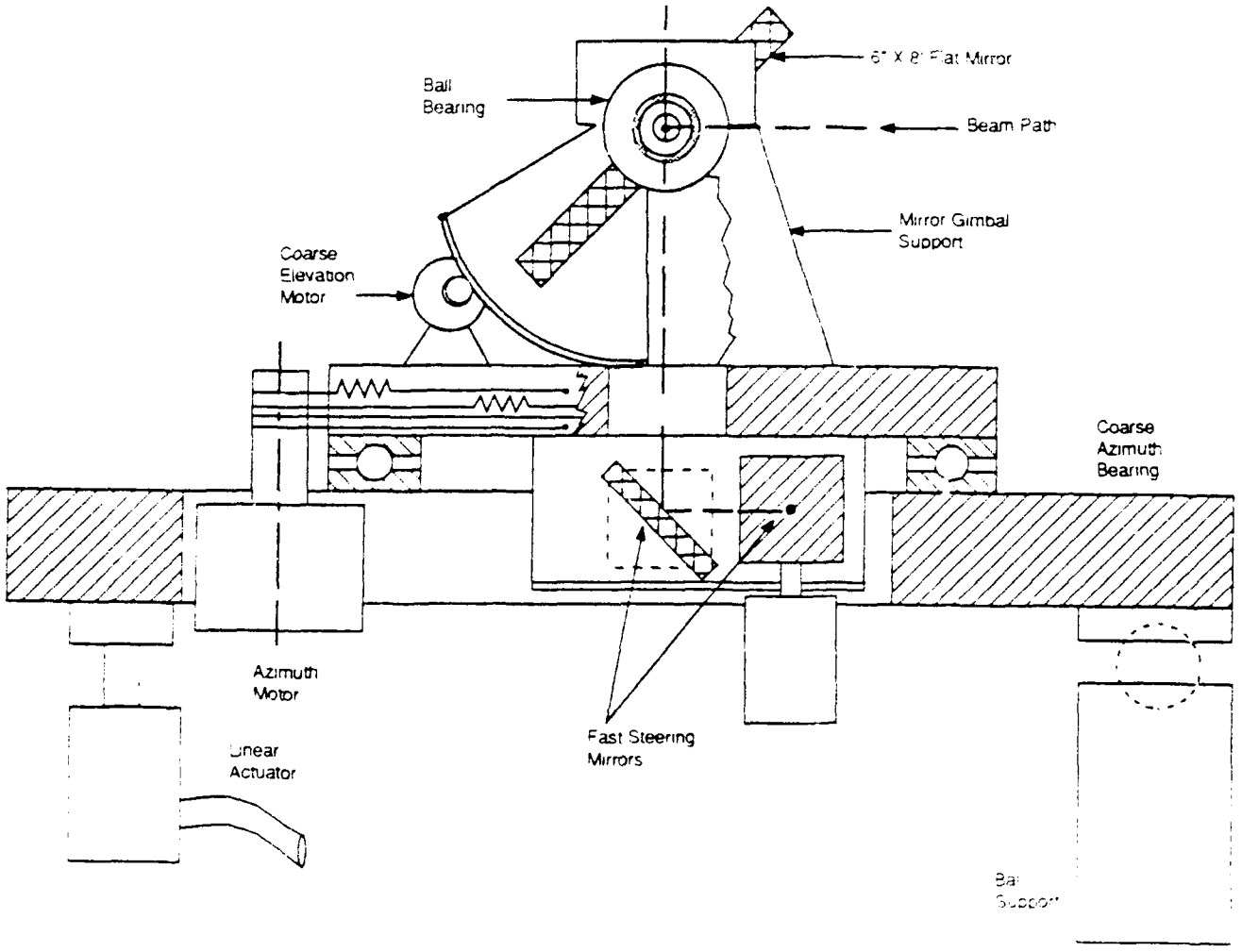

Figure 4-24. Demonstration Tracker

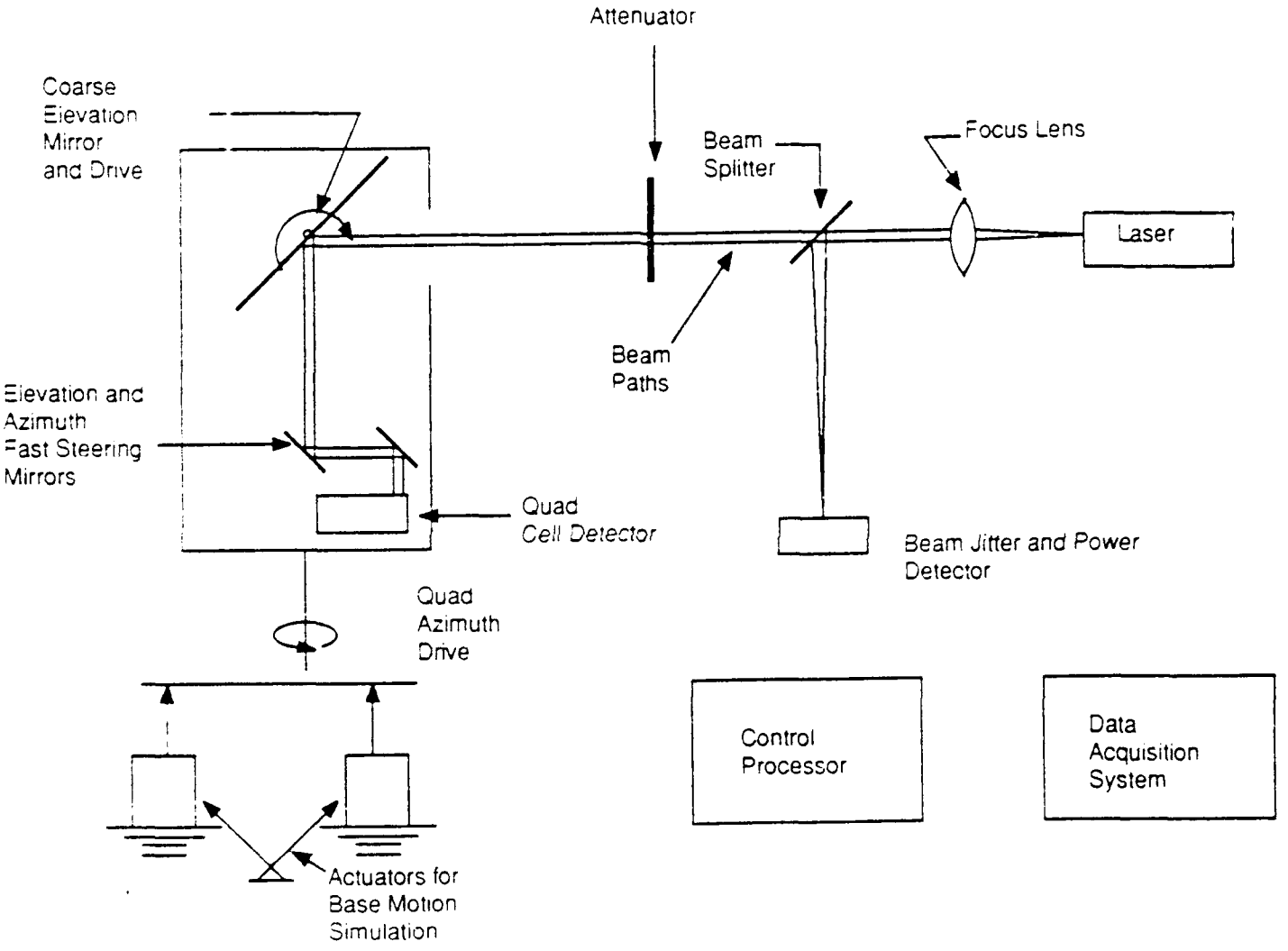

Figure 4-25. Optical System for Tracking Demonstration

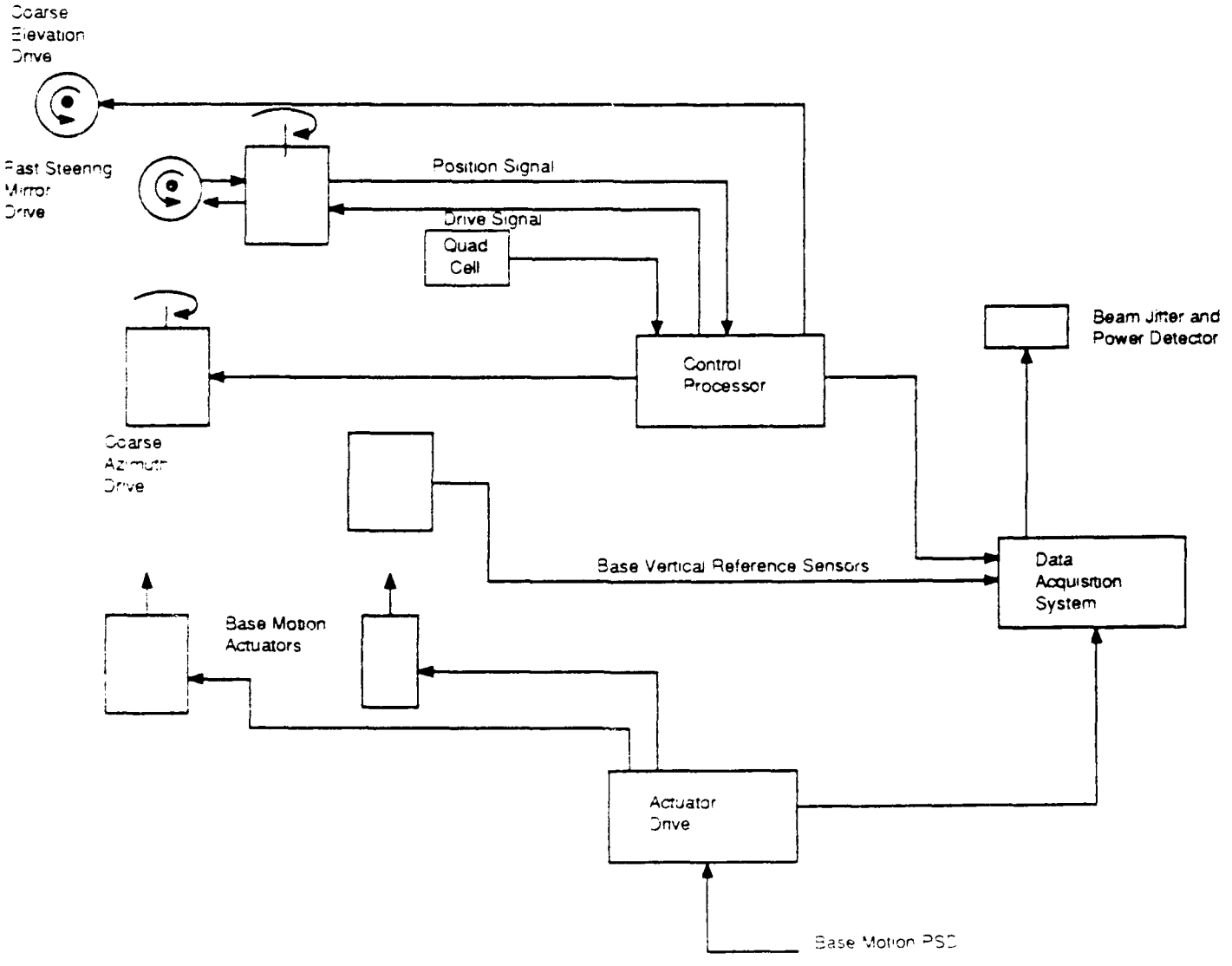

Figure 4-26. Signal Flow for Tracking Demonstration

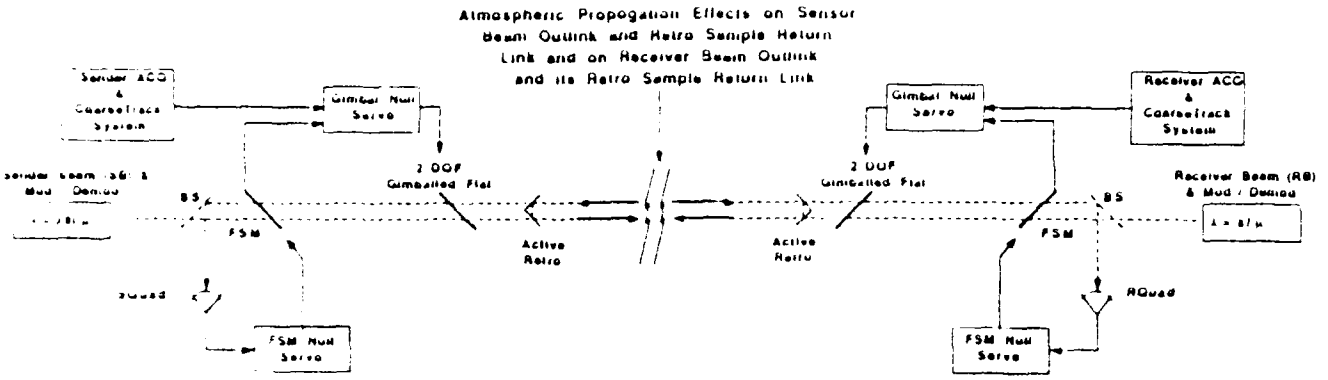

Figure 4-27. Candidate Configuration of Ship-to-Ship Communicator

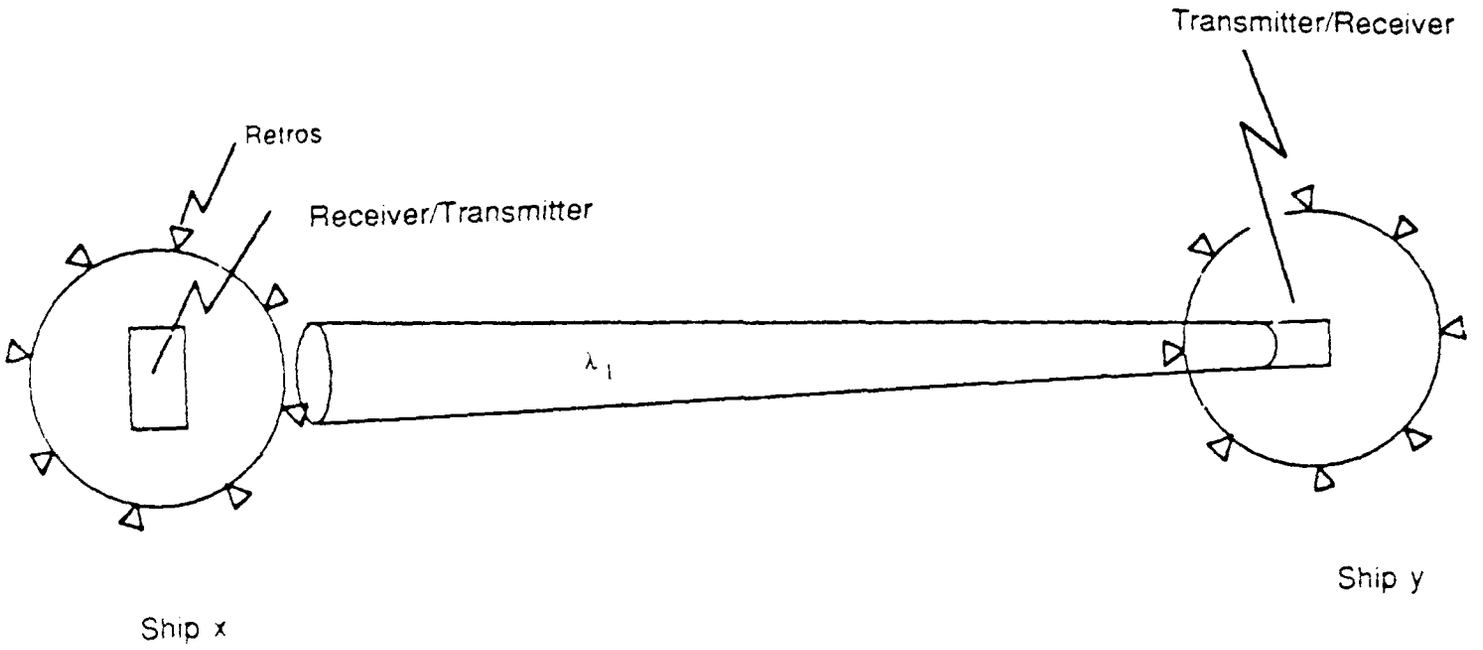

Figure 4-28. Ship y Acquires Ship x

d_{xtr} = diameter of the transmitting aperture (m)

d_{rcv} = diameter of the receiving aperture (m)

d_{cc} = diameter of the retro-reflector/corner cube (m)

τ_p = attenuation for one-way propagation

P_{xtr} = rated output power of the transmitter (w)

R = transmitter to receive range (m)

λ = spectral wavelength of the transmitter (m)

P_{rcvr} = power received by the aperture of the receiving station while the transmitter is on a different ship (as during communication of data) (w)

P_{rcvt} = power received by the aperture of the receiver while the transmitter is on the same ship (as during the acquisition and tracking of a friendly ship) (w)

We assume that the transmitter beam overfills the receiver aperture of the second ship during communication. and during tracking, the retro-reflected beam of the tracked ship overfills the receiver aperture of the tracker.

Then

$$P_{rcvr} = \frac{\tau_p P_{xtr} d_{xtr}^2 d_{rcv}^2}{4R^2 (1.22\lambda)^2}, \text{ (w)},$$

and

$$P_{rcvt} = \frac{\tau_p P_{xtr} d_{xtr}^2 d_{rcv}^2 d_{cc}^4}{4\pi (1.22\lambda)^4 R^4}, \text{ (w)},$$

Let $\lambda \approx 0.8 \times 10^{-6}$m,

and focal length of the receivers = 12cm.

The spot size of the receiver aperture in the detector plane (image plane)

$$= 2.34 \times 10^{-6} \text{ m}$$

which is $< 10^{-4}$m, the order of linear dimension of a detector.

Let the detector area be, $A_d = 10^{-6}$ m^2.

The D^* of an off-the-shelf Silican Avalanche-Photo detector (at 300°k) is.

$$D^* = 3 \times 10^{10} \frac{m}{w} \sqrt{Hz},$$

and the transmission of the receiver optics $\tau_o = 0.9$.

We can then calculate the minimum P_{rcvr} and P_{rcvt} required for SNR = 100 for the communication and the acquisition/tracking modes, respectively.

1) Assuming SNR = 100, and the bandwidth of communication to be 64MHz, then minimum required power received by the receiver aperture for SNR = 100 is:

$$P_{rcvr} = 2.963 \times 10^{-8} \text{ w}$$

with detector noise being 2.963×10^{-10} w, in the communication mode.

2) Similarly, for SNR =100, and the bandwidth required for tracking to be on the order of 400 Hz, the minimum required received power in the receiver aperture is:

$$P_{rcvt} = 7.4 \times 10^{-11} \text{ w}$$

with detector noise being $= 7.4 \times 10^{-13}$ w.

Finally, with P_{rcvr} and P_{rcvt} shown above and the optical path transmittance τ_p calculated earlier, we can estimate the required minimum transmitter power for SNR = 100 in the tracking and communication modes.

If one decides to use the same source as the transmitter in the above modes, it becomes obvious from above that the power requirement during the communication is more demanding than during tracking.

It can be seen that P_{rcvr} and P_{rcvt} are the detector white noise floor due to the signal bandwidth in the two modes, scaled up by the required SNR.

In any pulse code modulation, we must also remember the pulse height loss due to the finite bandwidth of the detector and the pre-amplifier. Thus,

for estimating the required transmitter pulse for peak power, we also need the effective integration time of the detector-pre-amplifier and must suitable upscale P_{rcvr} again to accommodate for the pulse height loss due to integration.

This is illustrated in the following feasibility study example:

Since low-power laser diodes are easy to modulate, for digital signal communication over optical links, they are the logical choice.

Let us choose a GA-Al-As diode laser, Model # PPl50M-785 manufactured by Opto-Electronics Company. Pertinent data supplied by the manufacturer are:

Peak pulse power, P_{xtrp}	$= 20 \times 10^{-3}$ w
Pulse rise time	= 0.04nsec
Pulse length, T_p	= 0.06nsec
Pulse repetition rate	= 50MHz
(Thus, Pulse period, T	$\geq$ 20nsec

We will assume the operating wavelength

$$\lambda = 0.8\mu m.$$

For the receiver detector, let us choose an Avalanche Photo diode, APD model #C30927 made by RCA Electrooptics. Pertinent data supplied by the manufacturer are:

Peak response wavelength	= 0.9µm
Responsivity, R	= 60 Amp/watt
Quantum efficiency, q	= 0.85
Detector integration time, T_{id}	= 3nsec

We will assume a combined detector-pre-amplifier integration time, T_i = 1 nsec.

Since pulse period of the signal T $\geq$ 20nsec and is larger than T_i, the pulse height loss factor due to integration time of the detector-pre-amplifier α, is

$$\alpha = \frac{T_p}{T_i} = \frac{0.06}{10} = 0.006$$

For receiver and transmitter aperture, let us assume

$$d_{xtr} = 0.03m$$

$$d_{rcv} = 0.1m$$

and one-way transmittance over a 15.3 km range at λ = 0.8µm

$$\tau_p = 0.318\sigma$$

as shown earlier

and optics transmittance,

$$\tau_o = 0.9.$$

The loss factor for this geometry, or the range pattern attenuation from the transmitter to the detector input, β, is

$$\beta = 3.0 \times 10^{-3}.$$

The peak power output of the detector pre-amplifier P_{dp}, is (from the above data)

$$P_{xtrp} \times \beta \times \alpha = P_{dp} = 3.6 \times 10^{-7} \text{ watt} > 10 \text{ times } P_{rcvr}.$$

The pre-amplifier pulse peak output during transmitter 'on' time is approximately a thousand times the amplifier noise floor, implying an effective signal-to-noise ratio (SNR, of 1000 for this configuration using the off-the-shelf components listed above.

4.4 Development of Evaluation Models

Two types of evaluation criteria were selected by ATA:

1) Measures of system performance;
2) Measures of system cost.

4.4.1 Performance Models

Two types of performance models were used:

1) Frequency domain simulation models;
2) Analytical predictions using equations.

4.4.1.1 Frequency Domain Simulation Models

ATA decided upon a beam-jitter-on-target measure of system performance.

ATA used frequency domain simulations to determine various performance factors (e.g., contributions to LOS jitter) of candidate control system configurations. The frequency domain models used a control-system performance-evaluation code, FRQRSP, for Frequency Response Simulation. This tool was used extensively for beam control system performance prediction during the Airborne Laser Laboratory (ALL) program and serves as the basis for several SDI beam control investigations.

The second type of performance models are equations. These equations relate candidate control system performance factors along with other characteristics of the systems to top-level performance factors which can be used directly to quantify the previously selected evaluation criteria; as, for example:

1) Aperture sizes;
2) Distance between the transmitter and receiver;
3) Laser power;
4) Optical efficiency of the transmitter and receiver elements;
5) Transmission of the atmosphere at the laser frequency;
6) Residual jitter of the LOS (i.e., beam jitter as predicted by the FRQRSP code)
7) Type of detection system used by the receiver;
8) Received signal-to-noise ratio (SNR).

The Bit Error Rate (BER) interrelates the most significant optical system parameters. A natural consequence in developing a BER equation is the receiver input signal-to-noise ratio ($\frac{Si}{Ni}$). Here we use these equations to parametrically change several of the critical component values to narrow the design for the optical system. Referring to Figure 4-29, the received power on the detector (P_{RCV}) is proportional to the ratio of the receiver

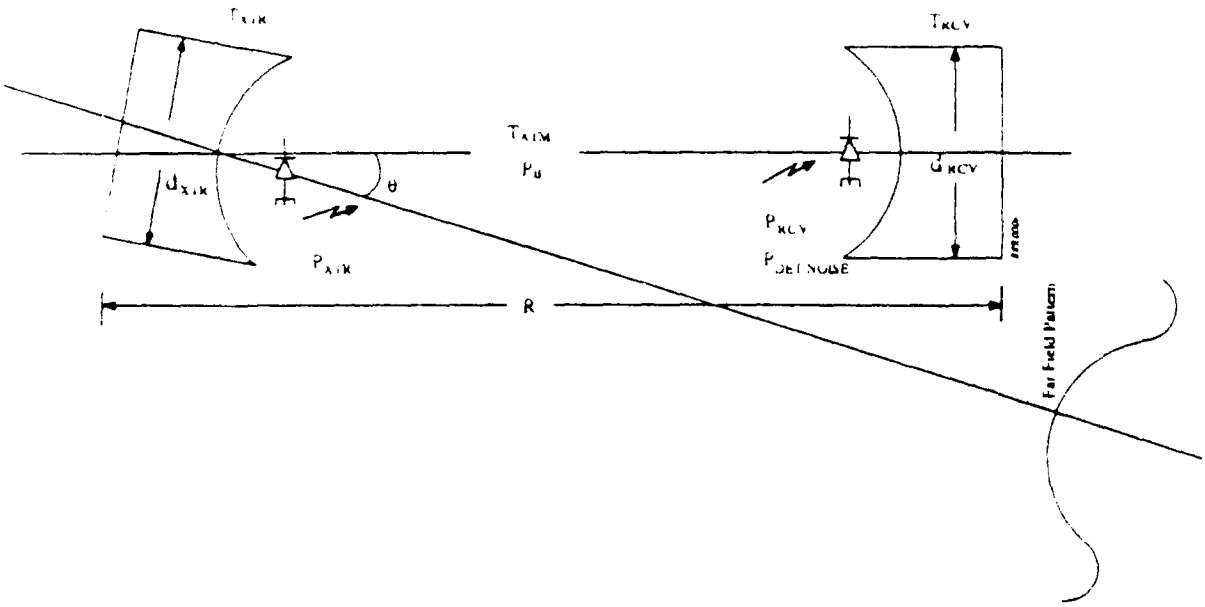

Figure 4- 29. Single Path Communication Parameter Identification

effective area to the transmitter far field radiation pattern. The other factors influencing received power are transmitted power, transmitter modulation efficiency, optical and atmospheric losses and pointing angle offset and jitter. In equation form, the energy per pulse (bit) on the detector from the transmitter is:

$$E_{RCV} = \alpha_{RCV} \cdot P_{XTR} \cdot \tau \cdot T_{XTR} \cdot T_{RCV} \cdot T_{ATM} [W]$$

where:

E_{RCV} = Energy Received per Bit [J]

T_{ATM} = Atmosphere Transmission

T_{RCV} = Receiver Optical Transmission

T_{XTR} = Transmitter Optical Transmission

τ = Pulse Width [S]

P_{XTR} = Transmitter Peak Power [W]

α_{RCV} = Fractional Energy Incident upon Receiver.

Here the far field pattern is assumed to be a two-dimensional Gaussian distribution about some off-axis pointing error angle θ, at range R, transmission aperture diameter d_{xtr} and effective beam width defined by σx and σy. For the far field pattern of the form:

$$\frac{1}{2\pi\sigma_x\sigma_y} e^{-1/2 \frac{(x-\bar{x})^2}{\sigma_x^2}} e^{-1/2 \frac{(y-\bar{y})^2}{\sigma_y^2}} d_x d_y .$$

We have 86% of the energy contained in $2\sigma_{xa}$ and $2\sigma_{ya}$, and assuming 5x diffraction limited optics:

$$5 \cdot R \left(\frac{1.22\lambda}{d_{XTR}}\right) \equiv 2\sigma_{xa} \equiv 2\sigma_{ya}$$

where:

R = Range between Transmitter and Receiver [m]

λ = Wave length of Transmitter [m]

d_{XTR} = Transmitter Aperture diameter [m]

$2\sigma_{xa}$ = Effective Airy disc null at Receiver with no x-axis jitter [m]

$2\sigma_{ya}$ = Effective Airy disc null in y-direction of Receiver with no y-axis jitter [m]

For an effective transmitter pointing error angle of θ, the center of the far field pattern will be $R \cdot \theta$ meters from the receiver center boresite. Because of the x and y symmetry, the direction off-axis is irrelevant and for computational simplicity we assume off-axis only from the y-axis (y=0). Refer to Figure 4-30 for the x-y axis coordinate system. Introducing x and y axis effective line-of-sight jitter, due to the platform base motion, atmospheric disturbances, etc.,

$$R\theta = \bar{x}$$

we have a far field pattern of:

$$FF(\theta, \sigma_{xjit}, \sigma_{yjit}, R, d_{XTR}, \lambda) = \left(\frac{1}{2\pi\sigma_x\sigma_y} e^{-1/2 \frac{(x-\bar{x})^2}{\sigma_x^2}} e^{-1/2 \frac{(y-\bar{y})^2}{\sigma_y^2}}\right)$$

where:

$$\sigma_x = \sqrt{\left(\frac{5R}{2}\left(\frac{1.22\lambda}{d_{XTR}}\right)\right)^2 + \sigma_{xjit}^2}$$

$$\sigma_y = \sqrt{\left(\frac{5R}{2}\left(\frac{1.22\lambda}{d_{XTR}}\right)\right)^2 + \sigma_{yjit}^2}$$

$\bar{x}$ = $\theta \cdot R$ = pointing error offset

σ_{xjit} = x-axis LOS jitter

σ_{yjit} = y-axis LOS jitter

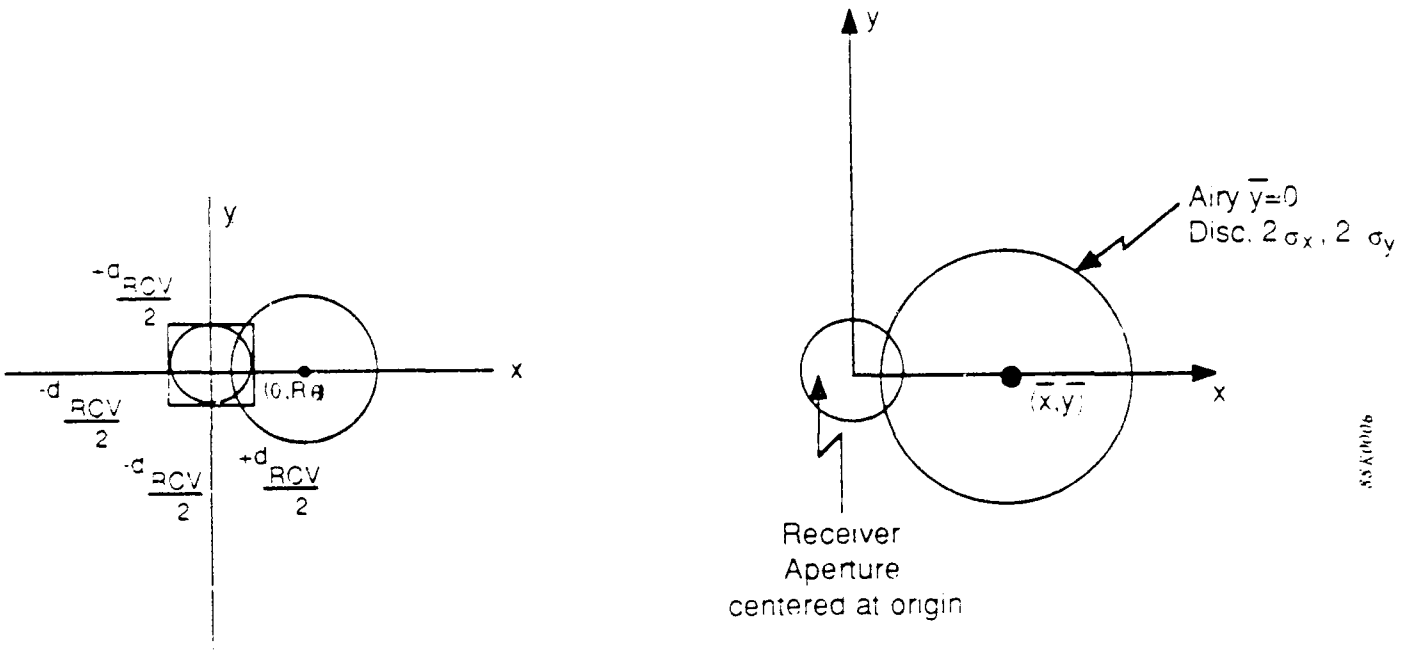

Figure 4-30. Receiver x-y Coordinate System

approximating the receiver aperture as a square simplifies the integration limits. With a receiver diameter of d_{RCV}, we have the receiver-collection coefficient α:

$$\alpha_{RCV} = \iint FF(\theta, \sigma_{xjit}, \sigma_{yjit}, R, d_{XTR}, \lambda) d_x d_y =$$

$$\int_{y=\frac{-d_{RCV}}{2}}^{\frac{d_{RCV}}{2}} \int_{x=\frac{-d_{RCV}}{2}}^{\frac{d_{RCV}}{2}} FF(\theta, \sigma_{xjit}, \sigma_{yjit}, R, d_{XTR}, \lambda)\, d_x d_y \quad \text{(equation *1)}$$

To arrive at a bit error probability, we need to calculate the noise power spectrum of the receiver output. Using Peebles Bit Error Probability solution for Amplitude Shift Keying (ASK) modulation we have:

$$P_E = \frac{1}{2} \operatorname{erfc}\left[\sqrt{\frac{\varepsilon}{2}}\right], \text{ for ASK}$$

$$P_E = \frac{1}{2}\left(1 - \frac{1}{\sqrt{2\pi\varepsilon}}\right) \exp\left[\left(\frac{-\varepsilon}{2}\right)\right], \text{ for noncoherent ASK}$$

where:

$\varepsilon = \frac{\eta_{DET} E_{RCV}}{\eta_o}$ is the energy per bit divided by twice the input noise spectral density

and

$$\frac{\eta_o}{2} = \frac{P_B}{w_{ch}} + \frac{P_{on}}{w_{ch}}$$

(Peebles, page 364) is Gaussian white noise input with power density $\frac{\eta_o}{2}$.

Here P_B is the background scattering power due to atmospheric conditions and solar flux. w_{ch} is the channel bandwidth of the communication system, and P_{on} is the detector output noise.

Combining items, we have:

$$\varepsilon = \frac{\eta_{DET} E_{RCV} \tau_{ch}}{2 (P_B + P_{on})}$$

where:

$$P_{ON} = \frac{2\eta_{DET}(Ge)^2(P_S+P_B)BR_L F}{h\nu} + 4kTB + P_{drk}$$

(from page 124 of Laser Satellite Communication)

where:

G = Avalanche Photodiode (APD) Detector Gain

ε = One Electron Volt [J]

η_{DET} = Detector Efficiency

P_B = Background Solar Power [w]

B = Bandwidth of the System [Hz]

R_L = Load Resistor [ohms]

F = Noise Factor

$h\nu$ = Energy in one Photon, Wavelength λ [J]

4kTB = Load Resistor Johnson noise [w]

P_{on} = Output Noise of Detector - Resistor Circuit [w]

P_s = Signal Power incident on Detector [w]

P_{drk} = Detector dark current noise power [w]

For ASK, assuming no separation between pulses and a channel bandwidth

$$B = \frac{\pi}{\tau}$$

we have the input signal-to-noise ratio to the ASK receiver demodulator as (Peebles, page 364-371):

$$\left(\frac{Si}{Ni}\right) = 2\varepsilon$$

that is, twice the average energy per bit per Hertz the noise power density.

We now show the graphical relationship of the input signal-to-noise ratio $(\frac{S_i}{N_i})$ versus the bit error rate P_E for an ASK (See Fig. 4-31).

Numerically integrating the appropriate equations, we arrive at a set of curves relating the optical system parameters to the input SNR. In examining Figure 4-32, it can be seen that at relatively small aperture sizes <1" cm, signal-to-noise ratios are quite acceptable in obtaining bit error rates less than 10^{-6} (using Figure 4-29 to relate bit error probability to SNR). Furthermore, the l mw of solar background power effects the SNR by less than 1 dB. The solar background of 1 nanowatt is a worst case rough order of magnitude estimate assuming no glints or direct line-of-sight with the sun and receiver (Deirmendjian). The values of the optical system parameters can be found at the end of this section.

We now show the $(\frac{S_i}{N_i})$ - ratio from the reflected power of a retro-reflector mounted on the receiving ship with a retro-reflector of aperture diameter d_{RR}. The reflected power from the retro is directed back toward the transmitter, but with the retro's far field pattern centered on the reflection receiver. We have as:

$$E_{RCV_{RR}} = \alpha_{RCV_{PR}} \cdot \alpha_{RR} \cdot P_{XTR} \cdot \tau \cdot T_{XTR} \cdot T_{PR} \cdot T_{RCV} \cdot T^2_{ATm} \quad [J]$$

where:

$$\alpha_{RCV_{PR}} = \iint_{x,y=\frac{-d_{PR}}{2}}^{+d_{RR}} FF(\theta, \sigma_{xjit}, \sigma_{yjit}, R, d_{XTR}, \lambda)\, d_x d_y \quad \text{(equation *2)}$$

and,

$$\alpha_{RR} = \iint_{x,y=\frac{-d_{RCV}}{2}}^{+d_{PCV}} FF(\theta=0, \sigma_{xjit}, \sigma_{yjit}, R, d_{RR}, \lambda)\, d_x d_y \quad \text{(equation *3)}$$

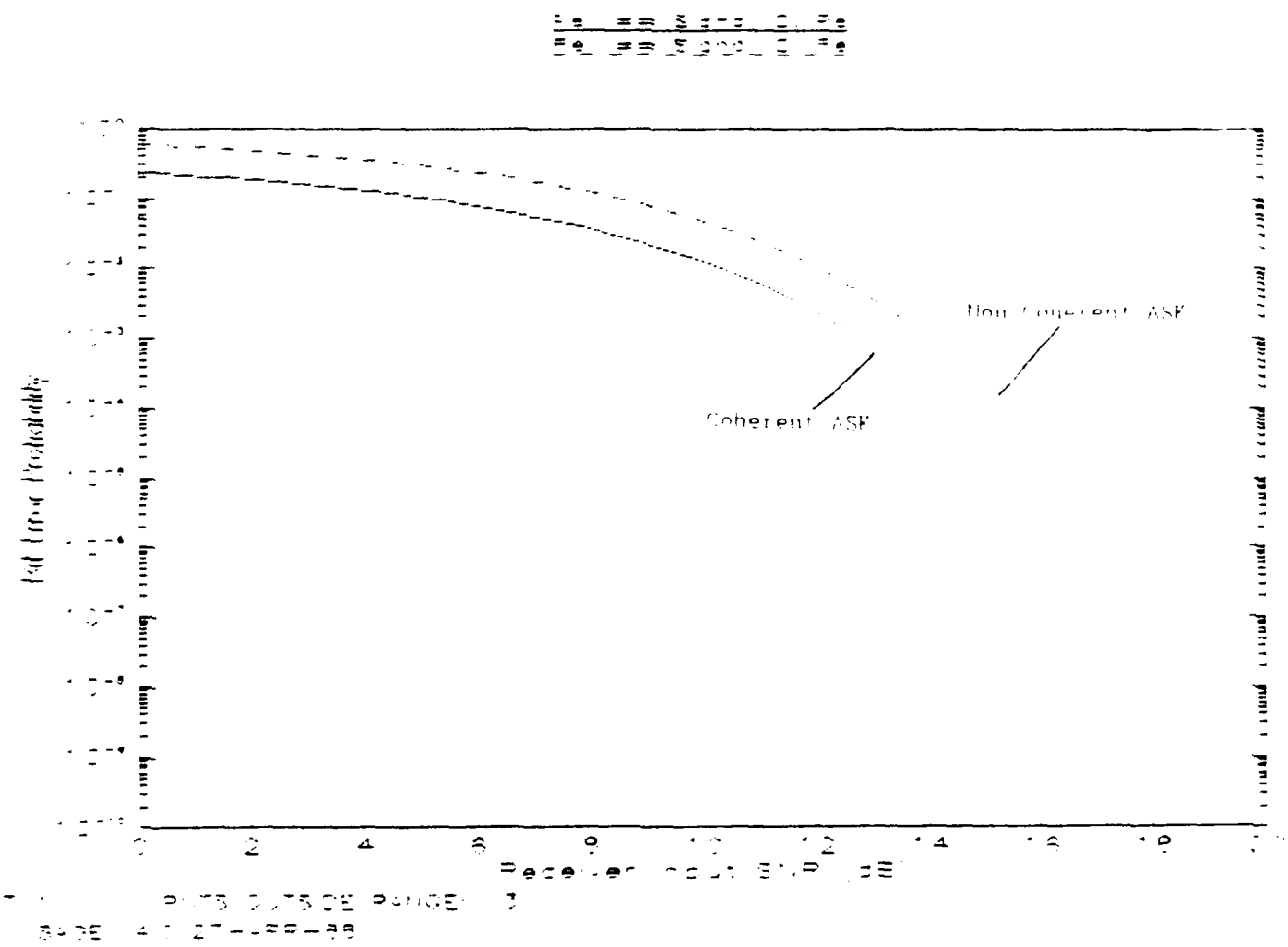

Figure 4-31. Bit Error Probability for a Given SNR

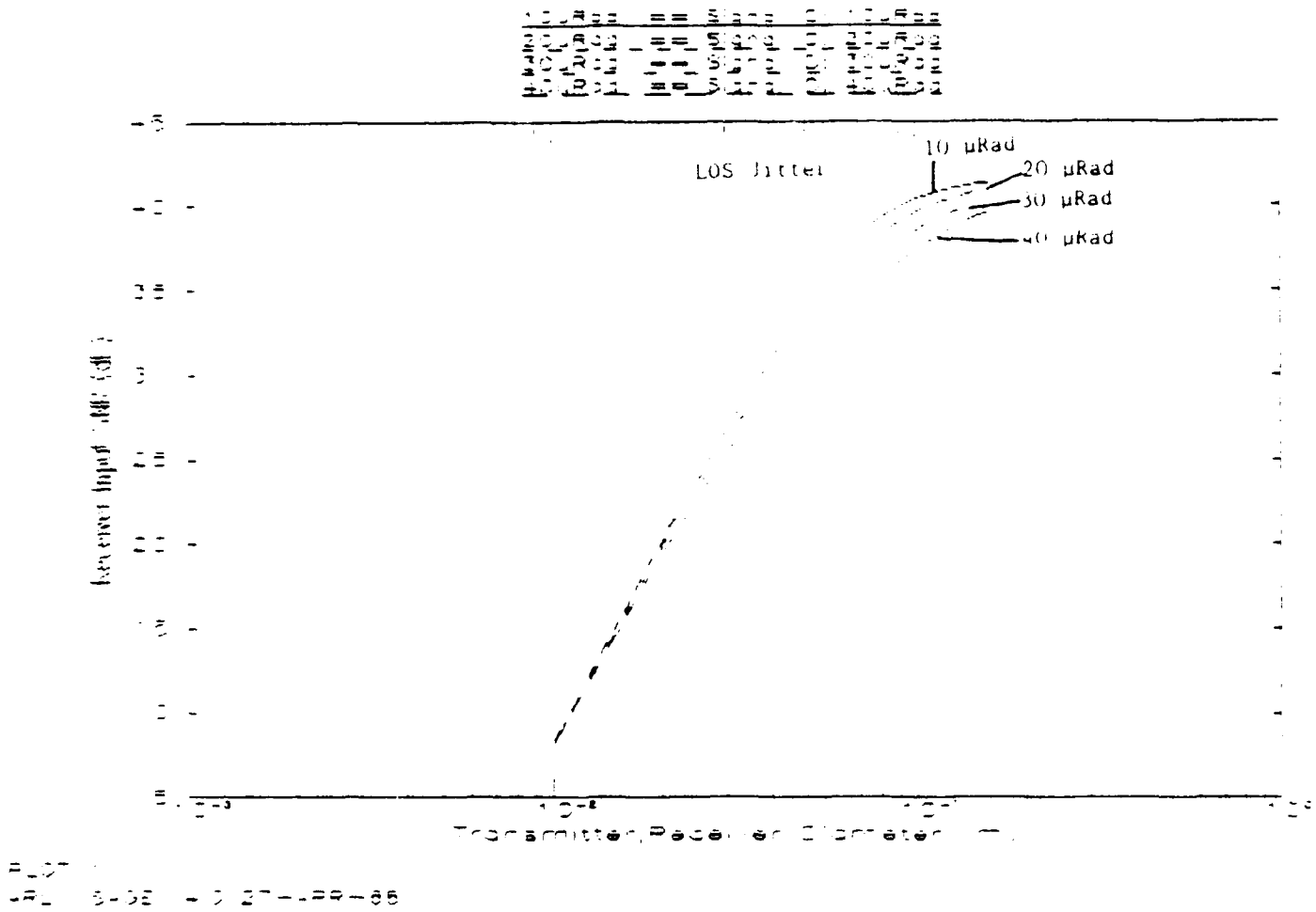

Figure 4-32. One-way Transmission SNR: 10 μrad Pointing Error Offset

and therefore, the $\frac{Si}{Ni}$ for the reflector receiver is:

$$\frac{Si}{Ni} = \frac{\eta_{DET} \cdot E_{RCV_{RR}} \cdot W_{ch}}{P_B + P_{on}} .$$

Again, numerically integrating appropriate equations we can show a graphical relationship between the optical system parameters and the SNR. As expected, as we increased the transmitter/receiver diameter, the amount of energy captured from the retro increases which boosts the SNR. However, by inspecting Figures 4-33 and 4-34, we see that for the large optics we may have a tracking problem with the low SNR values when the line-of-sight (LOS) jitter is above 30 μrad.

A caveat is in store in reference to the atmospheric attenuation used. Here, the transmittance is 0.1983 over the 16 km path length, which is only a rough order of magnitude estimation. Here, because the path length is twice the ship separation (to the retro and back) the effective atmospheric transmittance is about 4%. With different conditions orders of magnitude of change in SNR can be expected.

The values used for both one-way and reflected energies use the following constants:

$\lambda = 0.50 \cdot 10^{-6}$ m

$\tau = 10 \cdot 10^{-9}$ s

$T_{ATm} = 0.1983$

$T_{RCV} = 0.7$

$T_{XTR} = 0.7$

$T_{RR} = 0.8$

$P_{XTR} = 0.040$ W

$R = 16 \cdot 10^{3}$ m

$\theta = 10 \cdot 10^{-6}$ rad

$W_{ch} = B = \frac{\pi}{\tau}$ Hz

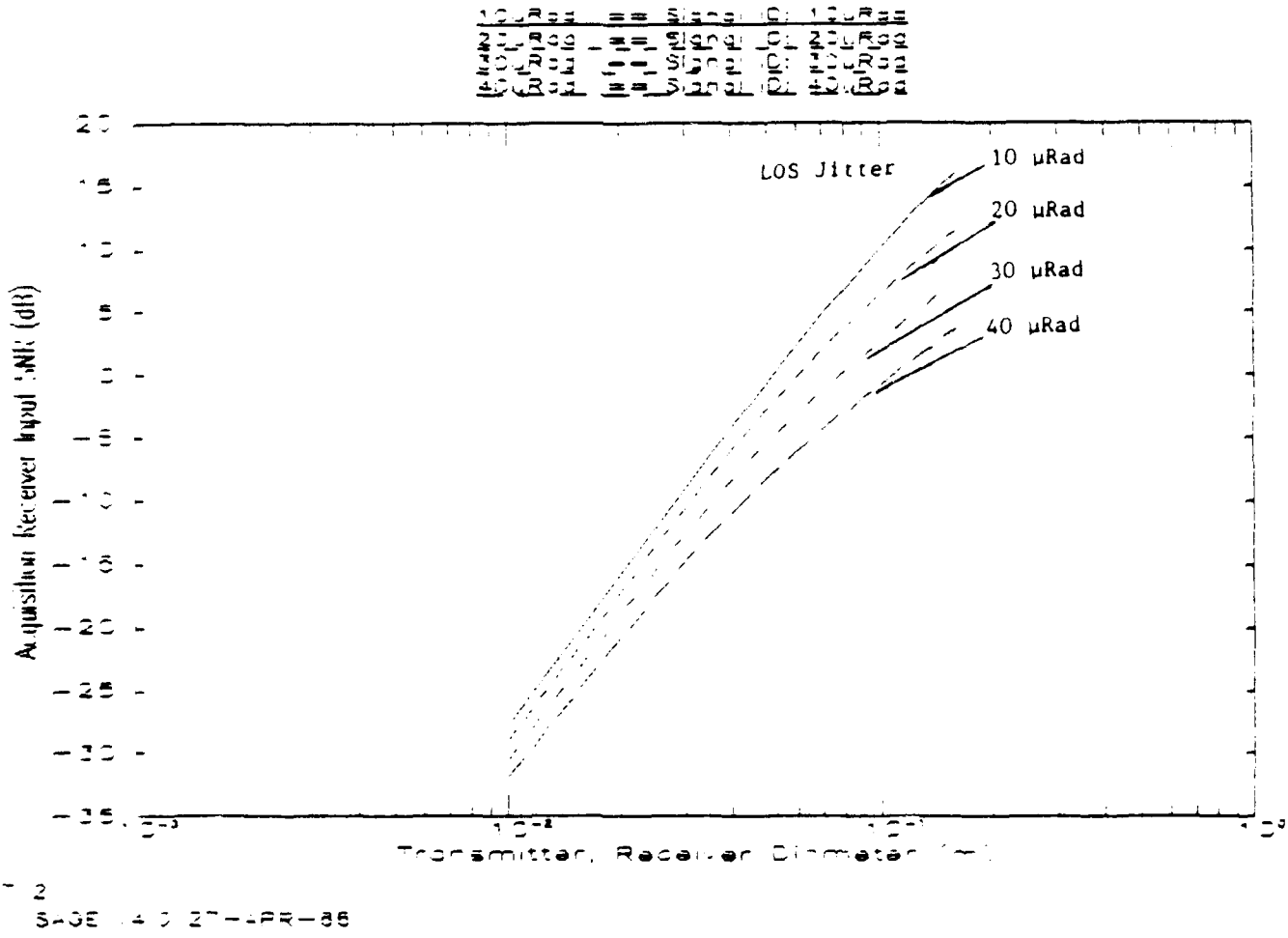

Figure 33. Reflected Signal SNR: 25 cm^2 Retro, 10 µrad Pointing Error Offset

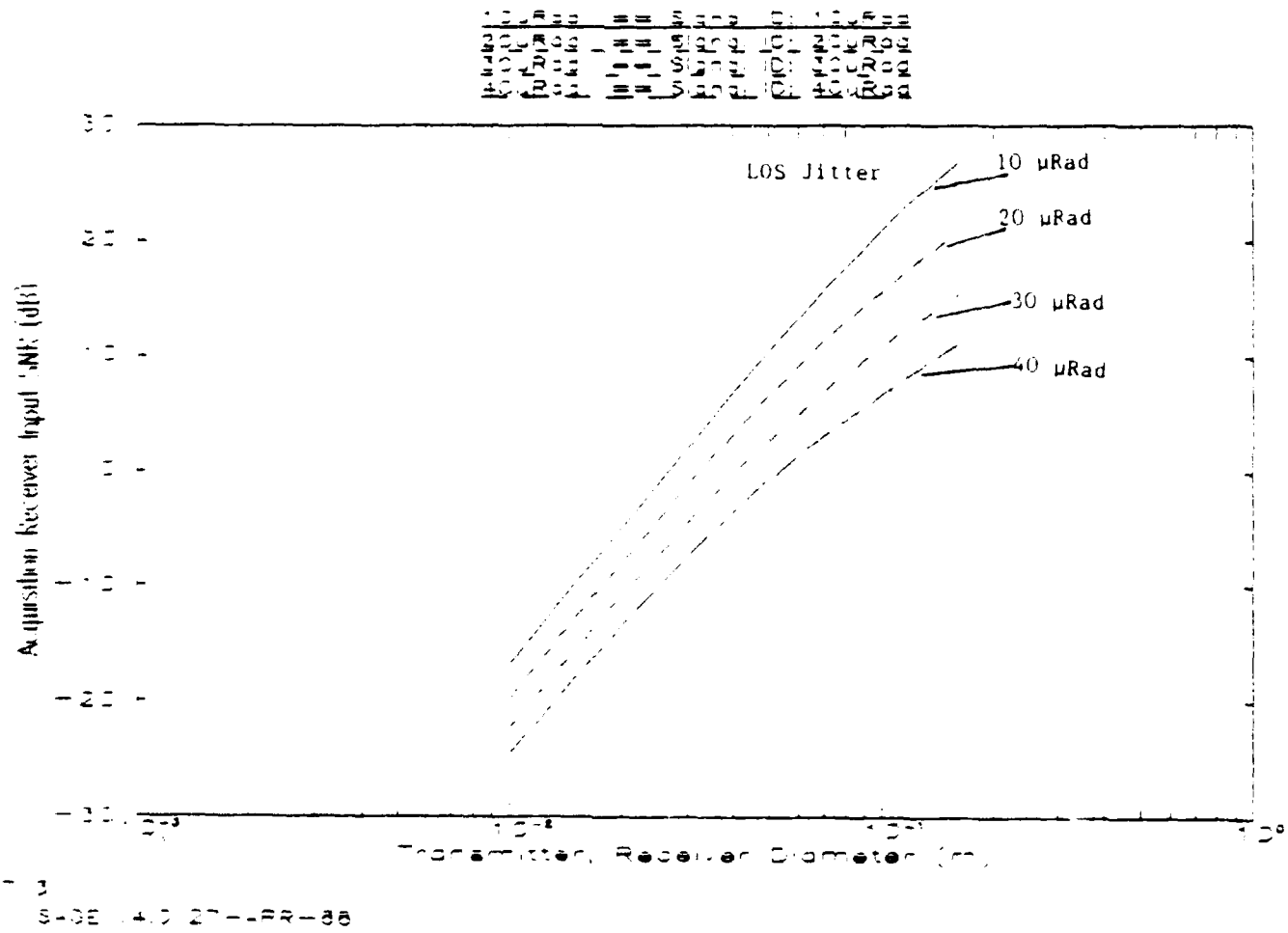

Figure 34. Reflected Signal SNR: 100 cm^2 Retro, 10 μrad Pointing Error Offset

η_{DET} = 0.6

F = 2.6 (Detector Noise Factor)

R_L = 50 Ω

T = 300° K

G = 200

$P_{dark} = 10^{-13} \cdot \sqrt{B}$

4.5 Evaluation of the System

The execution of the FRQRSP models provided the data needed to rank the system.

Figure 4-35 shows the Single Axis Model of Pointing Tracking System.

ATA used this model developed for Ball pointing and tracking experiment and input base motion and LOS disturbances and ran the model to achieve a residual track error of 3 nanoradians rms which is more than adequate.

Since these base motion and LOS disturbances did not contain high frequency disturbances, the spectrum shown in Figure 4-13 was used to provide more realistic high frequency disturbances.

4.6 Servo Model/Performance Estimation

Servo model/performance predictions are summarized in the following figures:

Figure 4-36 Nested Servo Block Diagram
Figure 4-37 Frequency Response Characteristics for 15 Hz Gimbal Servo
Figure 4-38 Frequency Response Characteristics for 350 Hz Fast Steering Mirror Servo
Figure 4-39 Frequency Response Characteristics for 15 Hz Gimbal and 350 Hz FSM
Figure 4-40 Baseline Nested Servos - LOS Disturbance Rejection
Figure 4-41 Baseline Nested Servos - LOS Input Cumulative RMS
Figure 4-42 Baseline Nested Servos Residual LOS Jitter Cumulative RMS
Figure 4-43 Baseline Nested Servos LOS Input Disturbance and Residual Jitter
Figure 4-44 Nested Servo Performance Summary 15 Hz Gimbal Servo/350 Hz FSM Servo

ATA, as a result of its analyses, concluded that:

1) Nested servo with typical bandwidths provides 10 microrad LOS stability;
2) Low-frequency induced motions are handled easily;
3) When a high-frequency disturbance envelope is selected, nested servos handle the envelope to 10 microrads with equal frequency power in error;
4) There is a choice of various implementation options.

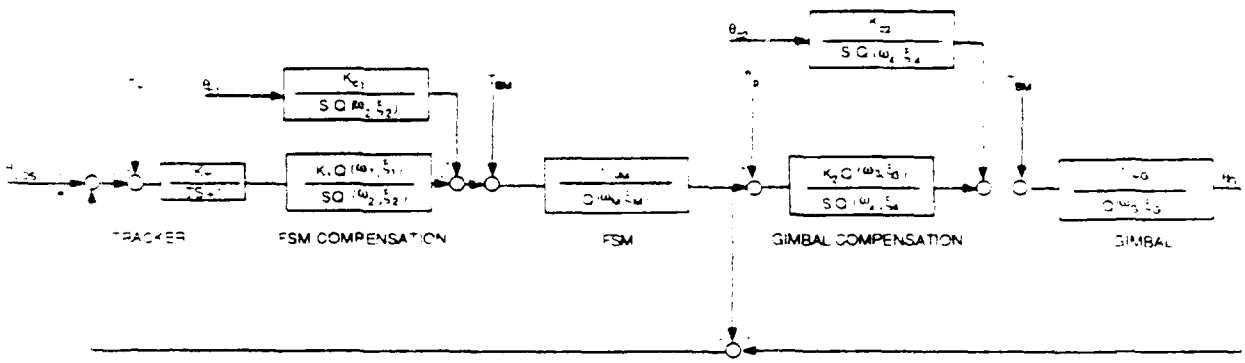

Figure 4-35. Single Axis Model of Pointing/Tracking System

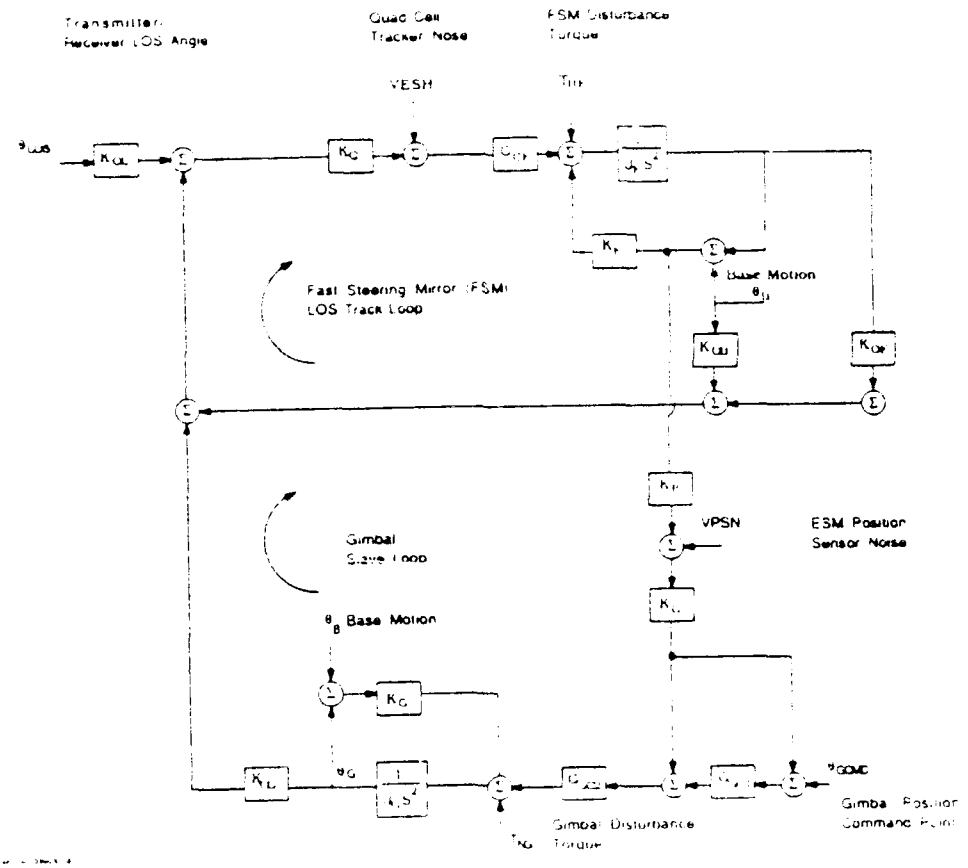

Figure 4-36. Nested Servo Block Diagram

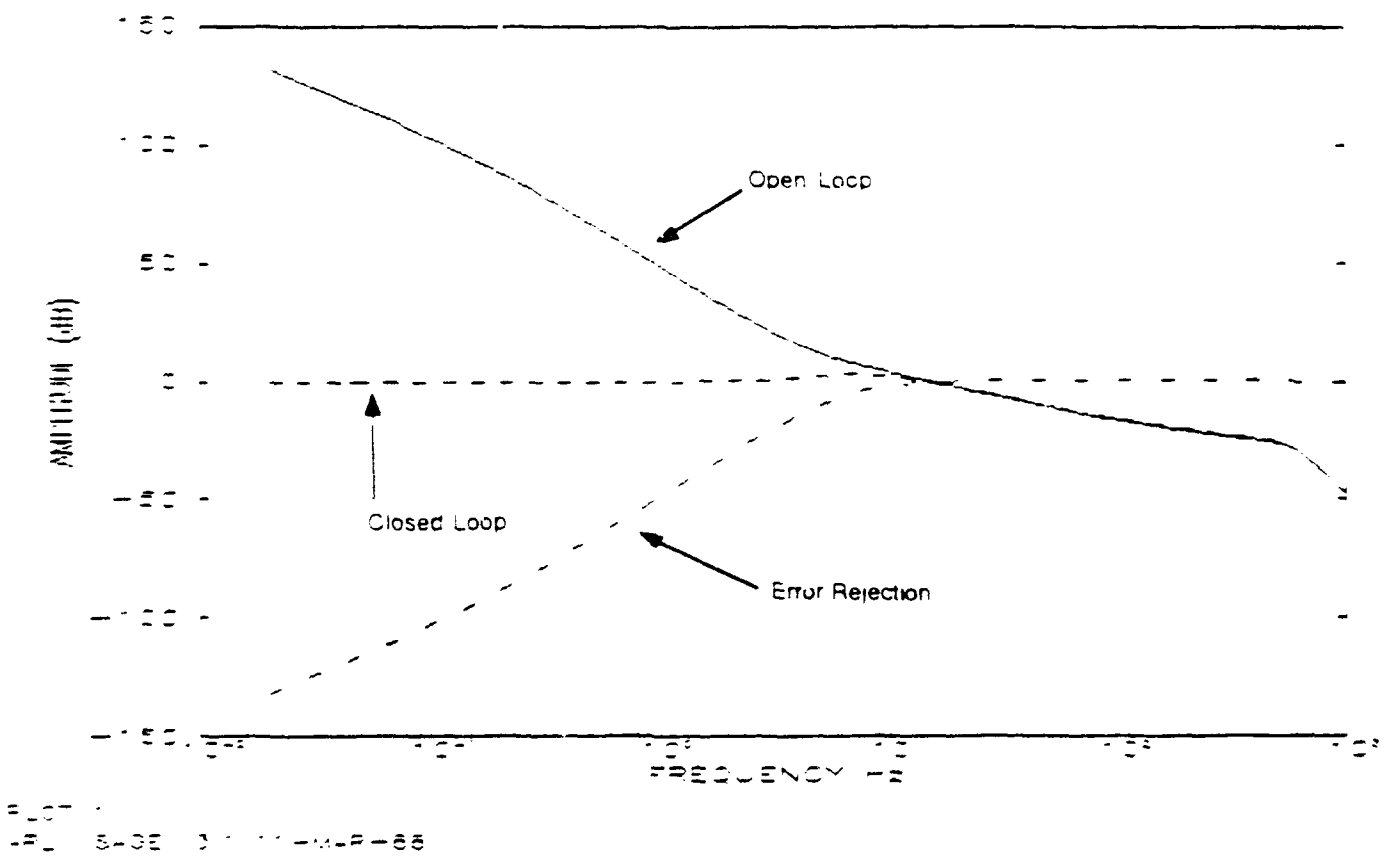

Figure 4-37. Frequency Response Characteristics for 15 Hz Gimbal Servo

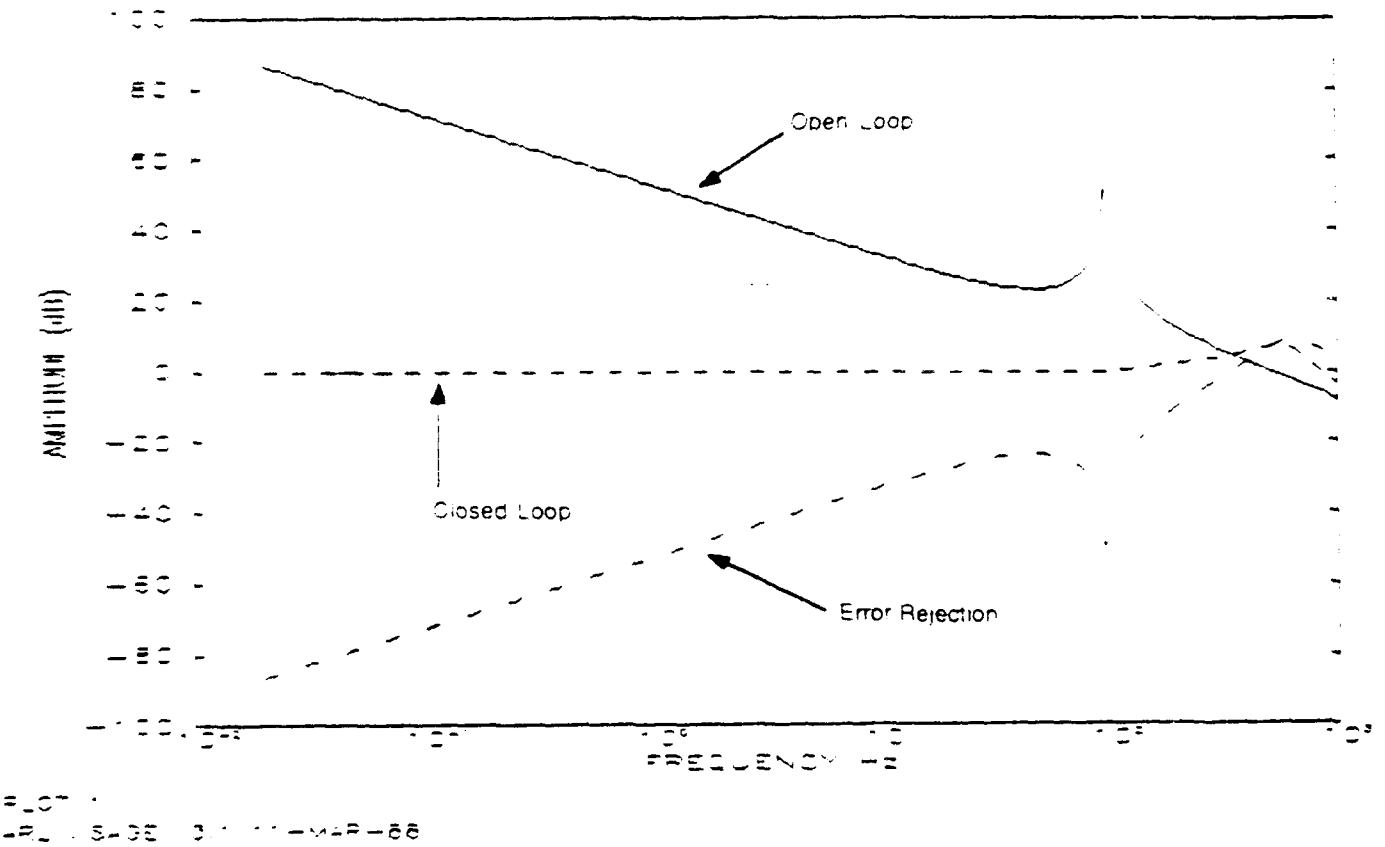

Figure 4-38. Frequency Response Characteristics for 350 Hz Fast Steering Mirror Servo

AD-A202 921

NAVAL OCEAN SYSTEMS CENTER, SAN DIEGO, CA
LOW-COST POINTING-AND-TRACKING SYSTEM FOR OPTICAL COMMUNICATIONS (PATSOC) BY: KH JOYCE

2 OF 2
NOSC TD 1287
UNCLASSIFIED
JUN 1988

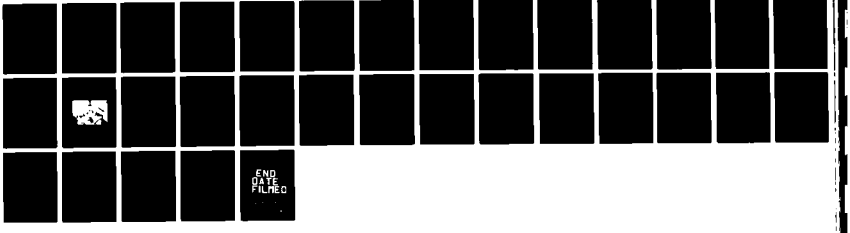

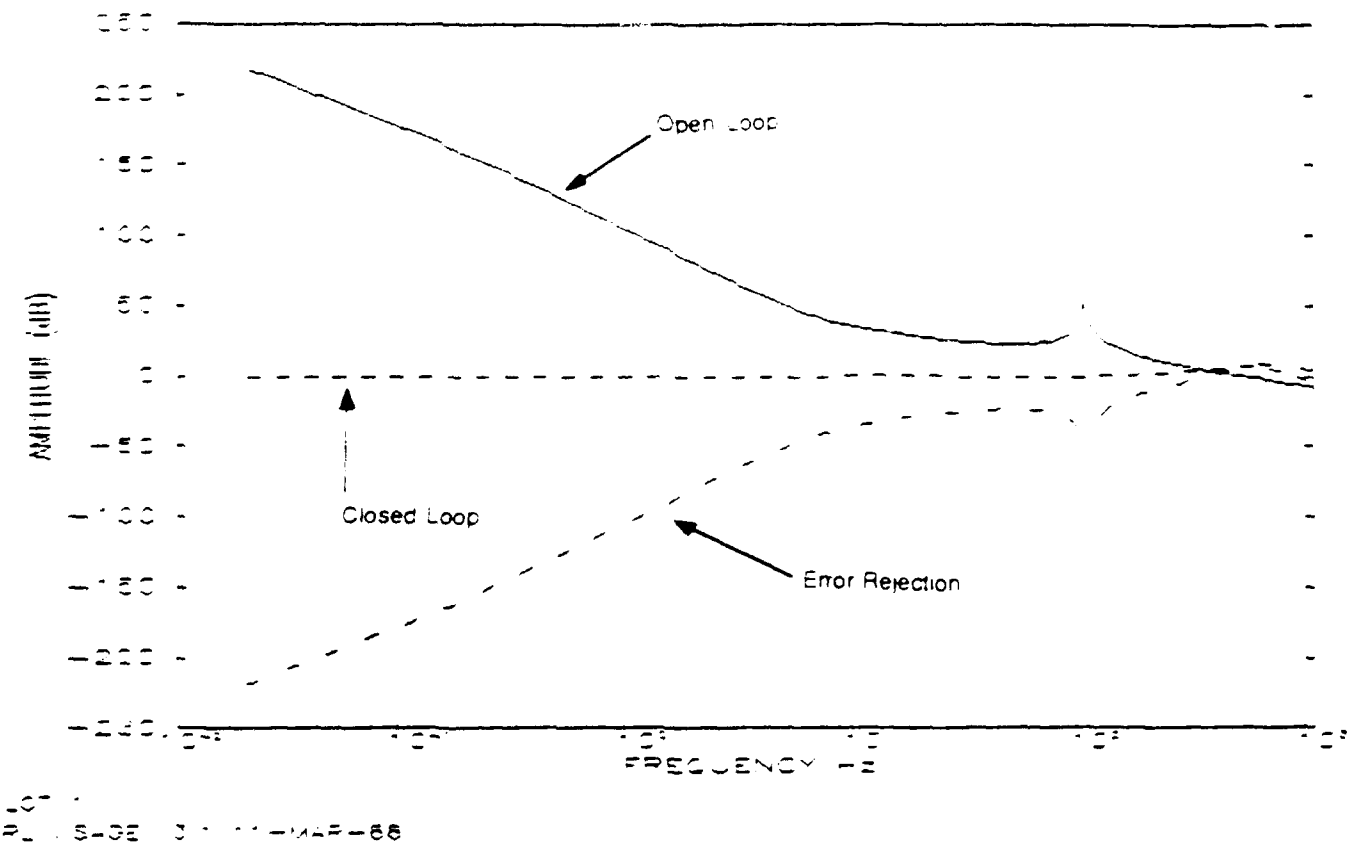

Figure 4-39. Frequency Response Characteristics for 15 Hz Gimbal and 350 Hz FSM

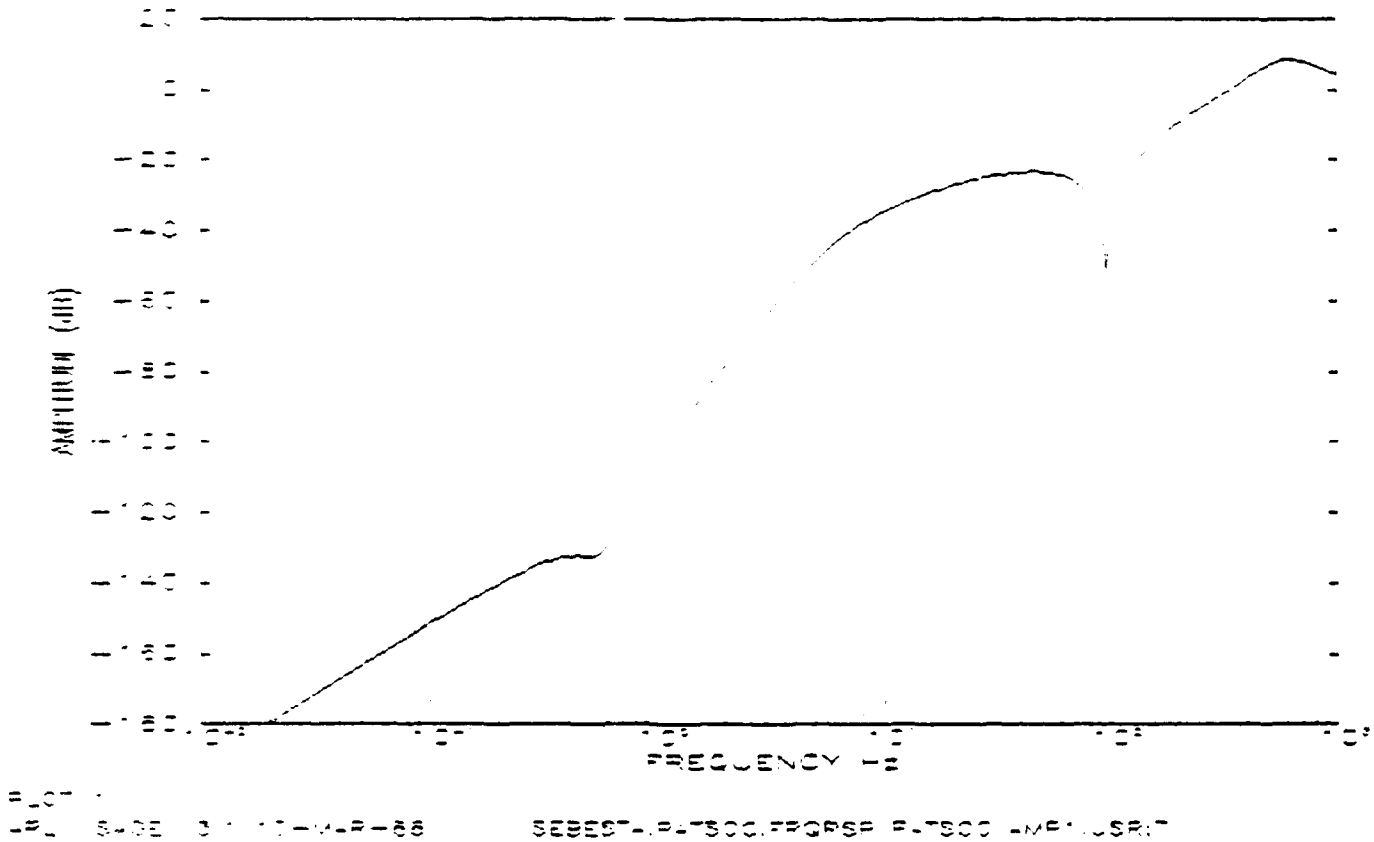

Figure 4-40. Baseline Nested Servos - LOS

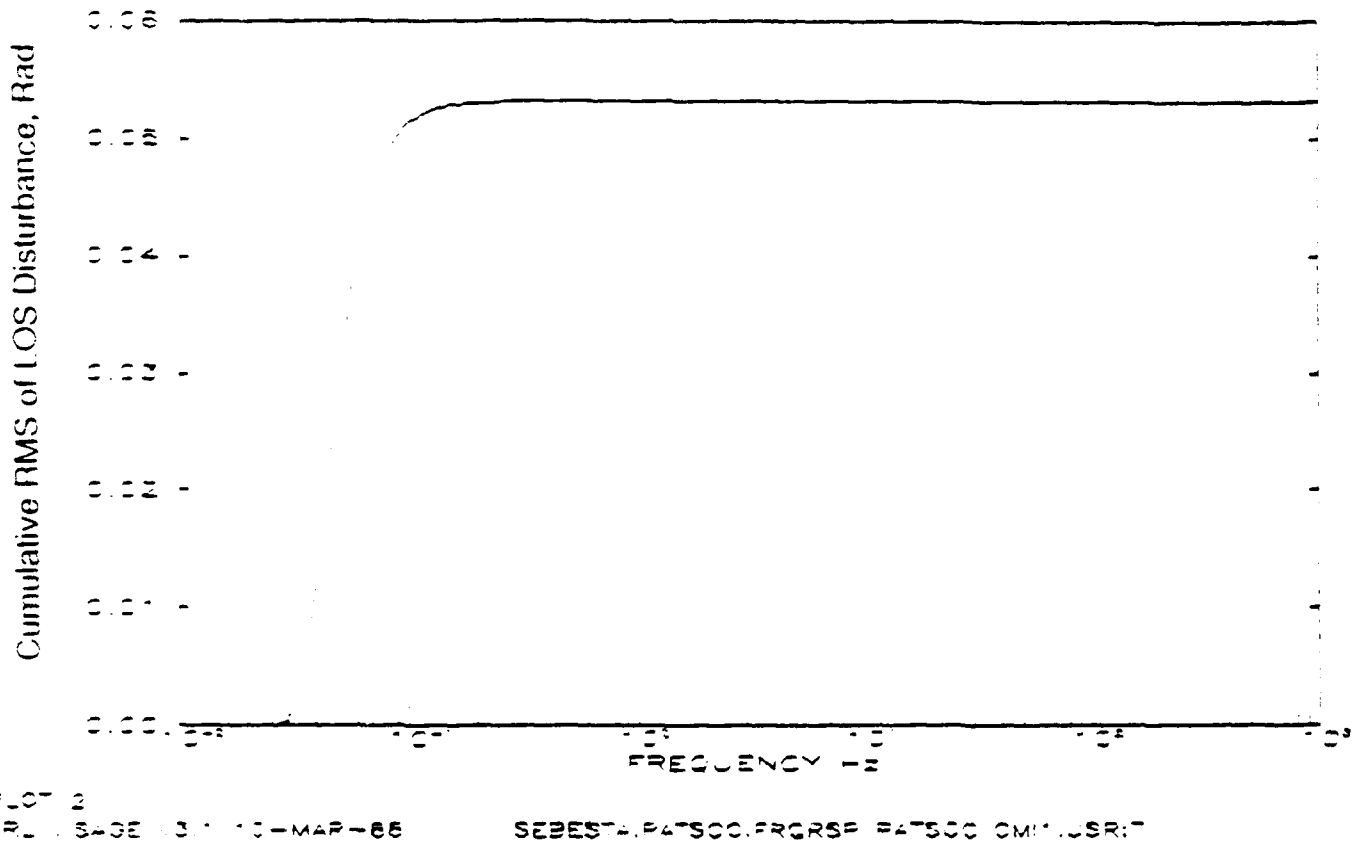

Figure 4-41. Baseline Nested Servos - LOS Input CUM RMS

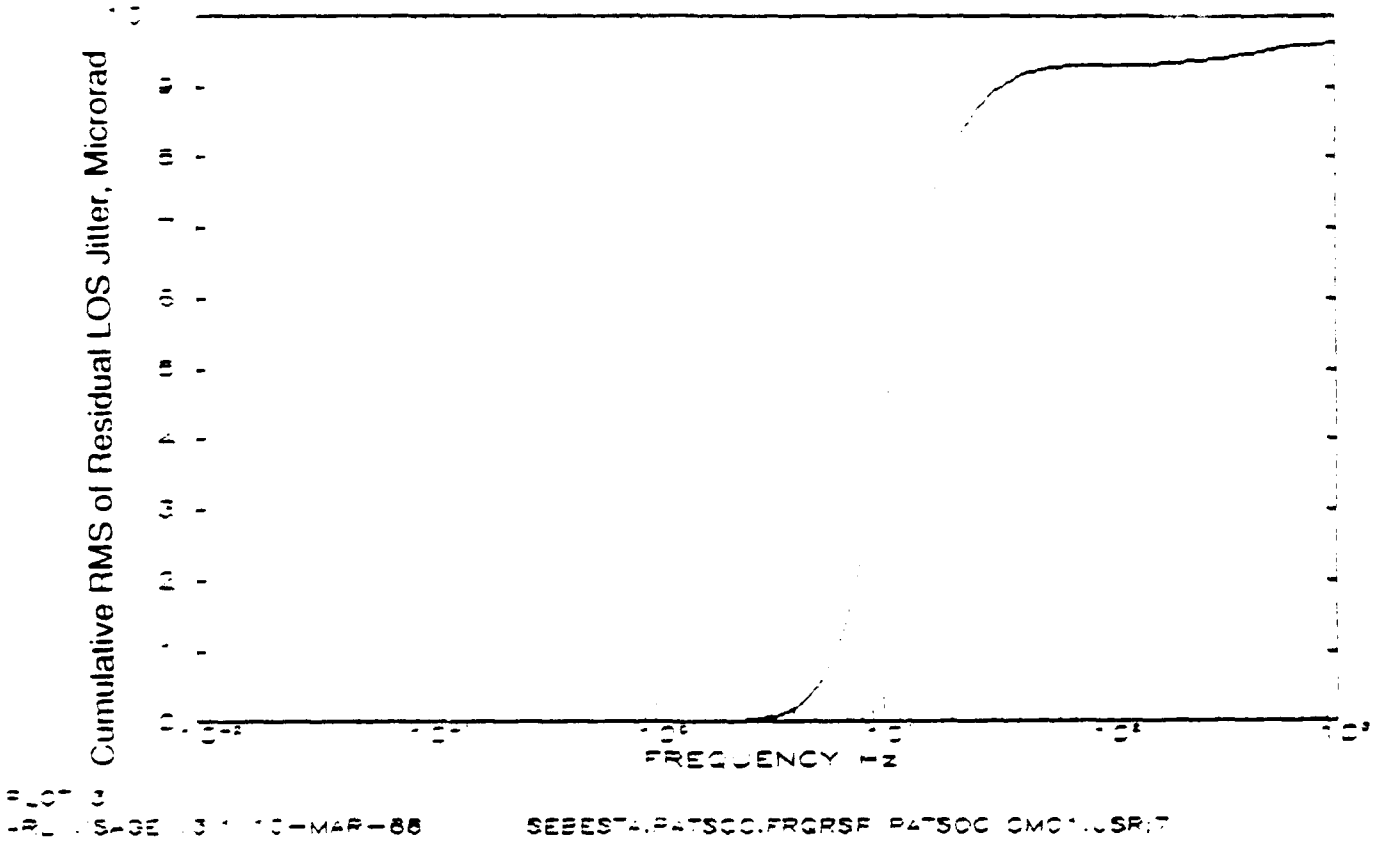

Figure 4-42. Baseline Nested Servos Residual LOS Jitter Cumulative RMS

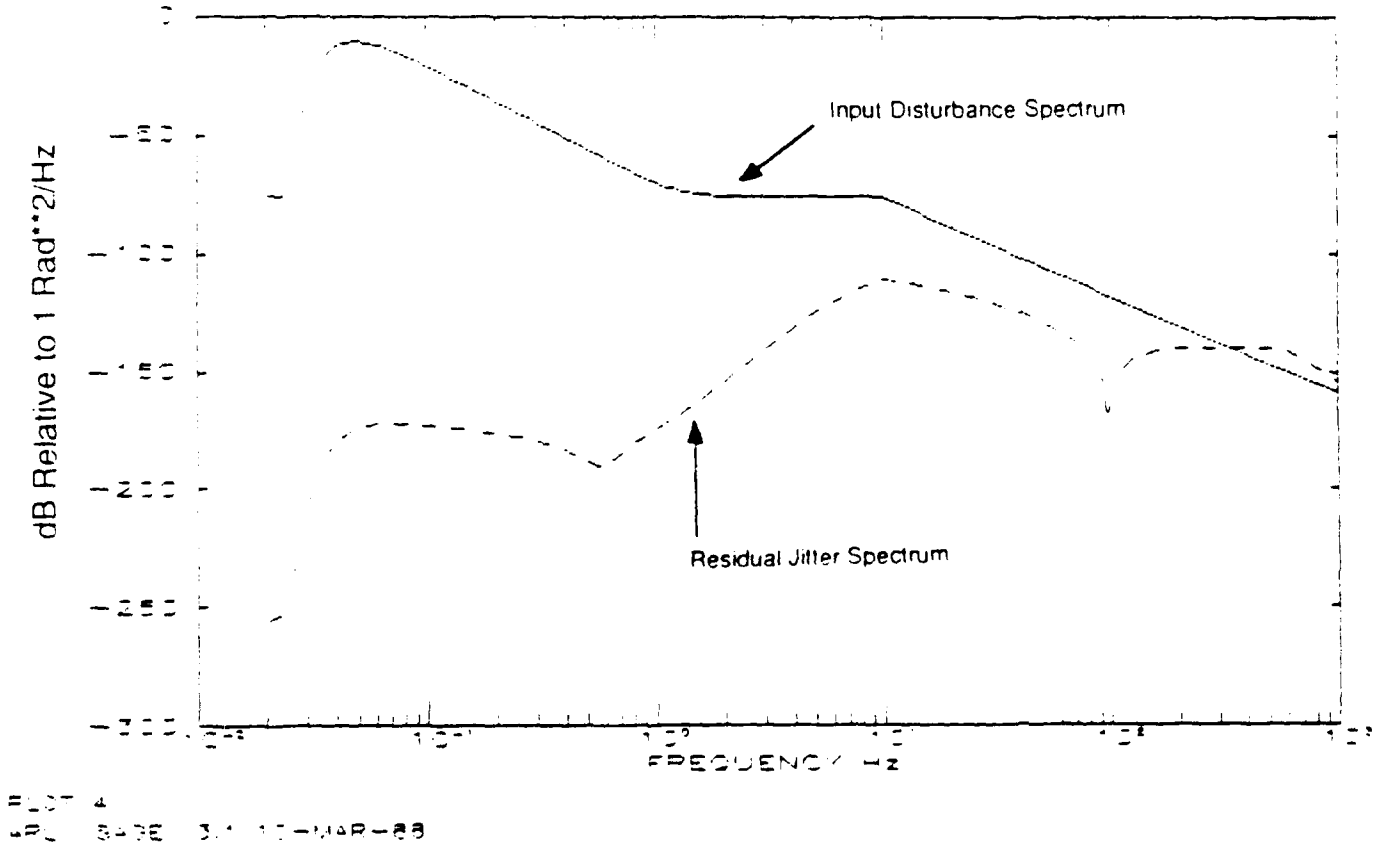

Figure 4-43. Baseline Nested Servos LOS Input Disturbance and Residual Jitter

ATA

NESTED SERVO PERFORMANCE SUMMARY
15 HZ GIMBAL SERVO/350 HZ FSM SERVO

BANDWIDTH (Hz)

	0.02 - 1	1 - 10	10 - 100	100 - 1000	Total (0.02-1000)
LOS Input	53 mrad	0.48 mrad	66 µrad	6 µrad	53.1 mrad
LOS Residual	0	4.4 µrad	8.2 µrad	2.4 µrad	9.6 µrad
FSM Angle	0.11 mrad	6.3 mrad	6.4 mrad	0.2 mrad	9.0 mrad

Figure 4-44. Nested Servo Performance Summary 15 Hz Gimbal Servo/350 Hz FSM Servo

5.0 OPTICAL SYSTEM

5.1 Laser and Optical Detectors

ATA is currently considering two types of lasers to be used as a beacon (see Figure 5-1). Specifically, they are GaAs type semiconductor laser diodes and a solid state Nd:YAG. Because of the proposed shared aperture system, we must also base the decision as to which laser to use on the suitability of the beacon laser to also be the transmitter laser.

- Semiconductor Diode Laser - GaAs Type. CW/Pulse Mode Operation
  - Small
  - Fairly Efficient
  - Potential for Long Lifetime
  - Inexpensive
  - Can be Directly Modulated by Varying Input Current
- Solid State ND:YAG Laser. CW/Pulse Mode Operation
  - Offers Higher CW Power Than Diode Laser, but Larger Than Diode Laser in Size
  - Can be Pumped by Diode Laser
  - Modulated via Q Switching or Cavity Dumping

Figure 5-1. Laser Options

GaAs lasers operate around 0.8 micrometer. They are small, fairly efficient and have demonstrated the potential for long lifetimes in accelerated lab tests. An advantage of the GaAs laser is that it can be directly modulated by varying the input current to the diode. Thus, it can be pulsed fast enough to achieve the required data rates.

Nd:YAG lasers operate around 1.06 micrometers. Although somewhat larger than diode lasers, Nd:YAG offer more power and a more collimated beam which means more power in the far-field at the antenna. The Nd:YAG is modulated via "Q" switching and/or cavity dumping. It is capable of high data rates (200 Mbits/sec). The Nd:YAG laser may be either flashed or diode pumped. A diode pumped Nd:YAG would make the most sense here in terms of size and longevity.

Attenuation of the beam power by absorption in the sea mist must be considered. The optimal wavelength for minimum attenuation resides around 0.45 micrometer. By frequency doubling either the diode or Nd:YAG laser, we can reduce the absorption by nearly two orders of magnitude from their natural values.

ATA recommends the use of the diode laser because of its simplicity of operation and small size.

ATA has investigated a diode-laser-pumped monolithic Nd:YAG crystal, presently being developed and used by Stanford University, for use as the Master Oscillator. This new laser has three advantages:

1) Extremely compact;
2) Stable frequency during operation;
3) Possible to finely tune the output frequency of the laser via controlling the temperature of the crystal. The tunability of the laser would allow easy multiplexing of the communication by allowing receiving, transmitting, and tracking to be done at unique wavelengths.

Figure 5-2 shows this design. This configuration may offer an attractive alternative in the future.

A number of vendors were contacted for information on optical detectors and laser sources for this project. ATA recommends the use of a silicon avalanche photodiode (APD) as the optimum detector because of its high responsitivity at the proposed laser wavelength. Specifically, this is the silicon APD model C30927 made by RCA Electroptics which is suitable over a wavelength band of 0.4-1.1 microns. The specifications for model C30927 are as follows:

Diameter	1.5mm
Peak Response	0.9 microns
Responsitivity	60 Amps/Watt
Quantum Efficiency	85%
Detector Integration Time	3.0 nanoseconds

Quantity	Approximate Cost
1-24	$1100
25-99	$1020

Additionally, a search was made for a GaAs-type laser source. A number of diode lasers made by Opto Electronics will satisfy the power and repetition rate requirements. They are all pulsed GaAlAs multimode diode lasers. The model numbers are PPL50M850, PP150M785, and PPL50M820, which operate at wavelengths of 0.85, 0.785, and .82 microns respectively.

All the models have the following specifications:

Linewidth	.5 nm
Peak Power	>20mW
Pulse Length	0.06 nm
Rise Time	0.04 nsec
Repetition Rate	50 MHz
Operating Temperatures	15-30 degrees C

The approximate cost of each laser is $7000.00.

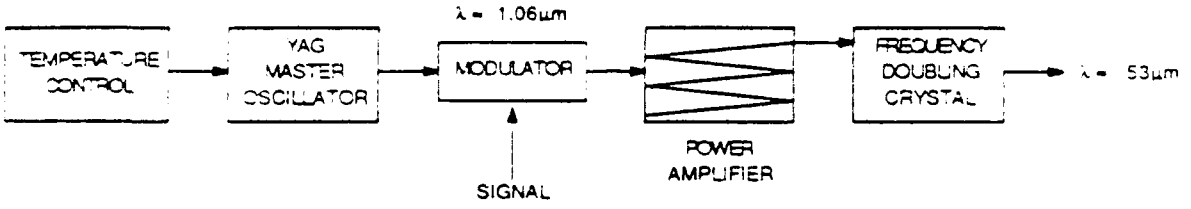

Figure 5-2. Possible Laser Design

5.1.1 Laser Safety

Throughout operation, the digital controller maintains less than the maximum safety limits for laser power operation. The controller governs the laser peak power using ranged direction information from an NTDS computer and optical time-domain reflectometry (ODTR) from the laser backscatter. Reflections from another ship or object can be used for ranging and, therefore, maintain safe laser operation.

5.2 Fixed and Steered Optical Elements

For the fixed optical elements ATA has considered the following. Material selection will be made on the basis of cost, durability, and stability. For mirrors, aluminum, pyrex, and Zerodur have been investigated. Metals are attractive for being lightweight and having low cost. Pyrex offers a higher optical quality at a cost that is still inexpensive. Zerodur offers high durability and stability since its coefficient of thermal expansion is effectively zero, but it has a high price. Selection of lens materials range between acrylic plastic and crown glass along with possible anti-reflection coatings.

For the steered optical elements, traditional, non-reactionless galvos and high-bandwidth, reactionless, electromagnetically-actuated beam-steering mirrors were considered. Steered optical components have been investigated, which incorporate a reaction mass for reactionless operation. The mass and the mirror are made of beryllium to provide a high stiffness to mass ratio

making high beamwidth operation (greater than 300 Hz) possible. Differential Impedance Transducers (DITS) will be incorporated to sense mirror position inside the assembly.

ATA investigated a Maksutov Cassegrain telescope design for the system. This design uses two spherical mirrors with a meniscus corrector lens placed in the entering beam to correct for spherical aberration. Spherical mirrors generally cost less than the aspheric mirrors used in a classical Cassegrain system. Optical design of the telescope will be based on a 15 cm clear aperture with a 1.5 degree field-of-view. This design would provide a simpler, cheaper option than the Ball RME telescope described in the next section.

5.2.1 Primary/Secondary Mirror Assembly

The relay mirror experiment (RME) being conducted by Ball Aerospace Corporation and ATA utilizes a telescope assembly for collecting radiation from a satellite source (Figure 5-3)

The design meets the requirements of the Optical Communication System (OCS) and a copy of this telescope may be incorporated directly in the OCS system. The specifications of this telescope are given in Table 5-1.

The filter, sensor and printed circuit are designed for infrared operation and would be replaced for the present application (Figure 5-4).

Figure 5-5 shows ATA's telescope design for this project.

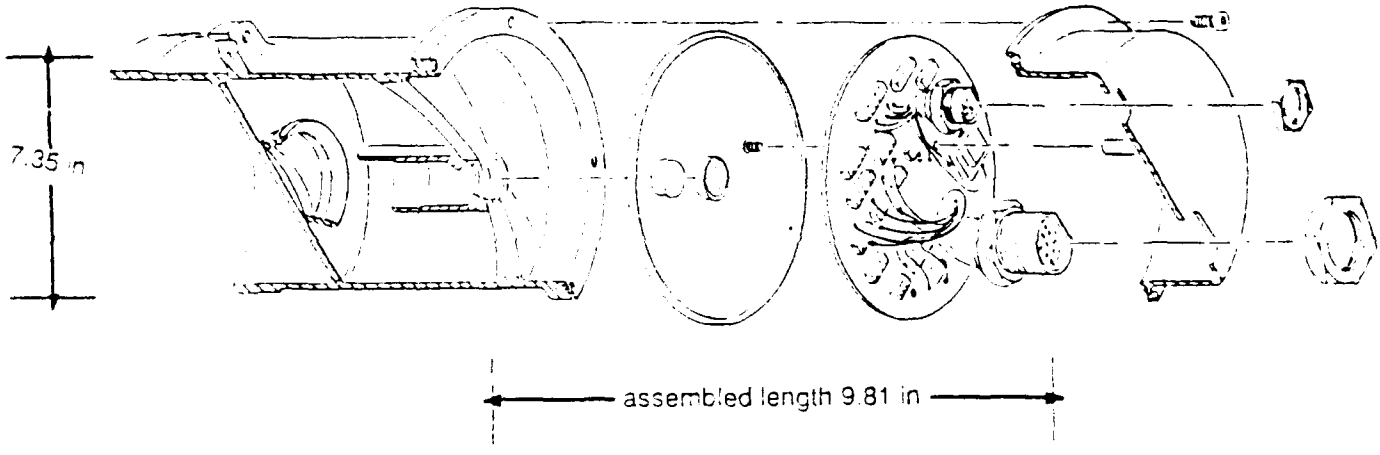

Figure 5-1. Ball Telescope/Sensor Assembly

Table 5-1. Telescope Specifications

Specification	Description
Overall Dimensions	4.81 x 7.35 in. dia.
Weight Total	10 lb
Telescope	8 lb
Sensor Assembly	2 lb
Telescope Assembly	Catadioptric with Mangin mirrors
Focal length	372 mm
Clear aperture	152 mm
Transmission efficiency	> 45%
Field-of-view	1.5° deg (full angle)
Field size at image plane	10 mm
Optical filter	High efficiency narrow bandpass
Multilayer multicavity design	Bahr Associates
Transmission efficiency	> 75 percent
Bandpass	7.5 nM
Blocking	10^{-5}
Printed Wiring Board Double-sided	6.5 in. dia.
Detector/Preamp Design	Previous design experience
IR enhanced silicon detector	Off-the-shelf part
Photovoltaic mode	
Ultra Low Noise Transimpedance Amplifier	
Analog-to-Digital Conversion	Covered in electronics section (6 bits)
Connectors	Data
	Power

SENSOR PRINTED WIRING ASSEMBLY

FUNCTIONAL BLOCK DIAGRAM

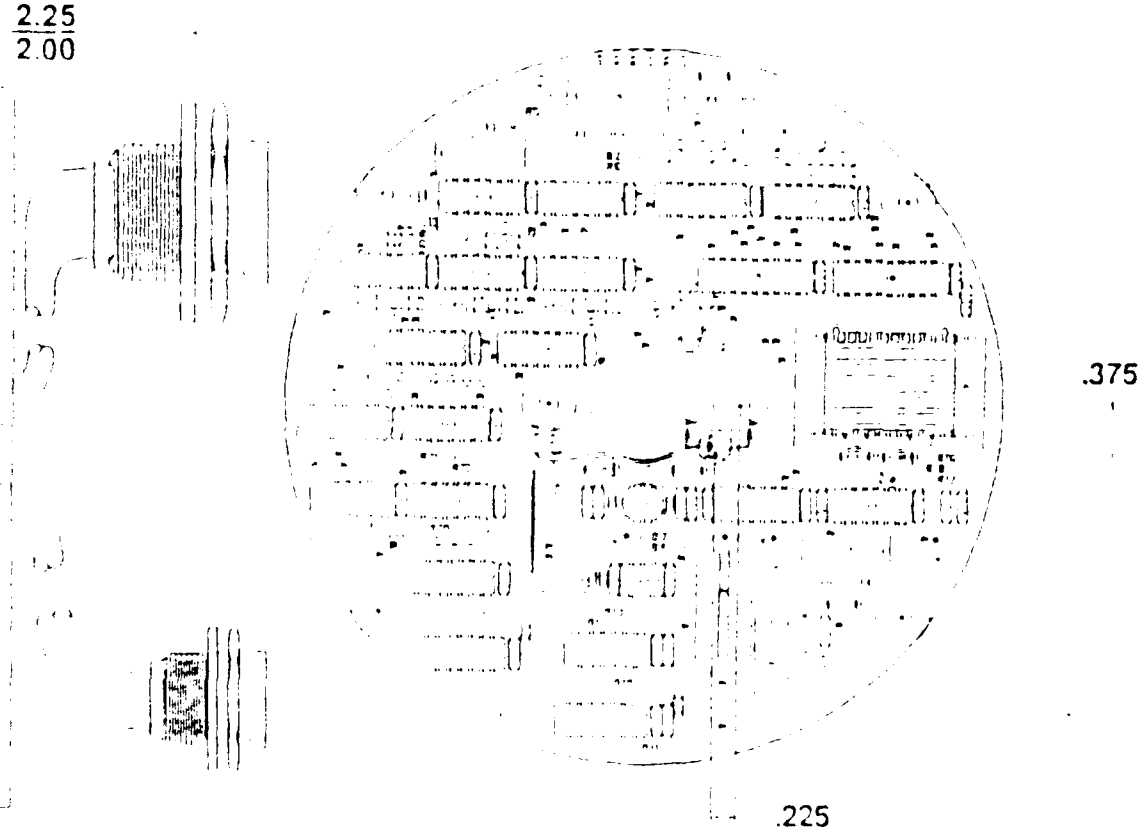

Figure [illegible]. Ball Sensor Printed Wiring Assembly

- Maksutov Cassegrain System Design

- Two Spherical Mirrors with Corrector Lens to Minimize Spherical Aberrations

- Inexpensive Design

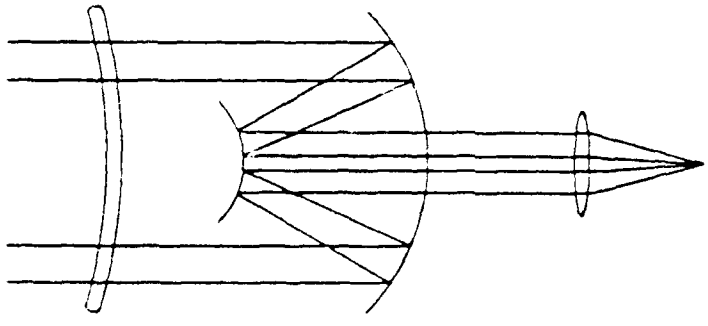

Clear Aperture: 15 cm
Field of View: 1.5 deg
Magnification: 5x

Figure 3-1 Telescope Design

5.2.2 Shared Aperture

The shared aperture design uses an isolated mount. It has an azimuth drive of plus or minus 180 degrees, a two-axis fast-steering mirror, and incorporates a signal generation processing module. The pointing flat can turn plus or minus 45 degrees and features an intelligent retro. There is a focus drive and a secondary spider.

Digital signal processors (DSPs) are relatively new types of processors used for enhancing the computational speeds often needed in signal processing applications. The DSPs are applicable in this control problem for the high-frequency control loop. Here, in place of ganging multiple, conventional-type processor modules together to implement a parallel processing approach, one DSP coupled with one conventional processor may indeed provide the necessary computational requirements.

5.3 Tracking Electronics

For the tracking electronics, quadrant cell detectors with both analog and digital signal processing were considered. Focal plane arrays with digital processing were also considered. Figure 5-6 shows a quad cell photo-detector.

A parametric study was performed to characterize optical system sensor limitations with the following system design parameters:

		Diameter (cm)
Optics	Receiver	15
	Transmitter	3
	Retro-reflector	3

Source GaAlAs Diode Laser, 820 nm, Peak Power ~ 30 mW

Detector Silicon Avalanche Photo Diode, $D^* = 3 \times \frac{10^{12}}{w}$ cm$\sqrt{Hz}$

1 mm Detector with 16 Hz Bandwidth Detector for Noise ~ 10^{-9} W

1 mm Detector with 300 Hz Bandwidth Detector for Noise ~ 10^{-11} W

All Components are off-the-shelf.

Results were:

1) Background power at receiver was estimated as:
   Sky illumination ~ 10^{-22} W
   Beam backscatter (0.5um particle size) ~ 10^{-12} W
   Solar backscatter from fog ~ 10^{-12} W.
2) Direct sunlight in field of view in sensor bandwidth completely blankets the signal ~ 60 mW.
3) SNR ~ 100 in absence of direct sunlight.

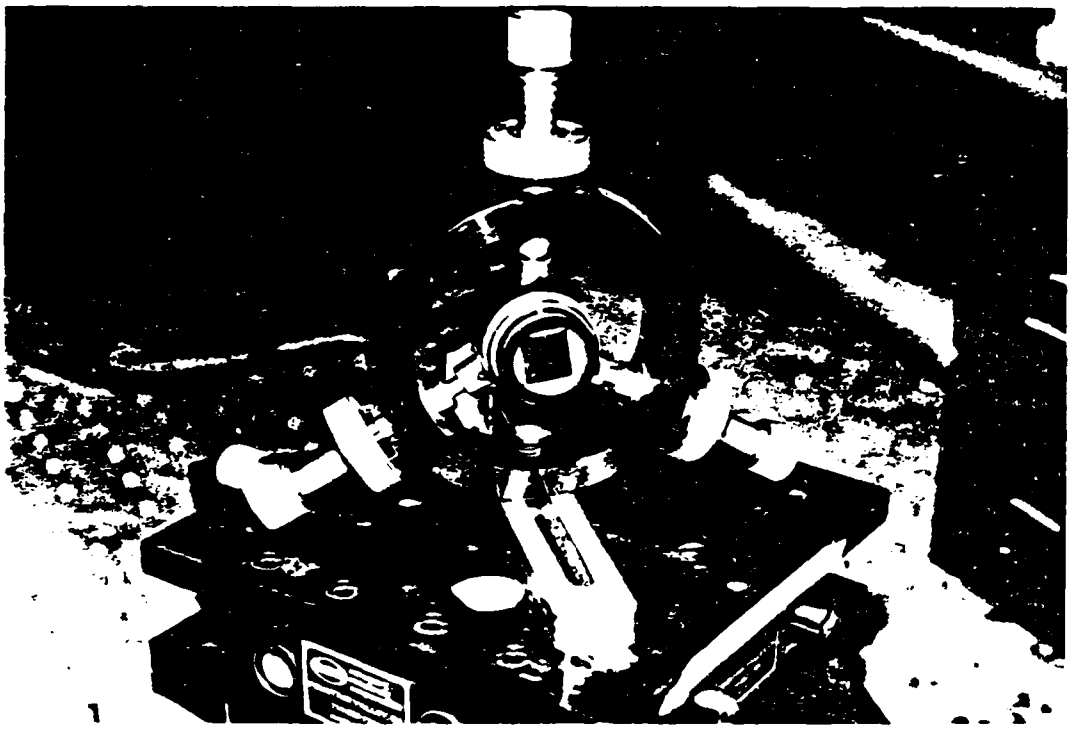

Figure 5-6. Quad-Cell Photodetector

ATA concluded:

1. Background power additions have negligible effects with a 20 nm bandwidth filter centered on the source wavelength.

2. Transmitter modulation may be used to reject direct solar input. Otherwise, the system is detector noise limited and not background limited.

ATA did a tracker sensor analysis for acquisition and fine tracking utilizing a quad cell and a conical scan.

Quad Cell:

Ideal control loop (no jitter) SNR ~ 100
Tracker Error ~ 0.03 μrad

With 10 μrad control loop residual error (= integrated uncorrected error) tracker error bound ~ 0.05 μrad; this is 0.08 cm in target plane at 15 km.

Conical Scan for Acquisition:

Beam waist optimized for minimum acquisition time = 0.01 sec and uncertainty in search area is 18m X 18m, SNR = 2

AC power return at receiver: $P_{AC} = 1.52 \times 10^{-11}$ W at 300 Hz

DC power return at receiver: $P_{DC} = 1.3 \times 10^{-11}$ W

Detector Noise for Δf = 300 Hz: $P_N = 6.4 \times 10^{-11}$

or $\frac{P_N}{Hz} = 3.69 \times 10^{-12} \frac{W}{Hz}$

Using a 2 Hz bandwidth filter center at 300 Hz, SNR ~ 2

Beam waist, optimized for reacquisition time = 0.02 sec and same uncertainty area, SNR = 1400.

Fine Tracking

The SNR was inversely proportional to the size of the search area.

Under the ideal control loop, the SNR is very large.

With 10 μrad control loop residual error search, area uncertainty is ± 4.5 cm in the target plane implying that the SNR is still very good.

Figure 5-7 gives the bit error probability for ASK communications. Figure 5-8 gives the bit error for a given SNR. Figure 5-9 shows the receiver input SNR and Figure 5-10 describes the optical impact.

- $PE = 1/2 \operatorname{erfc} \left\{ \sqrt{SNR} \right\}$ Coherent ASK
- $P \cong 1/2 \left(1 + \frac{1}{\sqrt{\pi SNR}} \right) \left\{ \exp \left(\frac{SNR}{4} \right) \right\}$ Non-Coherent ASK
- $SNR = \frac{\text{Energy Per Bit}}{\text{RMS Noise Power Density}}$
- No Burst Error Analysis Addressed
  - Digital Retransmission Relaxes Burst Error Problem

Figure 5-7. Bit Error Probability for ASK Communications

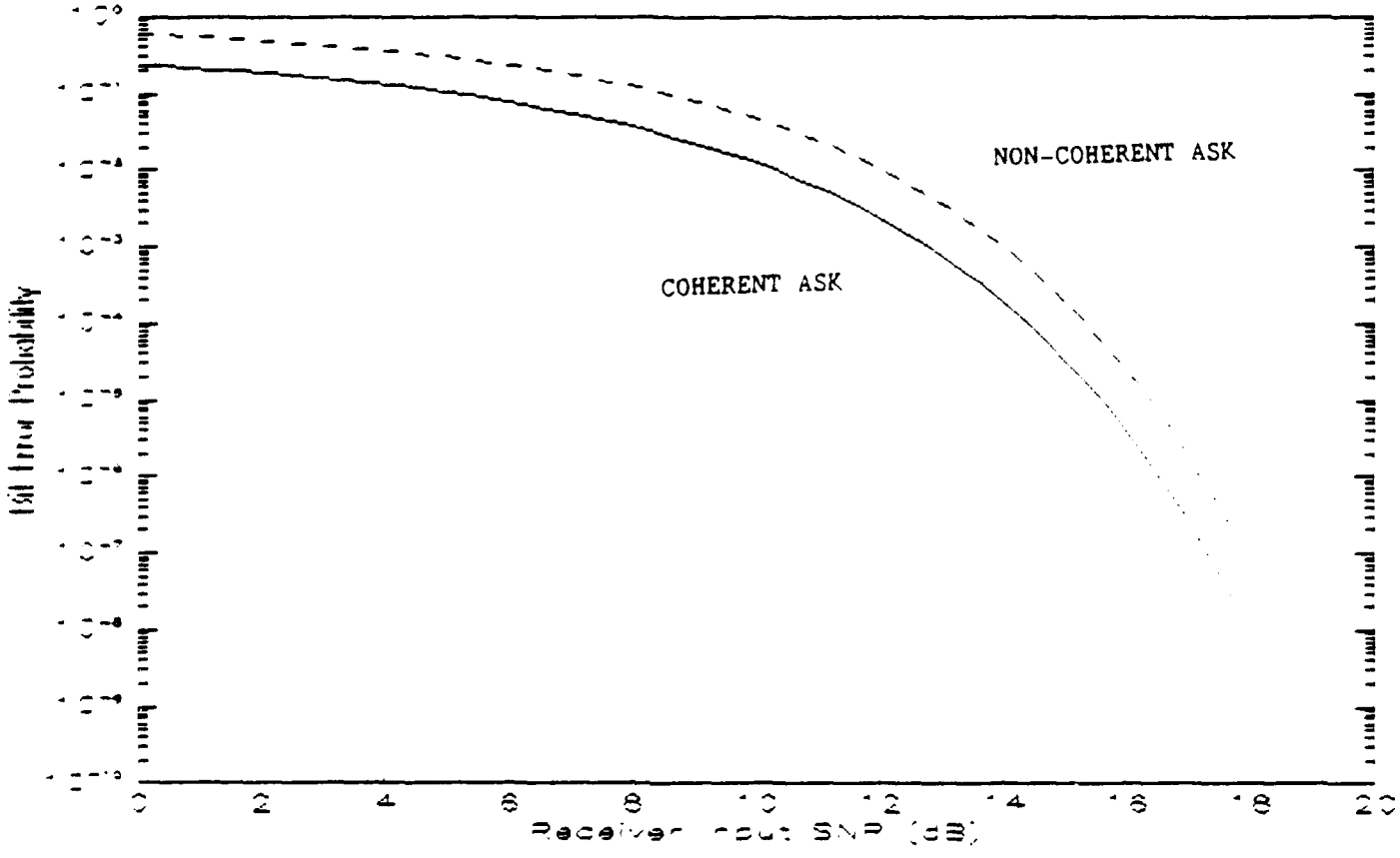

Figure 5-8. Bit Error For a Given SNR

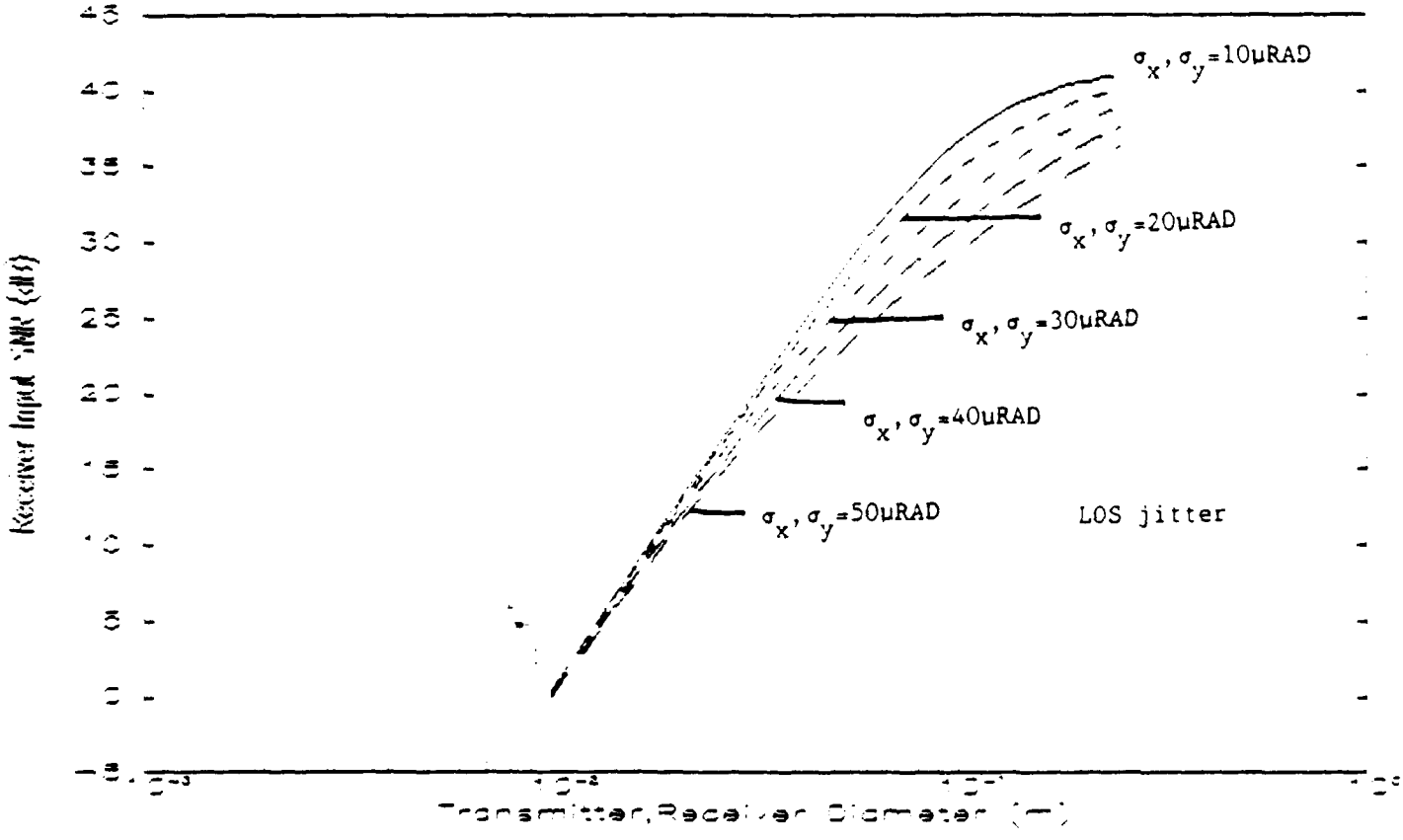

Figure 5-9. Receiver Input SNR: Tatm = 10%, Pointing Error = 1-urad

Operational Conditions:

10 cm Transmitter/Receiver
10% Atmospheric Transmission
35 mW Pulse Laser
10 urad Pointing Error
10 urad RMS x and y LOS Jitter

Implies:

- SNR > 1000 (30 dB)
- Pe < 10^{-10}
- Small, Light-Weight Optics

Figure 5-10. Optical Impact

5.3.1 Maximum Search/Acquisition Time

The baseline acquisition system will use a sequential search first in azimuth (horizon) direction followed by a search in the elevation direction. A 3 mrad by 3 mrad laser beam will perform a uniform azimuth scan at 1 Hz (per 360° revolution.) All target ships' receivers will be fitted with a 3 cm by 3 cm retro reflector at the center of their receiving aperture. Reflection from this retro will function as a friendly beacon for acquisition and tracking. The beam width of the retro-reflector is about 30 mrad. The acquisition sensors electronic bandwidth is assumed to be 300 Hz. Thus, from the instant the search beam encounters the retro, a detectable signal above the noise level will reach its peak in approximately 1 msec. Noting the time instant of the return pulse peak, and the location of search beam axis in the search time period, one could identify an area 0.3 mrad (in azimuth) by 3 mrad (in elevation) in the target space containing the target retro. If the azimuth search is limited to 180° of the horizon, the random acquisition time to acquire the retro-reflector is approximately 2.0 seconds. Next, the search beam will be focused down to 0.3 mrad by 0.3 mrad area and an elevation scan will be initiated, again at the 1 Hz rate (0.9 rad sec.) Thus, the elevation scan will be over in 5 msec or less, and the retro will be contained in a 0.3 mrad by 0.3 mrad area in a known direction. High-bandwidth fine tracking in that direction will be initiated immediately. The total acquisition and track initiation time is estimated to be about 2.5 seconds or less. Assuming a 30 mW tracker laser, a 15 km range, a round-trip path transmittance of 10% and a silicon avalanche photodiode of 1.5 mm diameter as the sensor, the signal-to-noise ratio at the detector output is estimated to be 50.

ATA's system is being designed to have a maximum search/acquisition time of one second, assuming a coarse (± 45 degrees azimuth, ± 22.5 elevation) indication of the receiver is available to the transmitter. The coarse indication can come from the radar or the last position of good communication.

6.0 DATA SYSTEM

Given a type of communication system, the signal noise ratio (SNR) determines the bit error probability. Simple, commonly available digital systems require the same "ball-park" SNR for PE~10^{-9}. Differences in requirements are 2 to 3 dB.

6.1 Type/Quantity of Information to be Transferred

ATA's design provides ansfer of real-time video-type information. In an ideal situation, up to 500 megabits/second of information will be able to be transferred. However, there is a cost-versus-bandwidth tradeoff to be considered if baseband video signals are to be transferred over a serial communication link, because data rates of several hundred megabits per second can be expected:

A 4.5 megahertz baseband video rate x 4 samples/cycle x 8 bits/sample x 2 channels = 288 megabits/second. If encryption, overhead and retransmission effects are included, 288 megabits x 30% encryption overhead x 10% protocol overhead x 25% transmission = 0.5151 gigabits per second.

For these data rates, the cost of implementing the communication system can be significant. Components such as laser diodes jump in price from the 20 megabits per second system to the 500 megabits per second system by a factor of about 10.

An attractive alternate is the use of a dot matrix laser printer/FAX machine. While these tend to operate at He:Ne frequencies of 630 nm and not 500 nm with information rates of 100 megahertz, with minor modifications they may provide the base for a relatively inexpensive demonstration of an optical communication system transmitter.

Here, existing off-the-shelf fiber optic communication transmitter-receiver pairs can be adapted for a line-of-sight link. Costs vary with bit rate and power requirements. At the low end, a 10 to 20 Mbps off-the-shelf system sells for approximately $6K to $8K, while a 500 to 1000 Mbps transmitter/receiver pair ranges in price from $10K to $20K. Obviously, this tradeoff is a factor the Navy will want to consider in deciding on the actual Phase II prototype. High power sources for commercial systems utilize 20-30 mw. Fiber optic systems are easily incorporated into Naval applications. See Table 6-1 on the off-the-shelf optical communication systems.

6.2 Maximum Transfer Time

ATA's initial system will be designed for the real-time case discussed earlier, i.e., 0.5 megabit/second. It will not be designed for burst or packet communications implying higher bandwidths, i.e., transfer time will not be considered accounted for in the retransmission factor discussed earlier.

6.2 Minimum Information Capacity of the System

Minimum information capacity refers to the requirements of a communication system for minimum functionality as a subsystem for ship-to-ship applications in emergency conditions. The requirements proposed assume only essential types of information necessary to be transmitted between ships.

The signal information bandwidth will be 20-50 megahertz. A 256 x 256 array of 8-bit pixels 20 times per second provides a 20 megabit second rate.

Ship to-ship communication for battle time situations may require secure information exchange among a fleet of ships with little or no delay. Information such as radar images, battle plan update charts, directives and vocal communication, and ship computer networking gives rise to a high data rate optical line-of-sight transmitter-receiver. For real-time transmission of this type of information, data rates derived from the following kinds of data transmission situations can be expected:

- 5 megabits per second for 10 radar images/sec x 256 x 256 pixels x 8 bits/pixel

- 2 megabits per second for 1 chart image/sec x 512 x 512 pixels x 8 bits/pixel

- 2 megabits per second for 10 vocal channels x 3000 Hz x 2 x 8 bits/sample

- 2 megabits per second for 100-19.2 k band computer connections at 19.2 k bound; 30% for encryption plus 10% protocol overhead.

In total, 20 megabits per second is a reasonable bit rate to transmit this quantity of information, using a 25% rate of retransmission due to any errored transmissions.

6.4 Maximum Error Rate of the System

Standard communication practices require that the maximum error rate will be one in a million or 10^{-6}. This rate was derived from the equations given in section 2.4 1.2.

6.5 Naval Tactical Data Systems (NTDS) Data Transfer

The digital controller will handle starting and stopping data flow across the channel and will request a retransmission as necessary as well as retransmit requested data. ATA will work with the customer to provide the protocol and encryption technology. NTDS computer-to-computer connections can be accomplished with a very high bandwidth transfer/communication link established for implementing a fleet command post in a single ship command room. Multiple links could be established for networking each ship to the control command center.

Aside from NTDS data, digitized video images (and voice channels) will be supervised by the digital controller in order to encode and decode each channel at the transmitter and receiver. The destination of each information channel is also supervised by the digital controller.

3. COST ELEMENTS

Costs are dependent upon various aspects of the systems, such as the three elements listed below:

1) Aperture size;
2) Number and type of optical elements;
3) Number and type of control loops.

The non-recurring development costs will not be used in evaluating the various systems. Not only are these costs much more difficult to estimate because of their subjective nature, but if the system is replicated many times, as we shall assume here, these costs tend to become a small part of system cost because of their allocation over a large number of systems. Table 3-1 gives some of the component weights, volumes and costs.

Table 3-1. Component Weights, Volumes, and Costs

	Weight (kg)	Volume	Cost ($)
Telescope and Optics and Sensors Assembly	8	[illegible] cm diam. [illegible] cm long	1,2[illegible]
Coarse Tracker Flat Mirror	1 kg	64 cubic cm	[illegible]-4[illegible] (quality dependent)
Quad Cell Detector	diam	[illegible] mm diam.	[illegible]
Coarse Tracker Gimbal	"	"	"
Fast Steering Mirror	1 kg	[illegible] cubic cm	[illegible],1[illegible]
Transmitter:			
35 mW Diode Laser	0.1	1[illegible] cub cm	[illegible],500
1W Nd:YAG	0.3	18[illegible] cub cm	[illegible]-12,000
Power Supply	2.3	"	2,[illegible]
Multiplexer/Modulator	2.3	"	1,[illegible]0
Receiver:			
Photodiode Detector	0.1	Small	1,[illegible]
Demodulator/Demux	1	"	1,[illegible]
Control Electronics:			
Microprocessor Boards	0.5	Phase II	[illegible],[illegible]

A I Boards	0.5	prototype	5000
D A Boards	0.5	12"x12"x12"	5000
Power Supply Connectors	1.0	total	5000
Stepper Motor Controller	0.5		2000

*To be supplied

The thermal control scanner, which is a driver for the fast-steering mirror, is available for $625.00 for model G325DT. The G300 series of fast-steering mirrors, 10-, 20-, and 30-millimeter size, range in price from $350.00 to $500.00. Both the scanner and the fast-steering mirrors are available from General Scanning Inc.

Ranking by cost alone at this point in the effort provides a reasonable approach. Most of the variation in pointing-and-tracking subsystem performance is due to overall configuration of the subsystem, not specific implementation. The implementation having the lowest cost was designated as the low-cost pointing-and-tracking subsystem. It is the design of this subsystem which is the principal result of this effort. It is this design which will be developed and implemented in Phase II of the effort. Table 7-2 gives some of the approximate costs for the Phase II effort.

Table 7-2. APPROXIMATE COSTS FOR PHASE II

TASK	LABOR ($K)	HARDWARE ($K)
1. Computer Models	30	0
2. Atmospheric Issues	30	0
3. Ship Motion	20	5
4. Tracking Demonstration	100	50
5. Glint Returns	30	0
6. Acquisition Demonstration	50	5
7. Communication Demonstration	100	70
TOTAL	$360K	$130K

These estimates will be defined in greater detail in our Phase II proposal.

8. BIBLIOGRAPHY

8.1 Recent Related Work by ATA Staff Members

Directed Energy Weapons," Report ATA-R-[illegible], Subtask Report, Contract F29[illegible]-[illegible]-116, Air Force Weapons Laboratory, KAFB, NM, October, 1986.

Laughlin, D.R., "MHD Angular Sensor Design and Evaluation," Applied Technology Associates, Inc., Report No. ATA-R-[illegible], July, 1985.

Laughlin, D.R., "MHD Angular Rate Sensor," Proceedings of the Annual Guidance and Control Conference, American Astronautical Society, San Diego, CA, February, 1987.

Morgan, F.E., "Stabilization Techniques for the CIGTF Seismically Stabilized Platform," AIAA Paper 82-1384-P, AIAA Guidance and Control Conference, August 1982.

Perrault, L.E., "Advanced Angular Sensor Concepts," Applied Technology Associates, Inc., Report Number ATA-R-[illegible], June 1984.

Schneeberger, T.J., "Statistical Analysis of Beam Control Systems," AFWL-TR-85-[illegible], Air Force Weapons Laboratory, KAFB, NM, September, 1986.

Sepetka, H.P., T.J. Schneeberger, et.al., "Performance Simulations of Beam Control and Diagnostic Systems," AFWL-TR-81-[illegible], Air Force Weapons Laboratory, KAFB, NM, September 1982.

Sepetka, H.P., et.al., "Precision Measurements and Active Control of the Seismically Stable Platform," Twelfth biennial Guidance Test Symposium, Holloman AFB, NM, October, [illegible]

Sepetka, H.P., L.K. Ebbesen, and L.D. Zirkle, "Advanced Control Laws for Precision Beam Pointing (U)," AFWL-TR-75-198, Air Force Weapons Laboratory, Kirtland AFB, New Mexico, April 1976.

Sepetka, H.P., L.P. Ebbesen, and L.E. Perrault, "Modeling and Simulation of Pointing and Tracking Systems," AFWL-TR-[illegible]-[illegible], Air Force Weapons Laboratory, Kirtland AFB, New Mexico, May 1978.

Sepetka, H.P., P.C. Lawrence, "Large Pointing System and Tracker Broadband Test System Simulation Models," AFWL-TR-[illegible]-[illegible], Air Force Weapons Laboratory, Kirtland AFB, New Mexico, October 1981.

Short, W.W., et al, "Statistical Analysis of Performance and Transfer System Performance," AFWL-TR-75-[illegible], Final Report, April 1976, (SECRET)

Short, W.W., et al, "Statistical Analysis of Pointing and Tracking System Performance," AFWL-TR-76-[illegible], Final Report, May 1977, (SECRET).

Short, W.W., and Schneeberger, T.J., et al. "Statistical Analysis of Beam Control System Performance," AFWL-TR-80-155, Final Report, October 1981, (SECRET).

8.2 Recent Related Work from DTIC LITERATURE SEARCH

Furham, R.S., "Intersatellite Link Design Issues," Report AFIT/CI/NR, 86-43T, Air Force Institute of Technology, WPAFB, Ohio, 1985 (AD A166-761)

Halley, P. (Editor), "Special Topics in Optical Propagation, AGARD-CP-300, Advisory Group for Aerospace Research and Development," North Atlantic Treaty Organization, 28th Meeting of the Electromagnetic Wave Propagation Panel, Monterey, CA, April, 1981.

Hanson, D.W., "Reduction of Anisoplanatic Errors," RADC-TR-81-122, Rome Air Development Center, Griffiss Air Force Base, New York, August, 1981 (AD-A106-689).

Kriksunov, L.Z., "Laser-Based Information Systems," FTD-TD(RS)T-0563-85, Foreign Technology Division, AFSCMD, WPAFB, Ohio, May, 1986. Translation from Sistemy Informatsiis Optichoskimi Kvantovymi Generatoriami, Kiev, USSR, 19[illegible] (AD-A168-418).

Leslie, D.H. et.al., "Technical Analysis of a Proposed Ship-to-Ship Chemical Laser Transmission Experiment," NRL Memorandum Report 4745, Naval Research Laboratory, Washington, DC, February, 1982 (AD-A112-804).

Maynard, J.A. et.al., "Airborne Flight Test System (AFTS)," Final Technical Report, McDonnell Douglas Aircraft Company, Contract F33615,76,C-1002, with HQ Air Force Space Division, Deputy for Space Communications Systems, Worldway Postal Ctr, Los Angles, CA, October, 1981 (AD-A115-100).

8.3 Recent Related Work at SPIE Conferences

Barry, J.D. and G.S. Mecherie, "Beam Pointing Error as a Significant Design Parameter for Satellite-Borne, Free-Space Optical Communications Systems," Optical Engineering, Vol. 24, No. 6, pp. 1049-1054, November/December, 1985.

Barry, J.D. and G.S. Mecherle, "Communication Channel Burst Errors Induced by Gaussian Distributed Mispointing." SPIE, Vol. 616, 1986.

Clarke, E.S. and H.D. Brixey, "Acquisition and Tracking System for A Ground-Based Laser Communications Receiver Terminal," SPIE Vol. 295, pp. 162-169, Control and Communications Technology in Laser Systems, 1981.

Coffelt, Everett L. & Ebben, Thomas, H., "Optical Transceiver Platform for laser Communication Experiments," SPIE, Vol. 616, Optical Technologies for Communication Satellite (1986), pgs. 22-28.

Hall, W.J. and J.D. Barry, "Precision Optical Pointing and Tracking from Spacecraft with Vibrational Noise," SPIE Vol. 616, pp. 2-10, Optical Technologies for Communication Satellite Applications, 1986.

Katzman, M., "Laser Space Communications Technology Status," SPIE Vol. 295, pp. 2-11, Control and Communications Technology in Laser Systems, 1981.

Kreft, L.A., et.al., "Analysis of Burst Error Occurrence on Optical Intersatellite Link (ISL) Design," SPIE Vol. 616, pp. 129-134, Optical Technologies for Communication Satellite Applications, 1986.

Legume, Moreau & Hibon, "Acquisition and Fine-Pointing Control for a 400 megabits per second Link between a Low-Earth Orbiter and a Geostationary Satellite," Sein. Electrog. SPIE, Vol. 616, 1986.

Lorenz, J.M. and K. Yong, "Acquisition Tracking and Fine Pointing of Space-Based Laser Communication Systems," SPIE Vol. 295, pp. 104-114, Control and Communication Technology in Laser Systems, 1981.

Nelson, R.O.; Eubem, T.E. and Manshalek, R.G., "Experimental Verification of the Pointing Error Distribution of an Optical Intersatellite Link, SPIE Proceedings, 1987.

Otagure, W.S., et.al., "Fiber-optic Gyro for Space Applications," SPIE, Vol. 616, Optical Technologies for Communication Satellite Applications (1986), Pgs. 205-212

Reiland W., et.al., "Optical Intersatellite Communication Links: State of the Laser Technology," SPIE Vol. 616 Optical Technologies for Communication Satellite Applications (1986), Pgs. 69-76.

Scott, P.W. and P.W. Young, "Impact of Temporal Fluctuations of Signal-to-Noise Ratio (Burst Error) on Free-Space Laser Communications System Design," SPIE Vol. 616, pp. 174-180, Optical Technologies for Communication Satellite applications, 1986.

Sein, E., et.al., "Acquisition and Fine-Pointing Control for a 400-Mbps Link between a Low-Earth Orbiter and a Geostationary Satellite," SPIE Vol. 6165, pt. 141-159, Optical Technologies for Communication Satellite Applications, 1986.

Young, P.W., et.al., "Pointing, Acquisition and Tracking Subsystem for Space-Based Laser Communications," SPIE Vol. 616, pt. 118-124, Optical Technologies for Communication Satellite Applications, 1986.

8.4 Other Recent Related Work

Bhattacharyya, Rameswar, Dynamics of Marine Vehicles, John Wiley and Sons, New York, 1978.

Dermendjian, D., "Scattering and Polarization Properties of Water Clouds and Haze," Applied Optics, Vol. 3, No. 2, 1964.

Gerber, A.; Davis, J., and Tinsley, J., "The Near-Ship and Ambient Marine Environment," I.R. (Received Oct. 14, 1984) Pgs. 604-612.

Hoffman, D., "Analysis of Measured and Calculated Spectra," The Dynamics of Marine Vehicles and Structures In Waves. Paper presented at International Symposium. Mechanical Engineering Publications, Ltd., London, 1-5 April 1974.

Hogan, B.J., "Reactionless Beamsteering Mirror May Aim Lasers for SDI," Design News, September, 1986.

Hudson, Infrared System Engineering, Wiley, pp 140-170, 1969.

Hurtman, Morris, Laser Satellite Communications, Prentice Hall, pp 42-43, 1987.

Masten, M.K. and H.R. Sebesta, "Line-of-Stabilization/Tracking Systems: An Overview," Proposed Paper, Automatic Control Conference, June, 1987.

Merritt, P.H. and J.E. Perrault, "Boresighting of Light Beams on Distant Targets Using Conical Scan Techniques," Proposed Paper, Automatic Control Conference, June, 1987.

Miratymon, "Laser Satellite Communications."

Nelson, P.D., et.al., "Experimental Verification of the Pointing Error Distribution of an Optical Intersatellite Link," Ball Aerospace Systems Division (BASD), Boulder, Colorado.

NRL DOCUMENT, Appendix B1: "N/H Test Results and Analysis of Tracking Capability," NMC 10602, prepared by Massachusetts Manufacturing Corporation, 9 Sept. 1981.

Peebles, A. Peyton Jr., Communication System Principles, Adison-Wesley Publishing, Inc., 1982.

Sher, L. (Editor), "Lessons Learned from the Airborne Laser Laboratory," AFWL-TR-83-5, June 1983, Confidential.

Van Dine, M.F., "Ship Relative Motions and Related Phenomenon," John Wiley and Sons, New York, 1976.

Approved for public release: distribution is unlimited.

The views and conclusions contained in this report are those of the authors and should not be interpreted as representing the official policies, either expressed or implied, of the Naval Ocean Systems Center or the U.S. Government.

END
DATE
FILMED

10/27/88

S.B.